Abstract

Al-Zayed, Ayman S., Tray Based Millimeter-wave Quasi-Optical Amplifiers and Dual Polarized Phased Arrays. (Under the direction of Amir Mortazawi.)

At millimeter wavelengths, spatial power combining techniques offer a viable approach to realize compact, reliable, lightweight, robust, higher-power and economical systems This work focus on the tray based perpendicularly fed array systems, several design issues such as bandwidth improvement, power combining efficiency, dual polarity and beam steering were addressed in this thesis.

A broadband tray based spatial power amplifier that employs dielectrically filled miniature horn arrays was investigated. Bandwidth improvement was achieved by replacing the patch arrays of an earlier design with the broadband dielectrically filled miniature horn arrays. This 5x5 spatial power amplifier with miniature horn arrays has a 3dB bandwidth of 1.32 GHz (13%), which is more than 4.5 times the 3 dB bandwidth of the perpendicularly fed patch array spatial power amplifier.

This work presents experimental and numerical investigations on a 49-element Ka-band amplifier array. This study is aimed at determining the origin of various losses in the amplifier array. Passive simulation data confirms that the load seen by the active devices is well matched and that most of the power is coupled to the LSE_{10} mode. This means that coherent power combining should take place if there is no phase and amplitude variation due to the active devices and phase correcting dielectric lenses.

This thesis presents a single aperture multibeam spatial power combining system that can support two separate polarizations. A Rotman lens is used as the power dividing network, which also has the ability to scan the beam over discrete angles. 1x9 dual polarized array was designed to demonstrate the beam steering in azimuth plane. The entire system is designed for the Ka band, with a center frequency of 32.6GHz. Through simulations and measurements, a ±30 degree scan range was achieved for the horizontal and vertical polarizations. The cross polarization for both the vertical and horizontal polarization ports was better than –16dB.

Tray Based Millimeter-wave Quasi-Optical Amplifiers and Dual Polarized Phased Arrays

by

AYMAN AL-ZAYED

A dissertation submitted to the Graduate Faculty of
North Carolina State University
in partial fulfillment of the
requirements for the Degree of
Doctor of Philosophy

ELECTRICAL ENGINEERING

Raleigh, North Carolina

2003

APPROVED BY:

Gianluca Lazzi	Griff Bilbro
Angus Kingon	Amir Mortazawi
	Chair of Advisory Committee

This work is dedicated to my parents, Family and Friends for their Support, Sacrifice

Encouragement, love and prayers

Biography

Ayman Al-Zayed was born in Alfeha, Kuwait. He received the B.Eng. (Honors) degree in Communication and Electronic Engineering from the University of Northumbria at Newcastle in 1995. Ayman then joined the Kuwait National Petroleum Company as and instrumentation and communication engineer. In 2000, he obtained the M.S. degree in Electrical Engineering from the University of Hawaii at Manoa. He then joined North Carolina State University and has fulfilled the requirements for a Ph.D. in Electrical Engineering. His research interests include microwave and millimeter-wave spatial power combining systems, phased arrays, and high frequency circuits and antennas.

Acknowledgements

I wish to extend my deepest thanks to my advisor, Professor Amir Mortazawi for giving me the opportunity to be part of his research group. I feel privileged to have been his student and to have had the chance to learn from his expertise in the field of microwave, as well as to interact with his personality. His guidance, encouragement, and patience have made this thesis possible.

I would also like to express my appreciation to my master's degree advisor Dr. Michael DeLisio for his support, friendship and contribution in my education.

I am honored to have Professors Gianluca Lazzi, Griff Bilbro and Angus Kingon as my dissertation committee members. Their helpful criticisms and valuable comments enabled me to complete this thesis.

I am grateful for the friendship and technical advices from the past and present colleagues Dr. Sean Ortiz, Dr. Mete Ozkar, Ali Tombak, Jin Zhang, Xin Jiang, Andy Guyette, Frederick Lecuyer, John Mazotta, Kevin Leong, Farshid Aryanfar, Dr. Abbas Abbaspour, Nader Behdad, Dr. Dimitri Peroulis, Navin Gupta, and Lora Schulwitz.

Special thanks to my family and loved one for always being there, for their support, understanding and love. I will always be indebted

Contents

List of Figures **viii**

1 Introduction **1**

1.1 Spatial Combining Technology ……...1

1.2 Perpendicularly-fed Patch Array for Spatial Power Combining……...5

1.3 Beam scanning using tray based Spatial power combiner……....7

1. 4 References……....8

2 Bandwidth Improvement in a Tray Based Spatial Power Amplifier **10**

2.1 Introduction and Motivation ……..10

2.2 Design of the miniture horn array……...13

2.3 Measured Results……17

2.4 Summary……21

2.5 References ..……22

3 Numerical and Experimental Investigations of Losses in a Tray Based Spatial Power Amplifier **24**

3.1 Introduction……24

3.2 Study of the cell spacing……27

3.3 FDTD Simulations……..…29

3.4 Effect of unit cell amplitude and phase variation……31

3.5 Thermal analysis…….33

3.5 Summary……..……...34

3.6 References……..…...……..36

4 Compact millimeter-wave tray based dual polarized multibeam active array 38

4. 1 Introduction and Motivation……..38

4.2 Dual polarized perpendicularly-fed patch phased array spatial combiner …….43

4.3 Dual polarized perpendicularly-fed patch phased array spatial combiner with phase shifters ……..…45

4.4 Dual polarized perpendicularly-fed patch array spatial combiner with Rotman lenses……49

4.4.1 Dual polarized patch antenna…….55

4.4.2 Microstrip to waveguide to aperture transition……..…59

4.4.3 Unit cell design …….62

4.5 Microstrip Rotman Lens……..…64

4.5.1 Microstrip Rotman Lens at X-Band……...69

4.5.2 Ka-band Microstrip Rotman lens……...78

4.5.3 Microstrip Patch Antenna Array fed by Rotman Lens……..…84

4.6 1X9 Dual polarized perpendicularly-fed patch array spatial combiner with Rotman lenses……90

4.7

References…….95

5 Conclusions and Future Work **100**

5.1 Conculsions ……100

5.2 Future Work……....103

Appendix A **105**

List of Figures

Figure **Page**

1.1 Power handling capacity from many solid state and tube devices as a function of frequency……..……..….2

1.2 Circuit level combiner. …….……..3

1.3 Quasi-optical grid oscillator.....3

1.4 Perspective view of the quasi-optical array employing perpendicular feed structure…5

2.1 Tile based spatial power amplifier with dielectrically filled miniature horn antennas……...…….12

2.2 Design concept of the unit cell……..12

2.3 The gain a Filtronic LMA 411 MMIC Amplifier…….14

2.4 The measure dielectric constant of paraffin was……...15

2.5 Simulated structure of the dielectrically filled miniature horn antenna using Agilent HFSS..……..16

2.6 The simulated and measured voltage standing wave ratio of the paraffin filled single horn……..18

2.7 The E-plan radiation pattern of a single horn antenna filled with paraffin at 9.22 GHz…….18

2.8 Small signal gain measurement of the spatial power amplifier with dielectrically filled miniature horn antennas……19

2.9 Small signal gain measurement of the perpendicularly-fed patch array spatial power amplifier…….19

2.10 Power compression curve of the 25-element spatial power amplifier……....20

2.11 Photograph of the 5x5 spatial power amplifier that employs dielectrically filled miniature horn arrays……...20

3.1 A photograph of the 7x7 amplifier array…….25

3.2 The small signal gain and return loss of the 49 element amplifier array……..25

3.3 The setup for measuring the loss of the spatial power combining array and the array topology……28

3.4 The insertion loss of several array spacing values versus frequency……28

3.5 The active reflection coefficients of the 49 cells Ka-band amplifier that is under investigation……..……...……30

3.6: Normalized field plots at a distance of 0.2λ from the array surface into the overmoded hard walled waveguide at time step = 3220……..... …30

3.7 The simulated insertion loss of the array fed by an ideal hard-horn versus the standard deviation of the phase…….……32

3.8 The simulated power compression of the array for a standard deviation in phase of 20° and 0.5 dB in gain…… ……33

3.9 The measured temperature versus time for the Ka-band 7x7 amplifier array……...34

4.1 Phased array approach of an electronically scanned transmitter……..……40

4.2 Drawing illustrating several unit cells with phase shifters on the trays that are stacked to from the array……46.

4.3 Dual polarized aperture coupled patch antenna fed by dielectric waveguides…….47

4.4 Details of the dual polarized patch antenna fed by two dielectric filled waveguide….47

4.5 Simulated return loss and isolation of the perpendicularly fed dual polarized antenna……..48

4.6 A prospective view illustrating several amplifying units on a tray that employs a microstrip Rotman lens to achieve beam steering……...……...50

4.7 Dual patch array used as the radiating element for the dual polarized tray based perpendicularly fed 7x7 patch array employing microstrip Rotman lenses used to achieve beam steering……..51

4.8 Dual polarized perpendicularly-fed patch array spatial power combiner with Rotman lenses……...53

4.9 A conceptual drawing of the perpendicularly fed dual polarized phased array feeding circuitry……..54

4.10 Dual polarized perpendicularly-fed patch array spatial power combiner with Rotman lenses and feeding circuitry……...54

4.11 The dual polarized patch antenna layout and it frequency response……...57

4.12 Simulated radiation patterns at 32.6 GHz for port 1 and port 2……..58

4.13 The microstrip to waveguide to aperture transition……61

4.14 The frequency response of the microstrip to waveguide to aperture transition……..61

4.15 Perspective view of the dual polarized perpendicularly-fed patch unit cell……...63

4.16 The frequency response of the dual polarized perpendicularly-fed patch…….....63

4.17 Calculated shape of the Rotman lens, optimized for a 30 degree scan angle…….66

4.18 Normalized Path length error ‘Δl’ versus the normalized aperture length ‘η’ for ‘***g'***= 1.076, at 10º, 20º and 30º……67

4.19 The simulated Rotman lens……70

4.20 The phase across the array ports when the lens is fed from the port that will produce radiation pattern with peaks at 0º……...71

4.21 The phase across the array ports when the lens is fed from the port that will produce radiation pattern with peaks at 30º…….....71

4.22 Calculated array factor of an antenna array fed by the simulated Rotman lens at 10 GHz……..72

4.23 A scanned photo of the fabricated Rotman lens……..72

4.24 The reflection coefficient of the input ports 1 and 4……...74

4.25 The coupling between the input ports and the coupling between array ports…….75

4.26 The phase across the array ports when the lens is fed from the port (1) the port that will produce radiation pattern with peaks at 0º……..75

4.27 Calculated array factor of an antenna array fed by the fabricated Rotman lens at 10 GHz……..76

4.28 The measured insertion loss of the X-band microstrip Rotman lens when it is fed from port 1……76

4.29 A photograph of the fabricated X-band Rotman lens…….77

4.30 Graphical representation of the dispersion relations for the modes that exist in a grounded substrate with ε_r=4.5 and d=0.508mm thick at 32.5 GHz……80

4.31 Plot of the effective dielectric constant as a function of frequency for a grounded substrate with ε_r =4.5 and dielectric thickness = 0.508 mm……...80

4.32 The simulated Ka-band Rotman lens……..82

4.33 The phase across the array ports when the lens is fed from port 1 which will produce radiation pattern with peaks at 0º. (Simulation)……83

4.34 Calculated radiation patterns of an antenna array fed by the simulated Rotman lens at 32.6 GHz……....83

4.35 The Mask of the Ka-band Rotman lens……..84

4.36 Array of microstrip patch antennas fed by Rotman Lens……...85

4.37 A photograph of the fabricated antenna array fed by Rotman lens…….87

4.38 Experimental setup for the measurement of the antenna array in the far field……...87

4.39 Measured radiation patterns of the microstrip patch antenna array fed by Rotman lens at 32.55 GHz……..88

4.40 The reflection coefficient of open ended transmission line with absorbing material (solid), and without absorbing material (dashed)……..…89

4.41 A comparison between the measured antenna array fed by the Rotman lens and the calculated radiation pattern of the Rotman lens with the input ports left open and without termination …….……...89

4.42 Auto CAD drawing of a 1x9 perpendicularly-fed patch array fed by Rotman lens...92

4.43 The mask of the 1x9 dual polarized antenna array…….92

4.44 Photograph of a 1x9 dual polarized patch array fed by Rotman lenses…….93

4.45 Measured radiation patterns for the vertical polarization at 32.6GHz……...93

4.45 Measured radiation patterns for the horizontal polarization at 32.6GHz……...94

5.1 Waveguide based dual polarized perpendicularly fed miniature horn array……...104

Chapter 1

Introduction

1.1 Spatial Combining Technology

The applications of microwave and millimeter-wave technologies have been growing in recent years, particularly in the commercial area. These applications include personal communication systems, indoor-wireless local area networks, railroad crossing alarm systems, satellite communication systems [1], automobile crash-avoidance systems [2] and remote sensing. Conventionally, high power sources at this portion of the electromagnetic spectrum are realized with vacuum tubes and gas lasers. These components have many disadvantages; they are usually heavy, bulky, and expensive, require high-voltage supplies, have high losses and are prone to single point failure. Also, in the millimeter-wave band, fabrication of conventional circuits becomes difficult and losses increase due to the skin effect in the metal walls. Solid-state devices can generate power at microwave and millimeter-wave region; however, the power of these devices is several orders of magnitude lower than that of vacuum tubes. A comparison of the available output power from vacuum tubes with the output power available from solid-state devices is shown in Figure 1.1. Consequently, and to overcome this, the output power of many solid state devices are combined. Traditionally this done using transmission line combining techniques as shown in Figure 1.2. The main and serious

disadvantage of this approach is the fact that for a large number of devices to be combined the power combining efficiency drops significantly. Resonant waveguide cavities are another typical technique to combine the power of many solid state devices. The disadvantages of this technique include, machining of the waveguides which become complicated especially at higher frequency, narrow bandwidths, and high conduction losses.

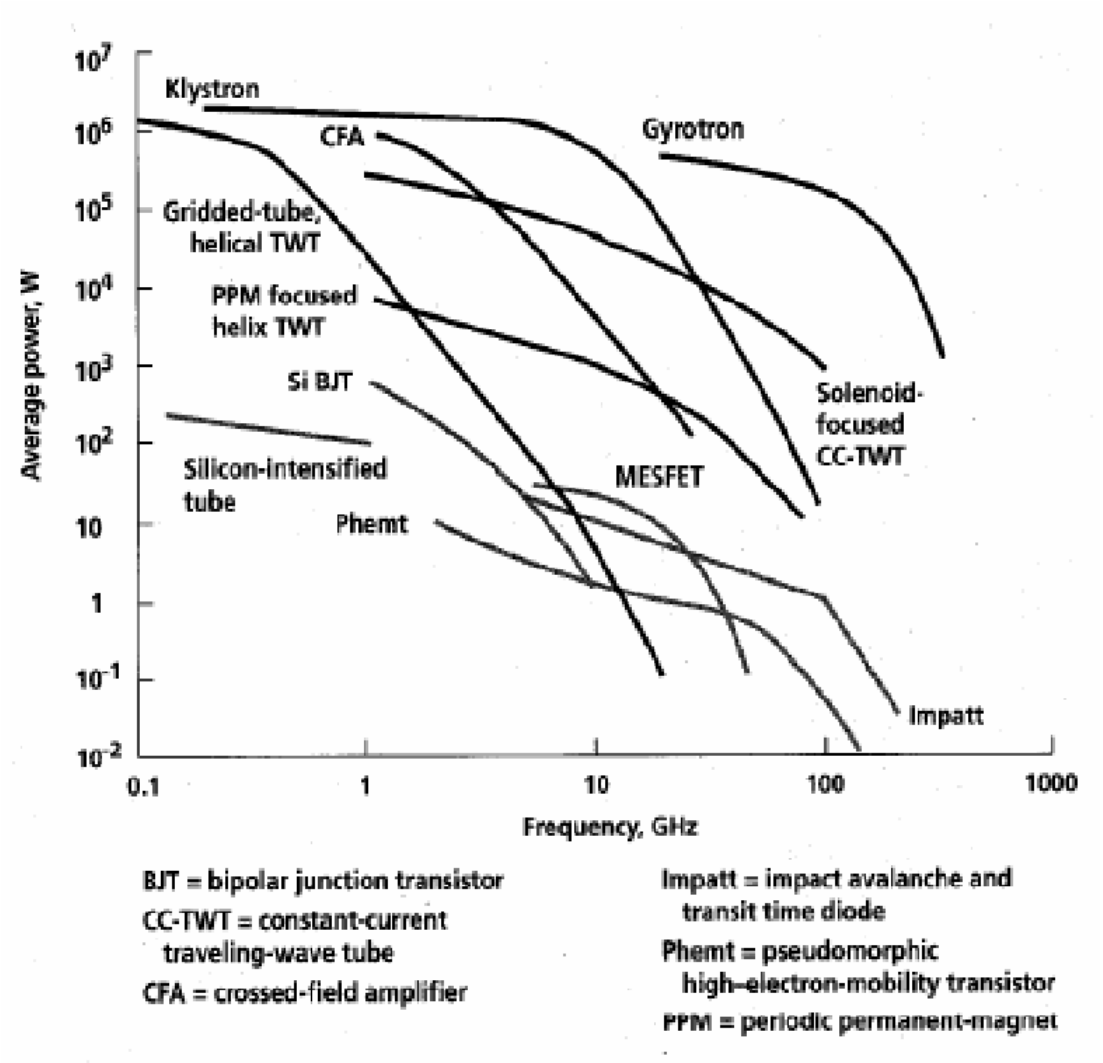

Figure 1.1: Continues power handling capacity from many solid state and tube devices as a function of frequency [3].

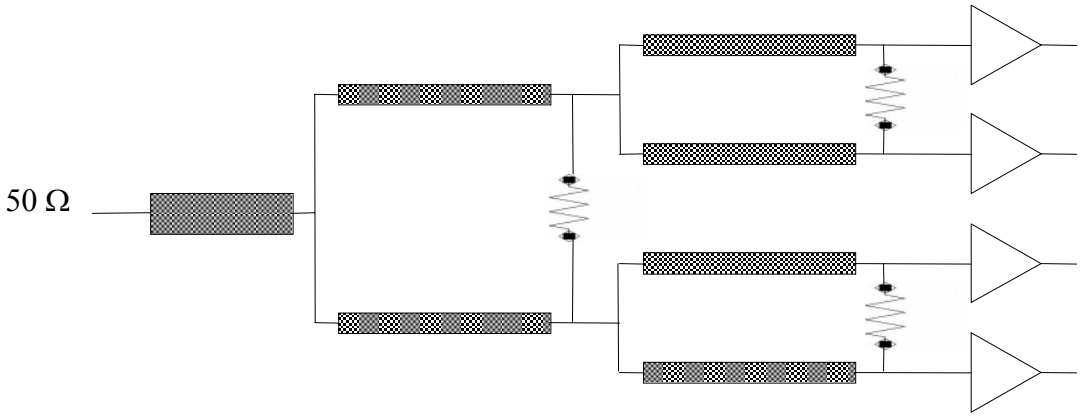

Figure 1.2**:** Circuit level combiner.

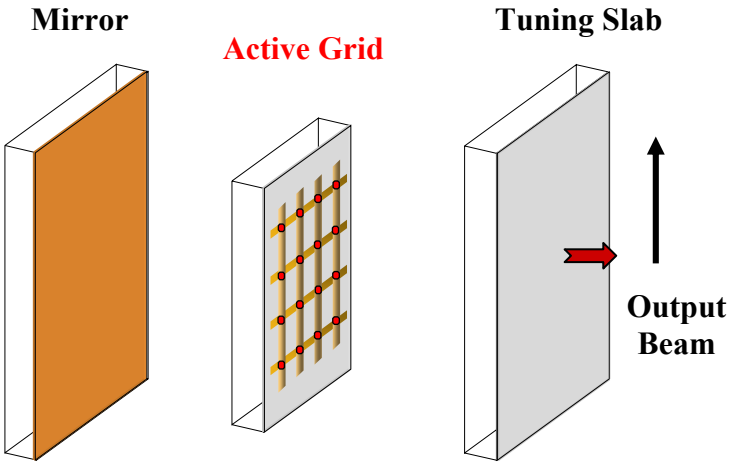

Figure 1.3**:** Quasi-optical grid oscillator.

Spatial (Quasi-optical) power combining techniques [4-5], such as quasi optical grids, tray based systems, and tile based systems provide an efficient means of combining the output power produced by many active solid state devices in free space. Furthermore, spatial combining circuits do not have limitation in the number of devices to be combined;

therefore, large RF power can be obtained from quasi-optical circuits, like the grid oscillator such as the one shown in Figure 1.3.

Spatial combining technology is still developing, and many circuits have recently been demonstrated such as amplifiers [6], oscillators [7], mixers [8], and multipliers [9].

Spatial combing circuits have many advantages that become more attractive when the frequencies increase.

(1) High power. By integrating a large number of devices a high total output power can be produced. More power can be generated by increasing the number of devices and the system size.

(2) Higher frequency. The higher the frequency the smaller the unit cell size, and therefore, more devices can be integrated per unit area.

(3) Less loss. Losses that are due to waveguide walls and feed networks are minimized because the power is combined in free space.

(4) Simpler analysis. The unit cell determines the impedance seen by the active devices, while the power scales with the total number of devices. Also, spatial combining circuits can be modeled using transmission lines, lumped elements, and simple circuits [11]. This can be simulated using computer aided design tools, such as, MDS, ADS, and HFSS.

(5) Monolithic Planar photolithographic techniques can be used to fabricate passive or active quasi-optic circuits.

(6) Failure tolerance. It was demonstrated [10] that when 20% of the active devices fail across the amplifier array a drop in gain of only 2.7 dB was measured.

(8) Low noise figure. The noise figure for an array would not be much worse than the noise figure of a single device, as the noise from each unit cell is uncorrelated.

1.2 Perpendicularly-fed Patch Array for Spatial Power Combining

Several architectures have been developed for spatial power combining, integrating solid state devices to generate noteworthy power levels at a different range of frequency bands. One of the well developed architecture is the tray based perpendicularly fed patch array spatial power amplifier [12]. Figure1.4. shows a conceptual drawing of the array.

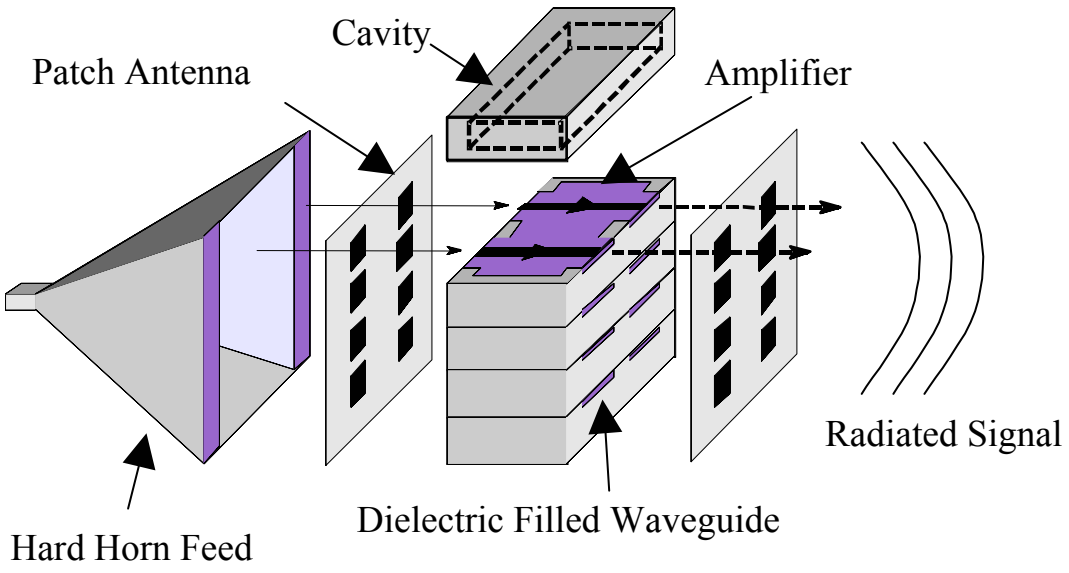

Figure 1.4: Perspective view of the quasi-optical array employing perpendicular feed structure.

In this figure, an array of microstrip patch antennas receive a signal of uniform amplitude and phase from a lens corrected hard horn feed on the left of the diagram. The signal is then coupled form the slots to the microstrip transmission lines located perpendicularly to the antenna layer. The signal is then amplified and then radiated through the aperture coupled patch antennas on the last layer. Using such structure, the power can be collected either in the far-field with a standard gain horn or with a hard horn feed.

This structure has many advantages over quasi optical grid arrays. The most distinguished advantage is that the amplifiers and biasing networks are located on trays, which are stacked to form the array. On another word, the amplifying portion of the unit cell occupies the space between the input and output microstrip patch antennas. This structure has the advantage of a minimal interaction between the radiated fields and the active devices. This isolation reduces the possibility of potential oscillations. Additionally, increased stability is provided, while delivering a robust and reliable design. The array is designed to have 0.5λ unit cell size. This spacing ensures that no grating lobes will be seen in the radiation pattern of such radiating structure. Another advantage is that the stacked trays provide thick ground plane for the removal of heat. Finally, this structure has the ability to use large device sizes, cascade devices and individual device biasing. Also more complex matching circuit can be used.

1.3 Beam scanning using tray based Spatial power combiner

At millimeter wavelengths, spatial power combining techniques offer a viable approach to realize compact, reliable, lightweight, robust, higher-power and economical systems. In many radar and communication applications it is mandatory to have a system capable of beam scanning and able to generate multiple beams from a single antenna aperture.

A complete structure of spatial power combiner requires electronic beam controllers for beam steering. Spatial or quasi-optical power combining techniques can be divided into two man categories, tile based and tray based. Extending the tile based spatial power combiner for beam control at higher frequencies faces technical challenges, the main one is the fact that amplifiers and phase shifter as well as the radiating elements share the same plane and therefore the unit cell size becomes large which lead to an undesired grating lobes and low radiated power.

Tray based structures such as the perpendicularly fed spatial power combiners have many advantages over the tile based structures. The most distinguished one is the reduced unit cell size which is typically on the order of 0.5 to 0.6λ in air. These unit cell sizes meet the constraint dictated by the requirements of angular coverage and grating lobe suppression. Since on the tray based structure the devices (such as amplifier and phase shifters) and matching networks are placed between the input and output antennas, therefore the devices and antennas are on separate planes. Two integration methodologies of dual polarized antennas, phase shifting components, feeding network and active devices were investigated in this thesis.

1. 4 References

[1] Yukio. Takimoto," Recent Development of MM-Wave Applications in Japan" Microwave Journal, pp. 214-226.May1996.

[2] G.R. Huguenin, "Millimeter Wave Radar for Automobile crash avoidance systems," Proceeding of the International Conference on Millimeter and Submillimeter Waves and Applications, SPIE Proceedings series, Vol.2250, Jan.1994.

[3] R. S. Symons, "Tubes: still vital after all these years," IEEE Spectrum., vol. 35, pp. 52-63, April. 1998.

[4] J.W. Mink, "Quasi-Optical Power combining of Solid-State Millimeter-Wave Sources," IEEE Trans. Microwave Theory Tech., vol. 34, pp. 273-279, Feb. 1986.

[5] R.A. York, "Quasi-Optical Power combining Techniques," in Millimeter and Microwave Engineering for Communications and Radar, J.C. Wiltse, ed., Critical.

[6] M.P. DeLisio, S.W. Duncan, D.-W. Tu, S. Weinreb, C.-M. Liu, D.B. Rutledge, "A 44-60 GHz Monolithic pHEMT Grid Amplifier," *1996 IEEE MTT-S Int.*

[7] Z. B Popovic, R. M. Weikle II, M. Kim, and D. B. Rutledge,"A 100-MESFET planar grid oscillator" IEEE Trans. Microwave Theory Tech, Vol.39, pp.193-200, Feb. 1991.

[8] J.B. Hacker, R.M. Weikle II, M. Kim, M.P. DeLisio, D.B. Rutledge, "A 100-Element Planar Schottky Diode Grid Mixer," IEEE Trans. Microwave Theory Tech., vol. 40, pp.557-562, March 1992.

[9] Moussessian, M.C. Wanke, Y. Li, J.C. Chiao, F.A. Hegmann, S.J. Allen, T.W. Crowe, D.B. Rutledge, "A Terahertz Grid Frequency Doubler," 1997 IEEE MTT-S Int. Microwave Symp Dig., pp. 683-686, 1997.

[10] S. Ortiz, M. Ozkar, A. Yakovlev, M. Steer, and A. Mortazawi, "Fault Tolerance Analysis and measurement of a Spatial Power Amplifier," *IEEE AP-S Int. Symp*., vol. 3, pp. 1827-1830, May, 2000.

[11] Polly Preventza, “Analysis and Design for Quasi-Optical Structures” Ph.D. Dissertation, California Institute of Technology, 1999.

[12] S. Ortiz and A. Mortazawi, “A perpendicularly-fed patch array for quasi-optical power combining,” *IEEE MTT-S Int. Microwave Symp. Dig*., vol. 2, pp. 667-670, 1999.

Chapter 2

Bandwidth Improvement in a Tray Based Spatial Power Amplifier

2.1 Introduction and Motivation

In 1986, Mink outlined comprehensively the use of active spatial power combining (quasi-optical) techniques to generate high power from active solid-state devices [1]. Since then, variety of power combining schemes has been presented in the literature. Remarkable power levels have been achieved at various frequency bands from amplifiers based on grids and arrays [2]-[4]. These spatial power combiners have been shown to have many advantages: insensitivity to single point failures that could be catastrophic in other combining configurations [8]-[9], noise figure levels comparable to those of single devices, and high output power levels resulting from the low loss spatial power combining method. However, there are some disadvantages and limitations associated with spatial power-combining techniques. Some of these limitations have been addressed by researchers, such as the removal of excess heat produced by the active devices [5]-[6], substrate mode effects that can cause low output powers and poor radiation patterns [10], narrow bandwidth and others.

The work presented in this chapter focuses on improving the bandwidth of a tray-based spatial power amplifier, implementing a perpendicularly-fed antenna. This is accomplished by replacing the microstrip patch antennas of a previous design shown in Figure 1.4 [7]-[8], with dielectrically filled miniature horn antennas, while all other design

parameters in the amplifier remain the same. A drawing illustrating this concept is shown in Fig. 2.1. In the figure, the horn antennas on the left receive a signal radiated from the transmitting hard horn. The signal is then coupled to a microstrip line from the dielectric filled waveguide, which feeds the miniature horn antennas. Two dielectric filled waveguide sections reside between the microstrip line and the horn antenna. The section near the horn serves as an impedance transformer, while the other serves as a transition between the waveguide and the microstrip line. Each microstrip line then feeds a MMIC amplifier. After amplification, the signal is radiated through the output of the dielectrically filled miniature horn antenna in the same way that it was received. Finally, the signal radiated from the miniature horn antennas are collected by a receiving hard horn located at the right of the figure. The hard-horns provide a uniform amplitude and phase to the array of miniature dielectric filled horn antennas, improving the combining efficiency of the system [11]-[12]. It is worth mentioning that this horn array amplifier is very stable, due to the minimal interaction between the radiated fields and the active devices. Other advantages of this topology are the ability to use large device sizes, to cascade devices, and to individually bias them.

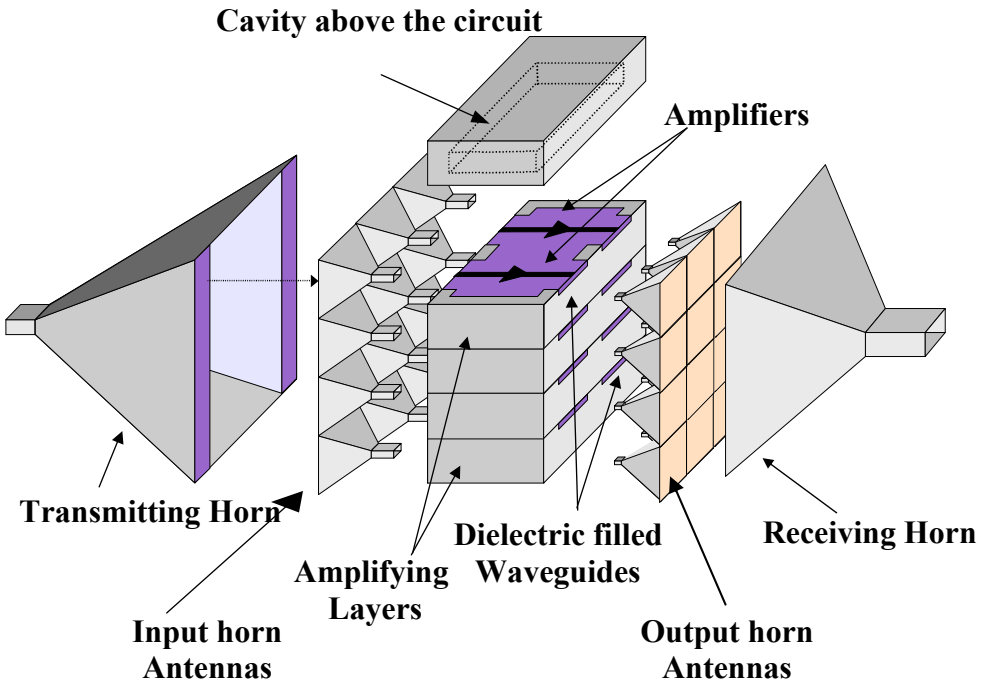

Figure 2.1: Tile based spatial power amplifier with dielectrically filled miniature horn antennas.

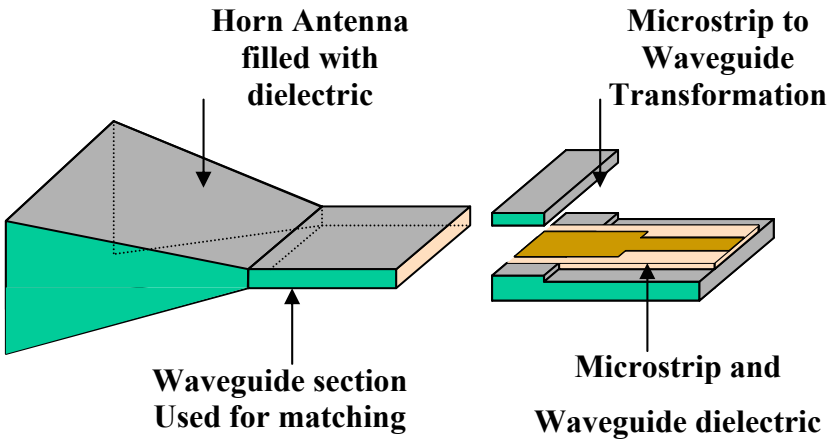

Figure 2.2: Design concept of the unit cell.

2.2 Design of the miniture horn array

The 5x5 spatial power amplifier presented in this paper takes advantage of the dielectrically filled miniature horn antennas as the receiving and radiating elements. These radiating elements were chosen for their potential to provide broad bandwidth. An illustration of the unit cell design is shown in Fig. 2.2. The signal received by the miniature dielectric filled horn will travel through a waveguide impedance transformer, and then through a second waveguide section, which provides a transition from the dielectric filled waveguide to the microstrip line. The waveguide impedance transformer uses the same dielectric as the miniature dielectric filled horn antenna. However, the second waveguide section utilizes the same dielectric as the microstrip line, by extending the microstrip line into this waveguide section.

The same design and hardware implemented in perpendicularly fed patch array amplifier [8] were used for this amplifier array. However, the microstrip patch antennas were replaced by miniature dielectric filled horn antennas. In both arrays, Filtronic (LMA411) MMIC amplifiers are used to provide the gain, with each having a small signal gain of 18 dB and gain flatness of ±0.8 dB between 8 and 14 GHz Figure 2.3 shows a Filtronic LMA 411 MMIC Amplifier. The output power at 1 dB compression is 17 dBm. Therefore for an ideally matched amplifier the maximum power is calculated to be 30.98dBm with is 1.25 watts.

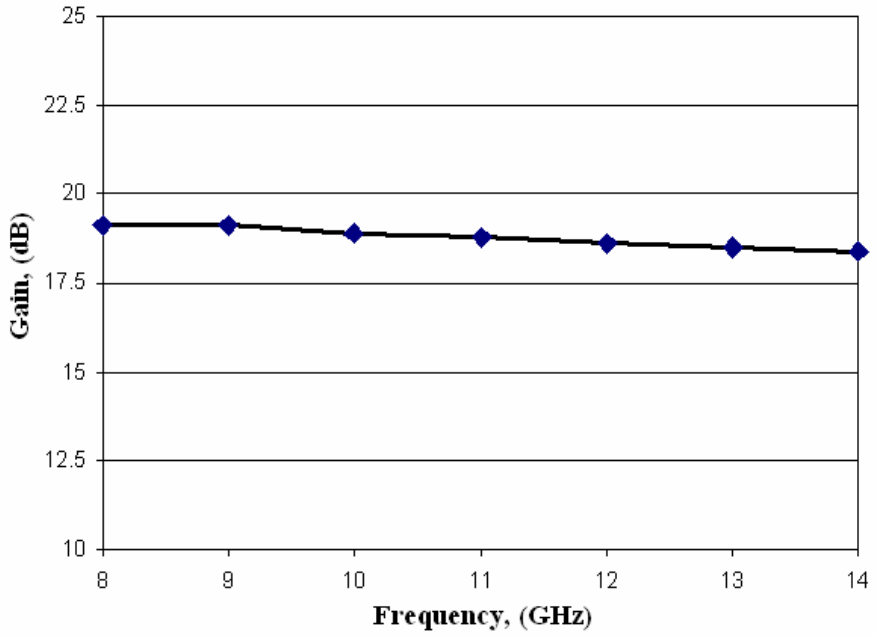

Figure 2.3: The gain a Filtronic LMA 411 MMIC Amplifier.

The microstrip lines were made from Roger's TMM3 substrate with a thickness of 0.38 mm and a dielectric constant of 3.27. The dielectrically filled waveguide has a height of 0.38 mm and is 11.43 mm wide. The impedance of the waveguide can be calculated using the following equation:

$$Z_o = \frac{377\frac{b}{a}\sqrt{\frac{\mu_r}{\varepsilon_r}}}{\sqrt{1-\left(\frac{f_c}{f}\right)^2}} \qquad 6.1$$

Where a and b are the width and the height of the waveguide respectively, f_c is the cutoff frequency and f is the operating frequency, μ_r and ε_r are the relative permeability and permittivity respectively. The waveguide dimension "a" is chosen so only one mode will propagate in this waveguide. Also "a" and "b" are designed so that the waveguide

impedance is the same as the microstrip line feeding the waveguide to microstrip transition..

The miniature dielectric filled horn was designed with the aid of Agilent High Frequency Structure Simulator (HFSS). The optimal horn design was chosen to give the largest bandwidth and directivity for the given aperture dimensions. The resulting length of the horn antenna (including the length of the waveguide impedance transformer) is 4.75 cm. The dimensions of the waveguide impedance transformer (which also serves as the throat of the horn) are 0.71 mm high, 14.73 mm wide and 4.88 mm long. It should be noted that this E-Plane horn is formed by flaring the walls of the rectangle waveguide in the direction of the E-field. Paraffin wax with a dielectric constant of 2.24 at 10 GHz [13] and dissipation factor of 0.0002 is used to fill the miniature horns and the waveguide impedance transformers.

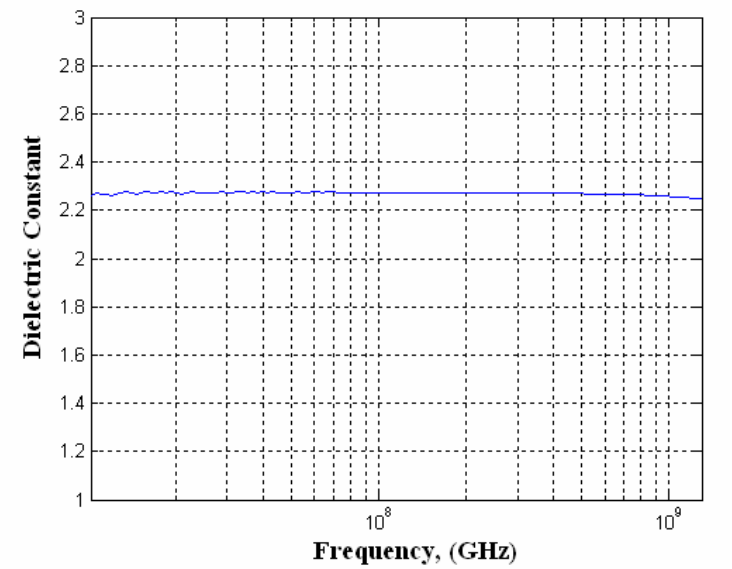

Figure 2.4: The measure dielectric constant of paraffin wax.

The dielectric constant of the paraffin was measured using Agilent E4991A RF impedance/material analyzer, and was found to be 2.28. Figure 2.4 shows the dielectric constant versus frequency (in log scale) up to 1 GHz for paraffin wax. It is worth mentioning that Polyethylene with a dielectric constant of 2.25 is a good alternative to paraffin.

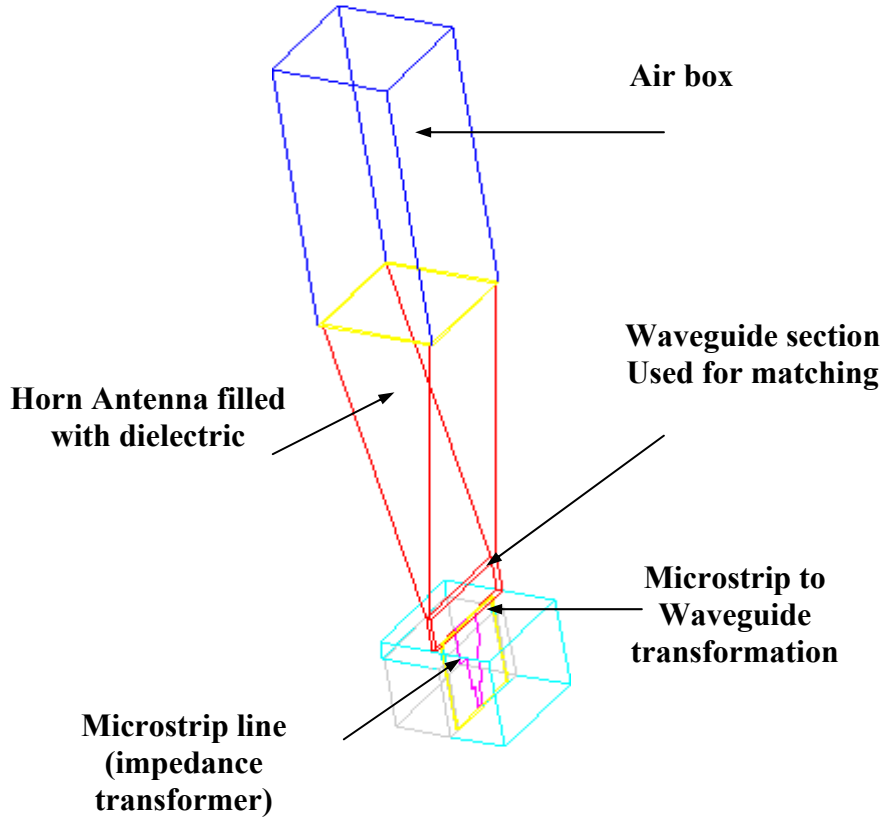

Figure 2.5: Simulated structure of the dielectrically filled miniature horn antenna using Agilent HFSS.

A single miniature dielectric filled horn antenna was designed, machined and tested to validate simulations. Figure 2.5 shows the simulated structure using Agilent HFSS. For the simulation of a single horn, radiation boundaries were assigned to five sides of the air box (no boundary condition is assigned to the aperture side). The simulated and measured

VSWR of this horn is plotted in Figure 2.6 and the E-plane radiation pattern at 9.22 GHz is shown in Figure. 2.7. A good agreement was obtained. The directivity of this horn was found to be 7 dB. The returns lose of an infinite array of horns can be found by carefully assigning boundary conditions to the sides of the air box [14].

2.3 Measured Results

Spatial power amplifier with 5x5 dielectric filled horn arrays was machined, assembled and measured. The small signal gain measurement was performed by placing the amplifier between two hard horns. The measured gain is shown in Figure. 2.8. The peak gain is 15.8 dB at 9.9 GHz, the 3-dB bandwidth is 1.32 GHz (13%) and the largest ripple is about 1.9 dB. The agreement is reasonable with simulation prediction.

It is to be noted that the previously published perpendicularly fed patch array quasi-optical amplifier has a gain of 16 dB and a 3-dB bandwidth of 280 MHz as shown in Figure 2.9. This bandwidth improvement was achieved by replacing the patch arrays with horn arrays keeping the rest of the parameters the same. Figure 2.10 shows the output power versus the input power for the horn array amplifier. This amplifier has 27 dBm (0.5 watts) output power under 1-dB compression. This amplifier has a power combining efficiency of 63%, based on half of the active array losses (2 dB). A photograph of the assembled tile based broadband spatial power amplifier is show in Figure 2.11.

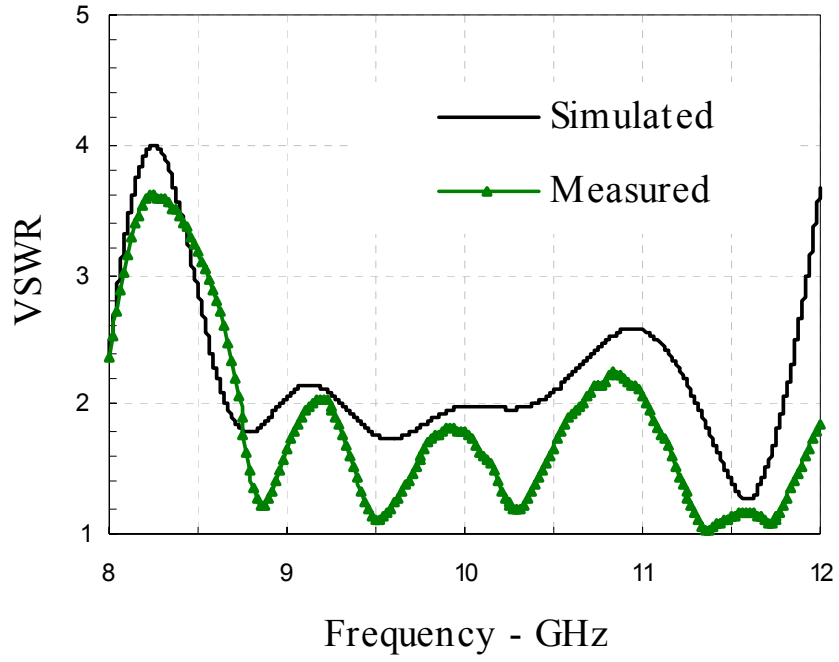

Figure 2.6: The simulated and measured voltage standing wave ratio of the paraffin filled single horn

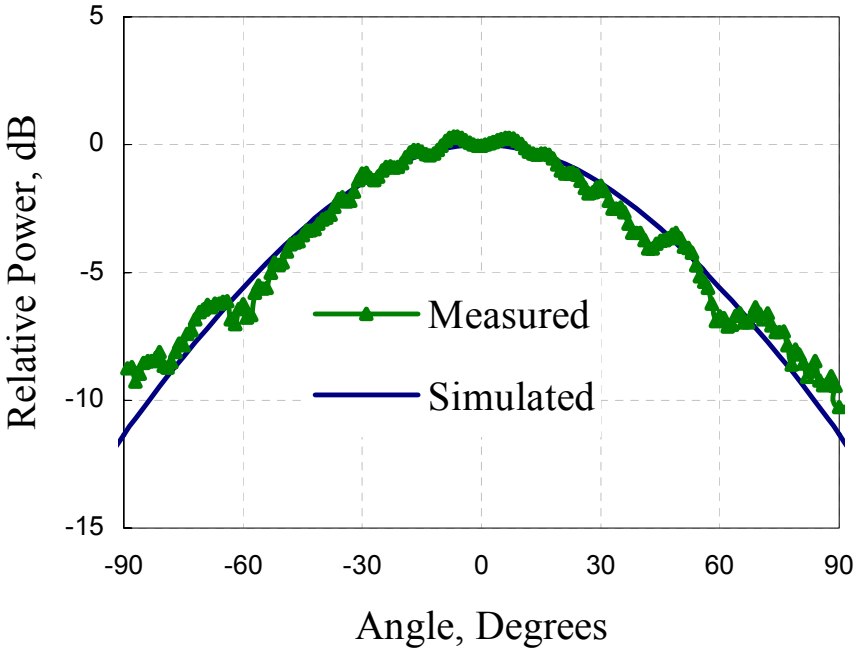

Figure 2.7: The E-plan radiation pattern of a single horn antenna filled with paraffin at 9.22 GHz.

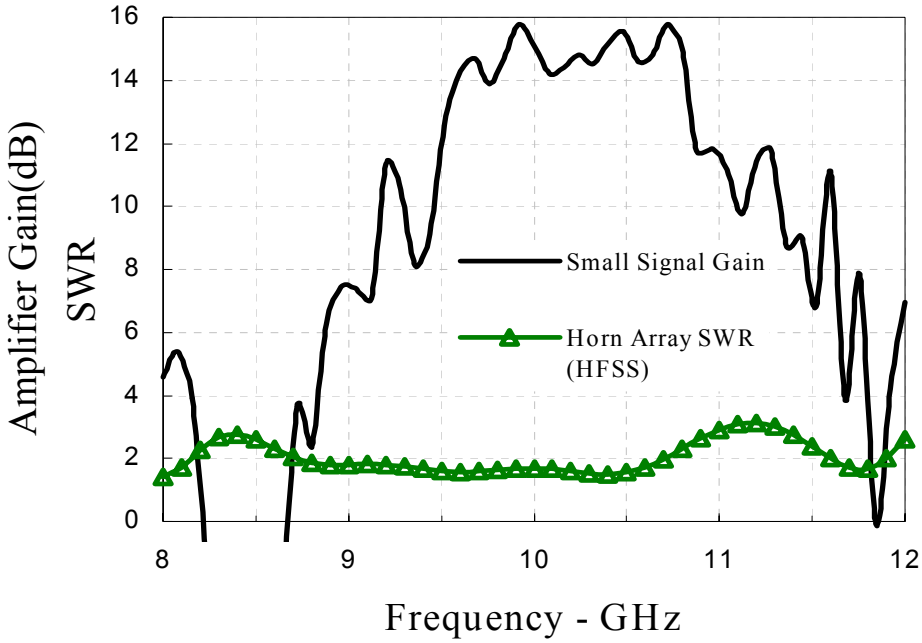

Figure 2.8: Small signal gain measurement of the spatial power amplifier with dielectrically filled miniature horn antennas.

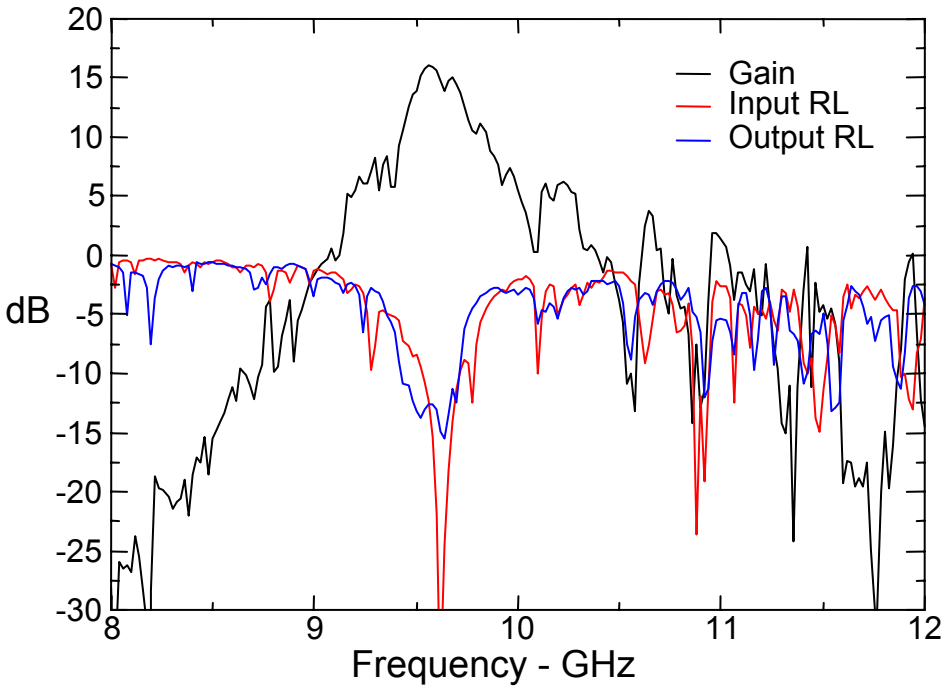

Figure 2.9: Small signal gain measurement of the perpendicularly-fed patch array spatial power amplifier.

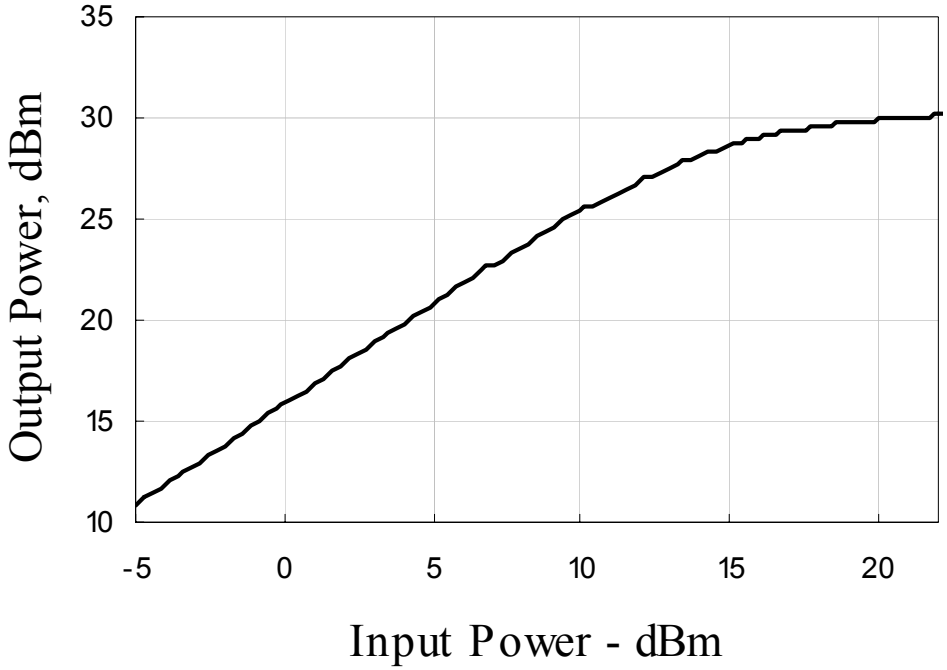

Figure 2.10. Power compression curve of the 25-element spatial power amplifier.

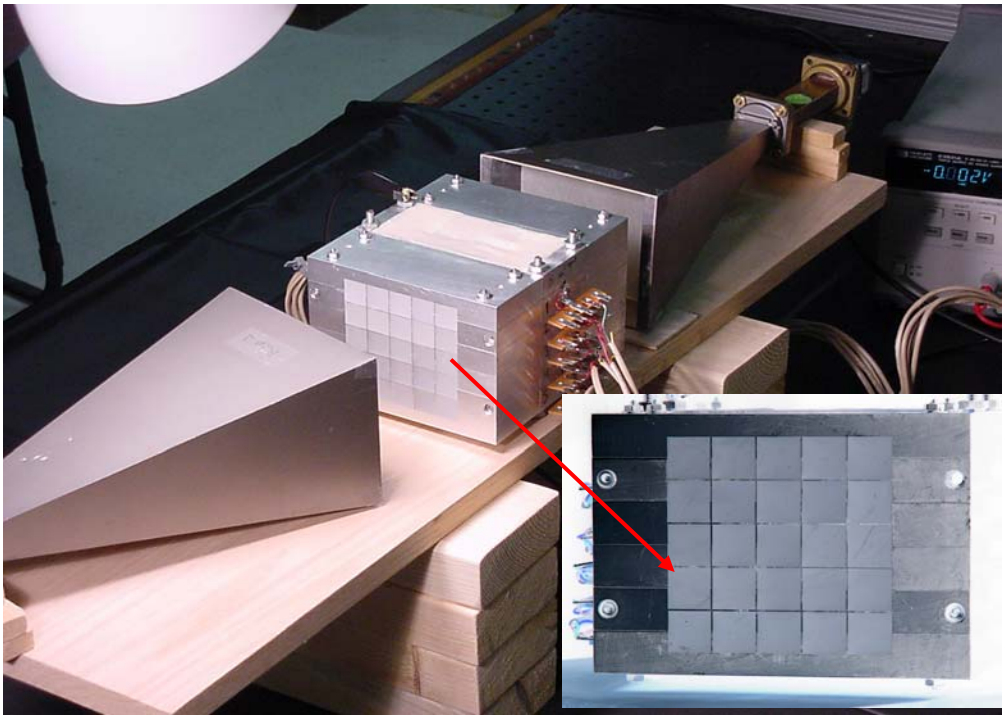

Figure 2.11: Photograph of the 5x5 spatial power amplifier that employs dielectrically filled miniature horn arrays.

2.4 Summary

In this chapter, a broadband tray based spatial power amplifier that employs dielectrically filled miniature horn arrays was presented. Bandwidth improvement was achieved by replacing the patch arrays of an earlier design with the broadband horn antennas. Dielectrically filled miniature horn arrays were employed for both the receiving and transmitting radiating elements of this 5x5 amplifier array. This 5x5 spatial power amplifier with miniature horn arrays has a peak gain of 15.8 dB at 9.9 GHz. The 3 dB bandwidth is 1.32 GHz, which is more than 4.5 times the 3 dB bandwidth of the perpendicularly fed patch array spatial power amplifier [8]. The output power was found to be 27 dBm at 1 dB compression. The measured gain and bandwidth agreed reasonably with simulations. This structure has the advantage of a minimal interaction between the radiated fields and the active devices. Additionally, increased stability is provided, while delivering a robust and reliable design. Gain, bandwidth and power measurements are consistent with simulation predictions.

2.5 References

[1] J. W. Mink, "Quasi-Optical Power Combining of Solid-State Millimeterwave Sources," *IEEE Trans. Microwave Theory and Tech.*, vol. MTT-34, no. 2, pp. 273-279, Feb 1986.

[1] D. Deckman, D. S. D. Jr., E. Sovero, and D. Rutledge, "A 5-watt, 37GHz monolithic grid amplifier, HBT grid amplifier," *IEEE MTT-S Int. Microwave Symp. Dig*., pp. 805-808, June 2000.

[2] N. -S. Cheng, P. Jia, D. B. Rensch, and R. A. York, "A 120-W X-band spatially combined solid-state amplifier," *IEEE Trans. Microwave Theory and Techs*, vol. 47, pp. 2557–2561, Dec. 1999.

[3] J. Sowers, D. Pritchard, A. White, W. Kong, and O. Tang, " A 36 W, V-band, solid state source," *IEEE MTT-S MO3C-1*, vol. 1, pp. 235-238, June 1999.

[4] A. Guyette, R. Swisher, F. Lécuyer, A. Al-Zayed, A. kom. S. L. lei, M. Oliviera, P. Li, M. P. De Lisio, *Sato, K.; Oki, A.; Gutierrez-Aitken, A.; Kagiwada, R.; Cowles, J*, "A 16-Element Reflection Grid Amplifier with Improved Heat Sinking" *Int.Microwave Symp Dig*., pp. 1839-1842, May, 2001.

[5] S. Ortiz, J. F. Hubert, L. Mirth, E. Schlecht and A. Mortazawi, "A 25 Watt and 50 Watt Ka-Band Quasi-Optical Amplifier," *IEEE Int.Microwave Symp Dig*., pp. 797-800, June, 2000.

[6] S. Ortiz and A. Mortazawi, "A perpendicularly-fed patch array for quasi-optical power combining," *IEEE MTT-S Int. Microwave Symp. Dig*., vol. 2, pp. 667-670, 1999.

[7] S. Ortiz, M. Ozkar, A. Yakovlev, M. Steer, and A. Mortazawi, "Fault Tolerance Analysis and measurement of a Spatial Power Amplifier," *IEEE AP-S Int. Symp*., vol. 3, pp. 1827-1830, May, 2000.

[8] R. A. York "Some Consideration for Optimal Efficiency and Low Noise in Large Power Combiners," *IEEE Trans. Microwave Theory Tech.*, vol. 49, Issue. 8, pp. 1477-1482, August. 2001.

[9] A. Al-Zayed, R. Swisher, F. Lécuyer, A. Guyette, Q. Sun and M. P. De Lisio, " Reduction of Substrate-Mode Effects in Power-Combining arrays," *IEEE Trans. Microwave Theory Tech.*, vol. 49, Issue. 6, part 1, pp. 1067-1072, June. 2001.

[10] M. A. Ali, S. Ortiz, T. Ivanov, and A. Mortazawi, "Analysis and measurement of hard horn feeds for the excitation of quasi-optical amplifiers," *IEEE Trans. Microwave Theory Tech.*, vol. 47, pp. 479-487, 1999.

[11] M. S. Gupta, "Power combining efficiency and its optimization," *Microwave, Antennas and Propagation, IEE Proceedings H,* vol. 139 Issue. 3, pp. 233-238, June 1992.

[12] D. M. Pozar, " Microwave Engineering", 2nd John Wiley& sons, 1998.

G. M. Turner, C. Christodoulou, "FDTD analysis of phased array antennas, " *IEEE Trans. Antenna and Propagation,* vol. 47, pp. 661-667, April. 1999.

Chapter 3

Numerical and Experimental Investigations of Losses in a Tray Based Spatial Power Amplifier

3.1 Introduction

Spatial power (quasi-optical) combining refers to combining the outputs of many active devices in free space. Several architectures have been developed for spatial power combining, integrating solid state devices to generate noteworthy power levels at a different range of frequency bands. Spatial combining also encompasses a broad rage of microwave circuits. These include amplifier, oscillators, beam controllers, and frequency converters. After much success in demonstrating the principles and concepts of spatial combining, researchers have directed there efforts on improving the structures and addressing important disadvantages and limitations associated with spatial power-combining techniques. These research investigations include increasing operating frequencies [1]-[2], optimizing for power [3], improving bandwidth [4], the removal of excess heat produced by the active devices [5]-[6], minimizing substrate mode effects [7]. The performance of a spatial amplifier array is affected by many factors. These factors are highly dependent on the type of amplifier array as well as the method of exciting the array. This chapter studies the performance of the Ka-band perpendicularly-fed patch array amplifier that is excited using hard-horn antenna shown in Figure 3.1.

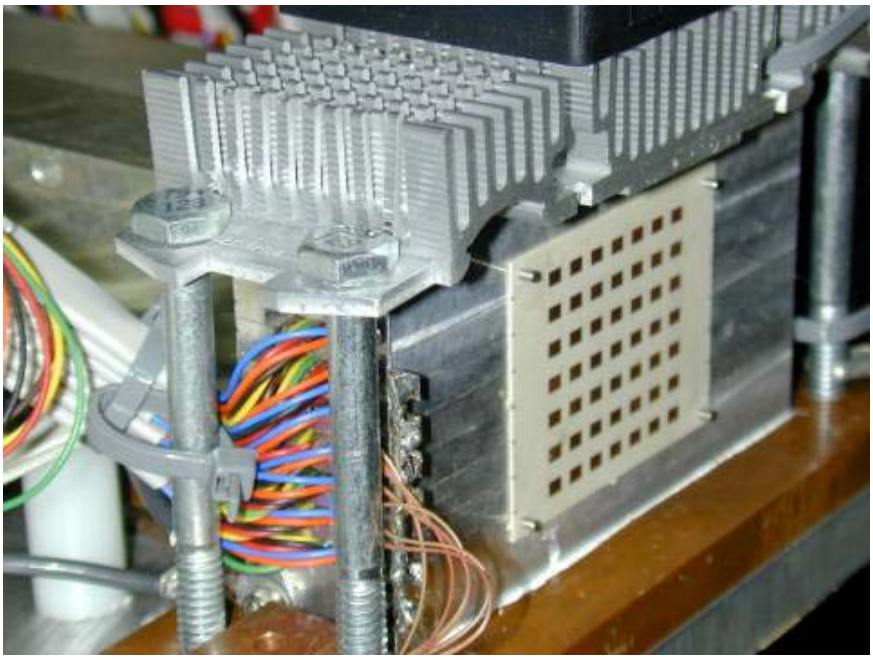

Figure 3.1: A photograph of the 7x7 amplifier array.

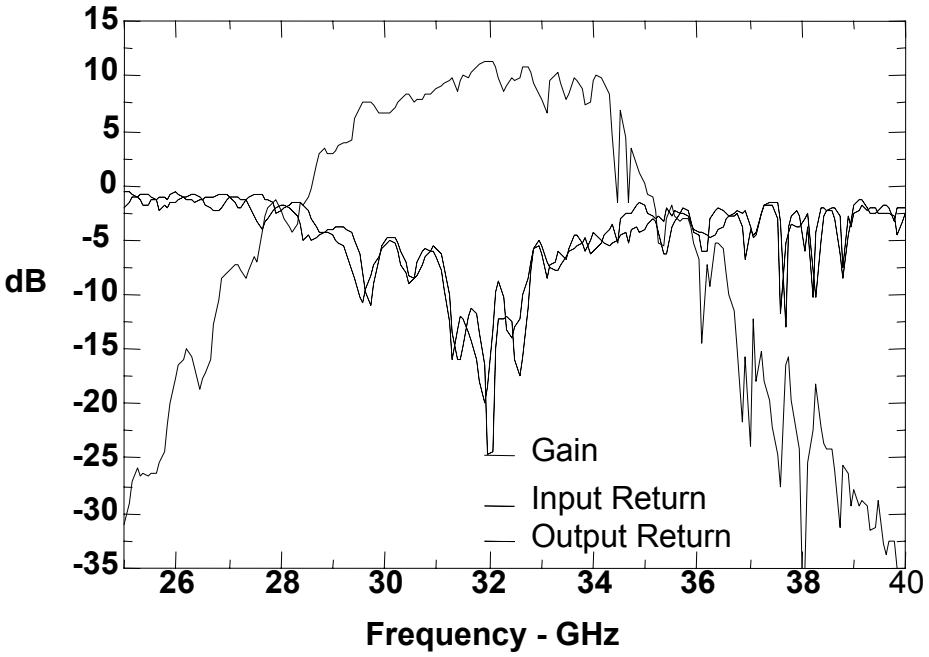

Figure 3.2: The small signal gain and return loss of the 49 element amplifier array.

This amplifier can produce 6 watts of power, however it exhibits high insertion loss (measured gain minus maximum gain) and therefore low power combining efficiency of 39%. Figure 3.2 show the gain small signal gain of this amplifier.

The patch antennas on the left of the diagram shown in Fig. 1.4 receive a signal radiated from the transmitting hard horn. Each of the microstrip patch antennas are coupled to slot aperture, which then feeds a dielectric filled waveguide. The dielectric filled waveguide is then coupled to a microstrip line, which then feeds the MMIC amplifier. After amplification, the signal is radiated through the transmitting patch antenna in the same way that it was received. Finally, the signal radiated from the patch antennas are collected by a receiving hard horn located at the right of the figure. Hard-horns and dielectric lenses are used to provide a uniform amplitude and phase to the array of patch antennas, improving the combining efficiency of the system [8]-[9].

To investigate the reasons for the low combining efficiency of this ka-bad amplifier several steps were undertaken. First: Experimental study of the unit cell spacing demonstrated a very good combining efficiency. Also a low insertion loss and a low ripple level were measured for an array with unit cell spacing of $0.5\lambda_o$, which is the case for active array. Second: FDTD simulations were performed on the structure. The results showed that the field distribution across the aperture is uniform, and that the active reflection coefficients of the 49 antennas are very similar again indicating field uniformity across the aperture. Third: Experiments were performed on the amplifier for the characterization of the unit cell amplitude and phase variation within the array. Measurements revealed that the amplitude and phase variations are very large. Fourth:

Analytical simulations explained that this large variations affecting this amplifier drastically, resulting in reduction of the combining efficiency and output power.

3.2 Study of the cell spacing

The Optimal array spacing can be determined either numerically or experimentally. The numerical formulation and simulation of large arrays within close proximity to hard-horn feeds is very time consuming. Therefore the optimal array spacing can be found experimentally. A simple passive spatial combiner was designed and fabricated. The array topology is the same as that used for the active amplifier. Figure 3.3 shows the passive insertion loss of an array of antennas between two hard- horn feeds. Each unit cell of the array consists of a receiving microstrip patch antenna, slot in the ground plane, and radiating microstrip patch antenna. The losses therefore are limited to the antenna efficiency and the hard-horn feed insertion loss. A Rogers TMM3 substrate with ε_r = 3.27, a dissipation factor of 0.002, and a thickness of 0.381 mm was used. The microstrip patch antenna has a length of 2.1 mm and a width of 3 mm, while the slot dimensions are 1.6 mm x 0.254 mm. Several experiments were performed as outlined in Figure 3.3. First the insertion loss of the two hard-horn feeds was measured by measuring the system without the antenna array. The loss at 31.6 GHz is approximately 1 dB [2]. The loss of the antenna array, including the hard-horn feeds, was then measured. Each antenna array had different array spacing and a different number of cells, since a maximum number of cells were placed within the horn aperture. Figure 3.4 shows the insertion loss versus frequency for several arrays with different spacing values.

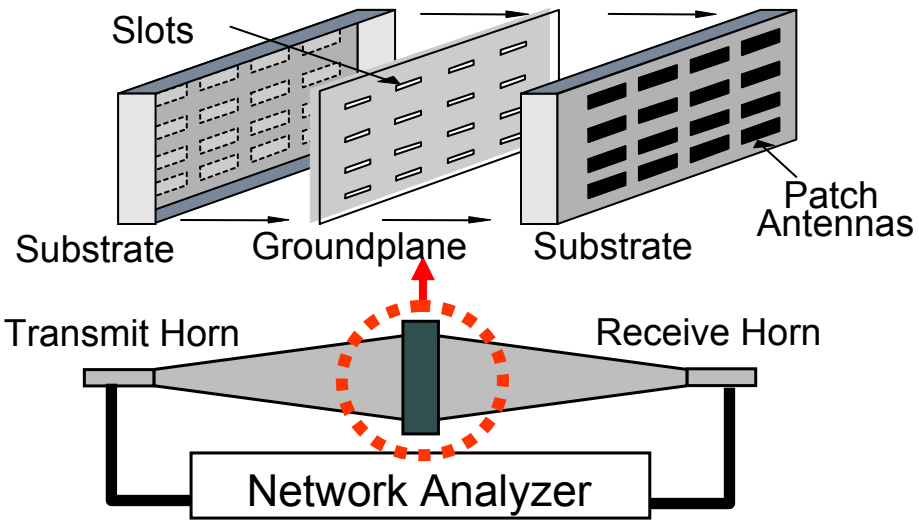

Figure 3.3: The setup for measuring the loss of the spatial power combining array and the array topology.

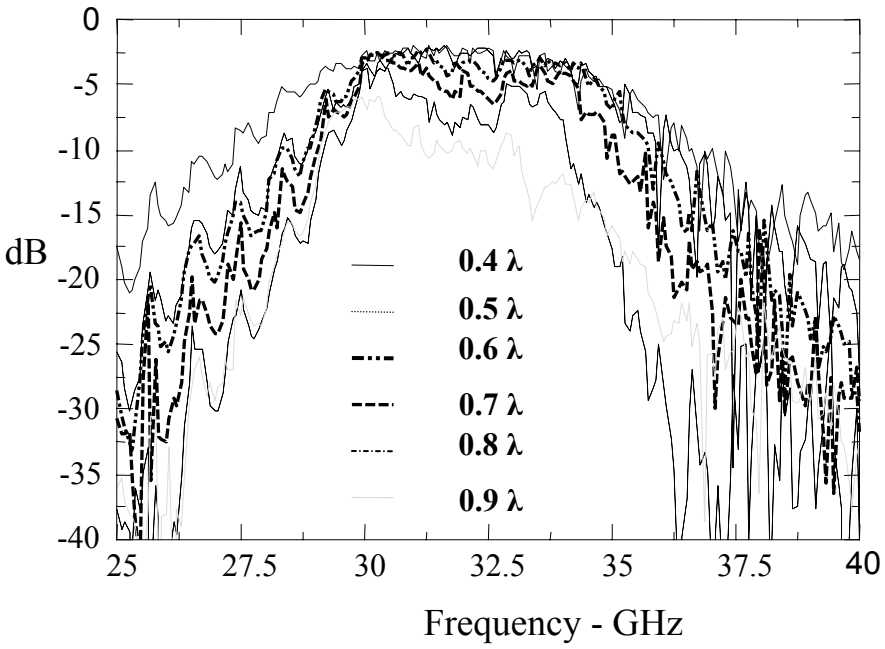

Figure 3.4: The insertion loss of several array spacing values versus frequency.

The loss with a cell spacing of $0.5\lambda_o$ and smaller is less than 2 dB at 31.6 GHz. From this point, the losses increase significantly with an increase in unit cell spacing. It is to be noted that the ripple level is reasonably low. The amplifier under investigation [2] was designed with a unit cell spacing of $0.5\lambda_o$. Therefore the total loss of this amplifier should be equal to this 2 dB plus losses due to the microstrip transmission lines (0.59 dB), the two dielectric waveguides (0.28 dB) and any mismatches. This 7x7 spatial amplifier uses 49 *Triquint TGA1073A*™ PHEMT MMIC amplifiers which have 19 dB of gain and an output power of 25 dBm under 1-dB compression. Assuming that there are no mismatches in this spatial amplifier system, the expected output power is calculated to be 11.13 watts, and the power combining efficiency is 72% based on half of the active array losses (1.435 dB). Also the gain will have low ripple level.

3.3 FDTD Simulations

The purpose of these passive simulations was to understand the causes of losses in the 49-element spatial power divider/combiner. The active reflection coefficients were obtained through the simultaneous excitation of all elements with a sinusoidally modulated Gaussian pulse while terminating the oversized hard waveguide. As can be seen in Figure 3.5 that the resonance frequencies for all of the elements are centered around 32.9GHz. This indicates an even division of power among the elements around this frequency. This also indicates that the active devices would roughly see the same load impedance. In addition, time domain field plots were obtained across the aperture of the hard walled waveguide when all of the passive elements were excited. Uniform field distribution across the aperture in Figure 3.6 means that most of the energy is being coupled to the

LSE_{10} mode of the hard horn. Therefore, the passive simulations tend to support the experimental observations that the losses due to power combining structure are quite low.

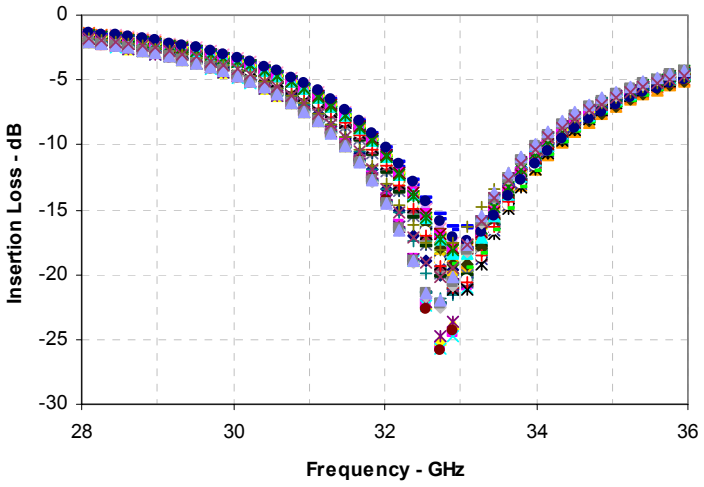

Figure 3.5: The active reflection coefficients of the 49 cells Ka-band amplifier that is under investigation.

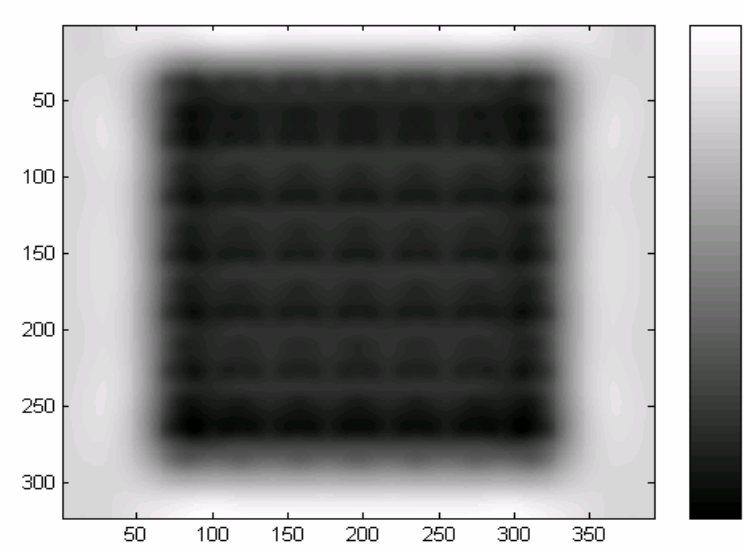

Figure 3.6: Normalized field plots at a distance of 0.2λ from the array surface into the overmoded hard walled waveguide at time step = 3220.

3.4 Effect of unit cell amplitude and phase variation

There are many factors, which can cause variations in the unit cell performance, such as variations in transmission line lengths and widths, bond wire lengths and loop heights, and active device performance. A statistical analysis can be obtained by cascading the various components, within a none-linear simulator such as Agilent – Advanced Design System (ADS) ^{TM}. These components are a non-linear device model of an amplifier cascaded with an ideal attenuator and phase shifter. The attenuator and phase shifter are then adjusted to represent the change in amplitude and phase from one cell to another. The phase and amplitude variations of the unit cell are modeled using Gaussian distribution with mean *m* and standard deviation σ. Each cell is then chosen randomly using this distribution. It will be assumed that the average phase and amplitude variations are equal to zero.

Figure 3.7 illustrates the insertion loss versus the standard deviation of the phase for two different values of the amplitude's σ. As expected, the loss increases as the probability increases for a large phase variation in the unit cells. This is also the case for a larger variation in the insertion loss or gain of the unit cell. A second test case is shown in Figure 3.8, where the ideal hard-horn is compared with the measured hard-horn for an amplitude σ of 0.5 dB and a phase σ of 20°. Under these conditions, the loss of the array is significantly larger in the actual hard-horn data than with the ideal field distribution. This is most likely due to an accumulation of phase and amplitude errors as is apparent when observing the accelerated roll-off in the insertion loss of Fig. 3.7. The results provided some insight into the effect of the device variations on the gain and combining efficiency of the system.

The unit cells were measured for both the passive and active array (amplifier under investigation [2]), using waveguide technique at the operating frequency of 31.9 GHz. The waveguide probes are placed nearly in contact with the antenna substrate. For the passive array, a variation of ± 1.1 dB in magnitude and ± 30° in phase was observed over the 49 unit cells. As for the active amplifier the magnitude varied by ± 1.8 dB and the phase by ± 40°. It is to be mentioned that only the amplifier that was probed is turned on, and the other 48 amplifier were turned off. This much of unit cell variations are without a doubt affecting this ka-band amplifier in many ways such as low gain amplitude as well as high ripple level. Also the power combing efficiency suffered. Therefore one can set a tolerable system performance (gain, ripple lever and power combining efficiency) and find how much unit cell variations are allowed.

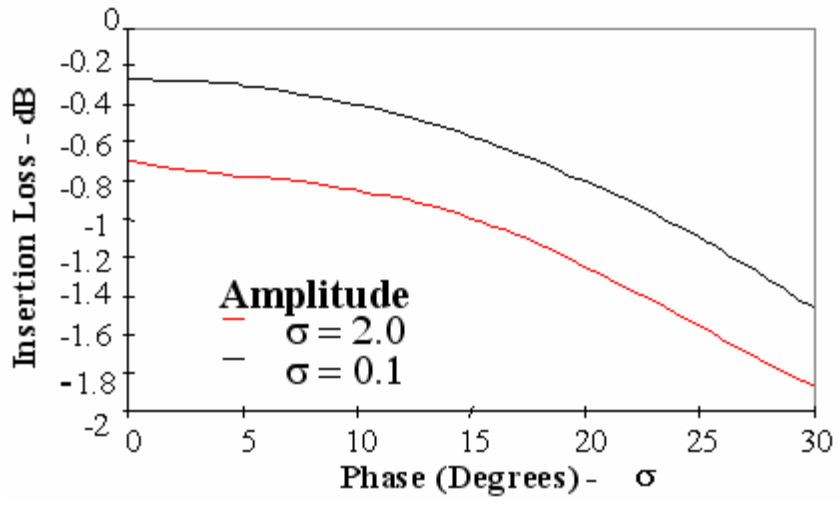

Figure 3.7: The simulated insertion loss of the array fed by an ideal hard-horn versus the standard deviation of the phase.

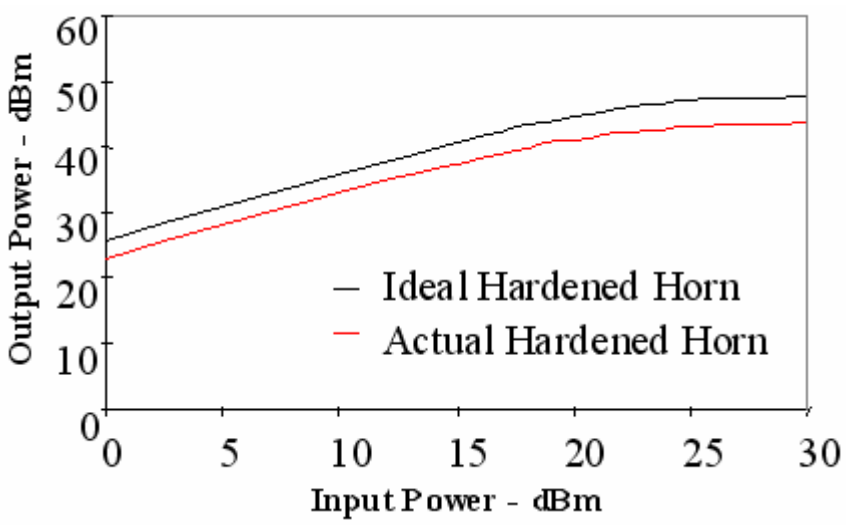

Figure 3.8: The simulated power compression of the array for a standard deviation in phase of 20° and 0.5 dB in gain.

3.5 Thermal analysis

Thermal measurements were carried out for this perpendicularly fed amplifier array, a thermocouple was placed beneath the center of each tray, and the temperature was measured and monitored for each tray. The temperature of the bottom tray was not monitored, and it was expected to be low as this tray was sitting on large and thick aluminum. Six thermocouples were needed to monitor the remaining six trays, the amplifier array was then turned on and the temperatures were measured. Figure 3.9 shows the temperature profile versus time for the 7x7 amplifier array. The temperature of the center trays heated up more quickly than the top or the bottom trays. The amplifier array temperature reached steady state after approximately 45 minutes. This amplifier array can run indefinitely with tray temperature not exceeding 38 degrees. The amplifier was then

turned off and temperature dropped back to the ambient room temperature. It is clear that the perpendicularly fed tray based structure have a very good heat removal performance.

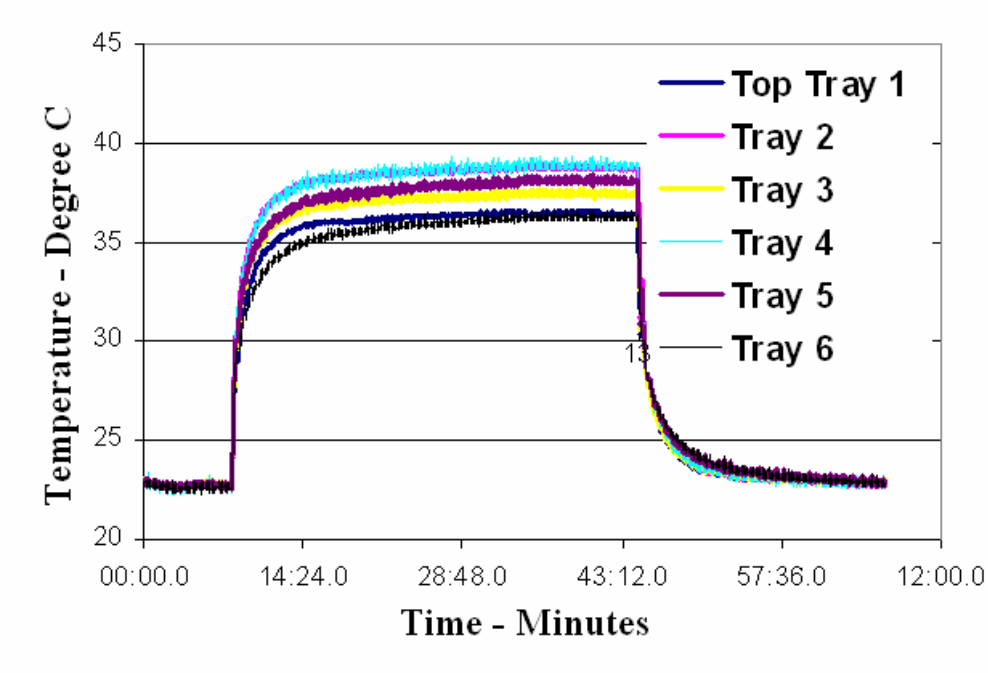

Figure 3.9: The measured temperature versus time for the Ka-band 7x7 amplifier array.

3.5 Summary

In this chapter the performance of a 7x7 Ka-band spatial power combining amplifier array fed by hard-horns was analyzed and the cause of the low combining efficiency was determined. Various design parameters were studied. Unit cell spacing study indicated that it is important that this spatial amplifier array fed by hard-horns have a unit cell spacing below 0.5λ, if losses are to be kept to a minimum. Based on this array measurement power and for an ideally matched system this amplifier should produce as much as 11.13 watts of power, with a power combining efficiency of 72%. Large unit cell

variations were measured for both the active and passive structures. FDTD simulated was performed on the array structure and found that this array has a uniform field distribution across its aperture and therefore should have good combining efficiency. Analytical study showed that this large amplitude and phase cell variations to the cause of this low combining efficiency. For a tolerable system performance, set in terms of gain, ripple lever and power combining efficiency, the maximum unit cell variations allowed can be found. Thermal analysis was performed on this system; this amplifier array can run indefinitely with tray temperature not exceeding 38 degrees.

3.6 References

[1] S. Ortiz and A. Mortazawi, "A perpendicularly-fed patch array for quasi-optical power combining," *IEEE MTT-S Int. Microwave Symp. Dig*., vol. 2, pp. 667-670, 1999.

[2] S. Ortiz, A. Al-Zayed and A. Mortazawi, "A Ka-band Perpendicularly-fed patch array for Spatial power combining," *IEEE MTT-S Int. Microwave Symp. Dig*., vol. 3, pp. 1519-1522, June 2002.

[3] W. A. Shiroma, and Z. B. Popović. "Feedback optimization of grid oscillators," *IEEE MTT-S Int. Microwave Symp. Dig.,* pp. 1053-1056, June 1997.

[4] A. Al-Zayed, S. Ortiz and A. Mortazawi, " Bandwidth Improvement in a Tile Based Spatial Power Amplifier," *IEEE MTT-S Int. Microwave Symp. Dig*., vol. 2, pp. 1313-1316, June 2002.

[5] A. Guyette, R. Swisher, F. Lécuyer, A. Al-Zayed, A. kom. S. L. lei, M. Oliviera, P. Li, M. P. De Lisio, *Sato, K.; Oki, A.; Gutierrez-Aitken, A.; Kagiwada, R.; Cowles, J*, "A 16-Element Reflection Grid Amplifier with Improved Heat Sinking" *Int.Microwave Symp Dig*., pp. 1839-1842, May, 2001.

[6] S. Ortiz, J. F. Hubert, L. Mirth, E. Schlecht and A. Mortazawi, "A 25 Watt and 50 Watt Ka-Band Quasi-Optical Amplifier," *IEEE Int.Microwave Symp Dig*., pp. 797-800, June, 2000.

[7] A. Al-Zayed, R. Swisher, F. Lécuyer, A. Guyette, Q. Sun and M. P. De Lisio, " Reduction of Substrate-Mode Effects in Power-Combining arrays," *IEEE Trans. Microwave Theory Tech.*, vol. 49, Issue. 6, part 1, pp. 1067-1072, June. 2001.

[8] M. A. Ali, S. Ortiz, T. Ivanov, and A. Mortazawi, "Analysis and measurement of hard horn feeds for the excitation of quasi-optical amplifiers," *IEEE Trans. Microwave Theory Tech.*, vol. 47, pp. 479-487, 1999.

[9] M. S. Gupta, "Power combining efficiency and its optimization," *Microwave, Antennas and Propagation, IEE Proceedings H,* vol. 139 Issue. 3, pp. 233-238, June 1992.

Chapter 4

Compact millimeter-wave tray based dual polarized multibeam active array

4. 1 Introduction and Motivation

Recently there has been great interest in the development of spatial power combining amplifiers for millimeter-wave power generation. Quasi-optical power combining technologies have made it possible to develop compact, lightweight, high power and reliable millimeter wave systems.

A complete structure of a spatial power combiner requires electronic beam controllers for beam steering. There are many military and commercial applications that require a multibeam antenna (antenna aperture with scanning capabilities); examples of the military application include missile seeking and guiding systems, target acquisition, situation awareness, combat identification, and millimeter wave imaging cameras which allow to see through dust and fog. There is a list of commercial applications such as satellite communications, surveillance systems, and automotive radar sensors for collision avoidance, blind-spot indicator and parking aid. Also radars for aircraft-guiding and landing systems [1], and road-pricing systems for charging road tolls [2].

Electronic scanning systems have many advantages over the traditional mechanical systems. They are more reliable, have higher scanning speed and have the ability to reposition the beam rapidly within the scanning range or coverage area of the antenna

aperture without physically moving the antenna. Electronic scanning systems can also track or image more than one target simultaneously.

The most popular electronic scanning system is shown in Figure 4.1. This simple phased antenna array uses a phase shifter before each antenna element to control and provide the constant phase difference between successive antenna elements needed for beam steering. A feed network is required to split the signal to these radiating elements. This method is useful and reliable. However, for a large number of antenna elements, this approach turns out to be expensive as the cost of the phase shifters become significant. Additionally, the bias lines needed to control each phase shifter make this approach less attractive. Also, losses associated with the feeding network, often comprise of power splitters and/or couplers, increase significantly with the number of array elements increases.

In many radar and communication applications, it is required to generate multiple beams from a single antenna aperture. In literature the most common techniques employ linear antenna arrays fed by Maxon (Blass), Butler matrix networks [3] or by microwave lenses. Both steering matrices can be realized using either waveguide or microstrip technology. However, there are disadvantages associated with both Maxon and butler feeding networks as they both require a large number of directional couplers, power dividers and crossovers. Therefore, the overall design becomes extremely complicated for a large number of ports. Another disadvantage is that the beam direction is inherently frequency dependant.

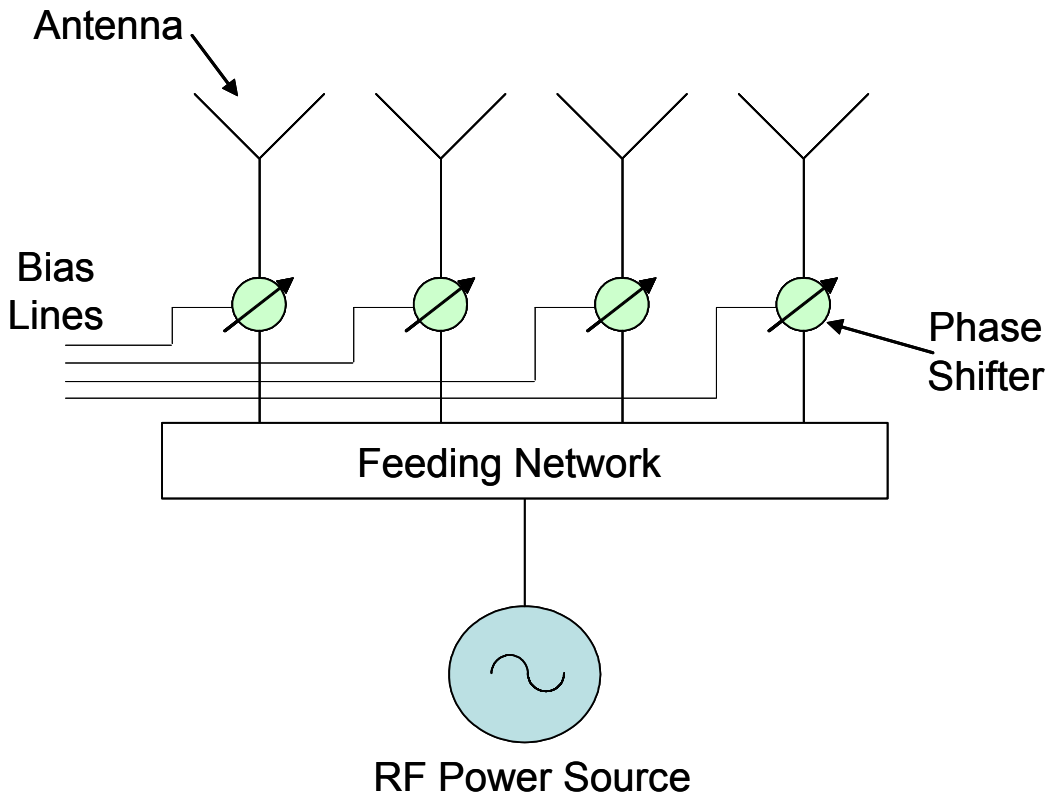

Figure 4.1: Phased array approach of an electronically scanned transmitter.

Microwave lenses provide an alternative way of feeding an array of antennas. The Rotman lens is the most popular among various microwave lens approaches, since the Rotman lens has three focal points while other lenses have two focal points. Therefore, the phase aberration or phase error across the aperture is less when the lens is fed from an intermediate input port (a point between two focal points/inputs). True time delay phase shifters, such as the Rotman lens, have a constant phase slope versus frequency, or a constant group delay. True time delay phase shifters are important as they present a constant time delay to each frequency component of a signal and therefore preserve the fidelity of narrow pulse (broadband) transmission. On the other hand, non-true time delay

phase shifters cause the beam to scan as the frequency of the transmitted signal varies, which is undesirable. In this chapter, the Rotman lens is chosen to be the phase shifting element for the dual polarized phased array, more detail is given in the coming sections.

It is worth mentioning that few phase shifterless beam scanning techniques [4]-[7] have been reported. For example, recently Liao and York [5] demonstrated a new technique for beam steering. They eliminated the need for phase shifter by using antenna-coupled oscillators. By choosing the correct frequencies of the end oscillators in the chain, the main beam could be continuously steered over 30º. Also, Tombak and Mortazawi [6] demonstrated a novel phased array based on the extended resonance power dividing method. This method eliminates the need for separate power splitter and phase shifters making this system less complicated to design and cheaper to mass produce. They measured a scan range of 20º. These ideas are interesting; however, more study is needed on the tradeoffs, limitations and two dimensional scanning.

The challenge is to develop a compact, reliable and low cost millimeter-wave radar system with futures such as dual polarization, multibeam capabilities and high power. At millimeter-waves a single solid state device can not produce enough output power; therefore, this system should have the potential of incorporating many active devices or amplifiers to achieve high power levels.

Two integration methodologies of dual polarized antennas, phase shifting components, feeding networks and active devices are investigated in this chapter. Both of these approaches are based on the microstrip to reduced height waveguide transition, and modifying the perpendicularly-fed patch array spatial power amplifier (which was

discussed in the pervious chapters and shown in Figure 1.4). This two dimensional spatial combiner will be modified to achieve both dual polarizatins and beam steering.

The first approach is to redesign the perpendicularly fed spatial power amplifier by adding an extra feed using a reduced height waveguide orthogonal to the exiting one. These two dielectrically filled waveguides will be used as apertures to excite the dual polarized patch vertically and horizontally. Phase shifters will be integrated into the trays in order to demonstrate beam steering in the azimuth and elevation for each polarization.

In the second approach, a microstrip Rotman lens will be incorporated in the tray based spatial power combiner. The lens and will be used as the phase shifting element and a power divider. This approach reduces the cost and circuit complexity of the system, the scan angles that can be obtained from these lenses are discrete.

In this technique, the signals at the output ports of these microstrip Rotman lenses will couple to the dielectrically filled waveguides though the microstrip to dielectrically filled waveguide transitions. Each reduced height dielectrically filled waveguide is used as an aperture to excite or couple the signal to the microstrip transmission line that feeds the patch antenna. By switching the input signal of the Rotman lens from one input port to another, beam steering can be realized in one polarization.

To obtain dual polarization, a second Rotman lens is introduced to the bottom of the metal tray. The second lens is placed half way between the top and bottom trays and in between the unit cells of the upper tray. The signals at the output of this Rotman lens will couple to the patch antenna in the same manner as in the top lens but to a different polarization. Therefore, beam steering can be realized in the azimuth plane for two polarizations. By

adding one phase shifter at the input of each Rotman lens the beam can be steered in the elevation plane for both polarizations. It is to be noted that one polarization can be used for transmission while the other can be used for reception.

More detailed explanation of the two integration methodologies are given in the next sections.

4.2 Dual polarized perpendicularly-fed patch phased array spatial combiner

As mentioned in the previous chapters, at millimeter wavelengths, spatial power combiners offer many advantages. Quasi-optical or spatial power combiners are compact, reliable, high power, lightweight and economical. Many techniques for obtaining dual polarizations [8]-[14], and beam steering [15]-[18] were demonstrated recently. Alexopoulos demonstrated electronic beam scanning using active surfaces [19]. The RADANT project comprises a three dimensional array of varactor diodes for beam steering [20]. Lam demonstrated a monolithic design of a periodic grid loaded with diodes for scanning the beam electronically [21]. The purpose of this project is to demonstrate a compact millimeter wave dual polarized multifunction array system.

Spatial or quasi-optical power combining techniques can be divided into two main categories, tile based and tray based. A Tray based structure, such as the perpendicularly fed patch array, was chosen for the design of this dual polarized phased array. This structure has many advantages. This topology offers the designer enough room to place

amplifiers and biasing networks in the space between the input and output antennas. Also, one can use large device sizes, cascade devices and individually bias them. Therefore, solid state phase shifters can be easily integrated into the design to demonstrate electronic beam steering. The most notable feature in the perpendicularly fed array is the reduced unit cell size, which is difficult to achieve in tile based arrays.

In the tile structures and grids [lam] the active devices, such as the amplifiers and the phase shifters as well as the radiating elements, share the same plane and therefore the unit cell becomes congested, which leads to a unit cell size larger than half of a free space wavelength needed to ensure a radiation patterns without grating lobes. In addition, these active devices interfere with the radiating element making the electromagnetic simulation difficult and less accurate. The perpendicularly fed topology utilizes a microstrip to dielectrically filled waveguide transition or feed. This feed places the devices and antennas on separate planes, isolating the radiating elements from the active devices. Another advantage of using the perpendicularly fed tray based structure rather than the tile based structure is that it is superior in the removal of heat. The thick ground planes formed from stacking the trays provide a good heat sink.

4.3 Dual polarized perpendicularly-fed patch phased array spatial combiner with phase shifters

The perpendicularly fed spatial power combiner that was presented in the pervious chapters is modified to demonstrate a perpendicularly fed dual polarized array with beam steering capability. As shown in Figure 4.2, another dielectrically filled waveguide was introduced into the structure and placed orthogonally with respect to the original dielectrically filled waveguide. Each waveguide aperture will be used to excite the square patch antenna in one polarization, therefore dual polarization can be realized. In other words, the two waveguides are orthogonal to each other and feeding the same square patch antenna with two different polarizations. Both vertical and horizontal polarization can be beam steered in the azimuth and elevation planes.

A conceptual view of the antenna implementation is shown in Figure 4.3. In this figure, a signal input into the microstrip line is coupled to the dielectrically filled waveguide through the microstrip to waveguide transition. The signal is then radiated by the aperture coupled patch antenna placed on the dielectric filled waveguide. This description is applied for both polarizations. A more detailed drawing of the patch antenna can be seen in Figure 4.4.

The complete system that consists of two input microstrip lines, reduced height waveguides and aperture coupled patch antennas can be simulated using Agilent HFSS^{TM}. To demonstrate the concept, the system was designed and simulated at X-band. The waveguide height was chosen to be the same as the slot, while its width was chosen to have a cutoff frequency below the design frequency to ensure the propagation of the

dominant mode only. The dielectric constant of these waveguides is 9.2 which is Rogers TMM10. This relatively high dielectric constant was needed to shrink the width of these waveguides and to fit them within the patch antenna.

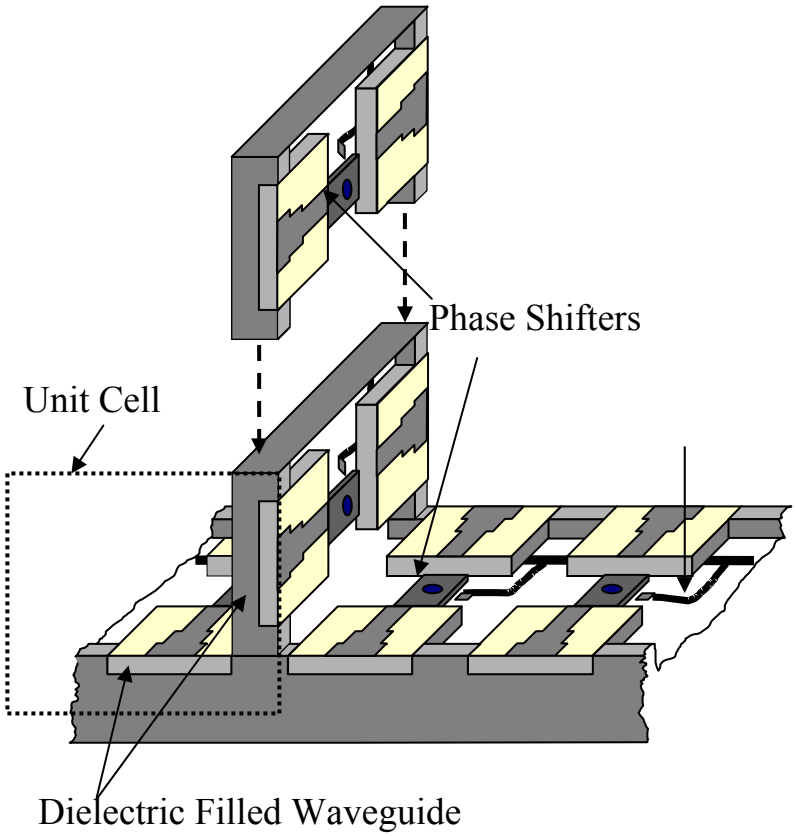

Figure 4.2: Drawing illustrating several unit cells with phase shifters on the trays that are stacked to from the array.

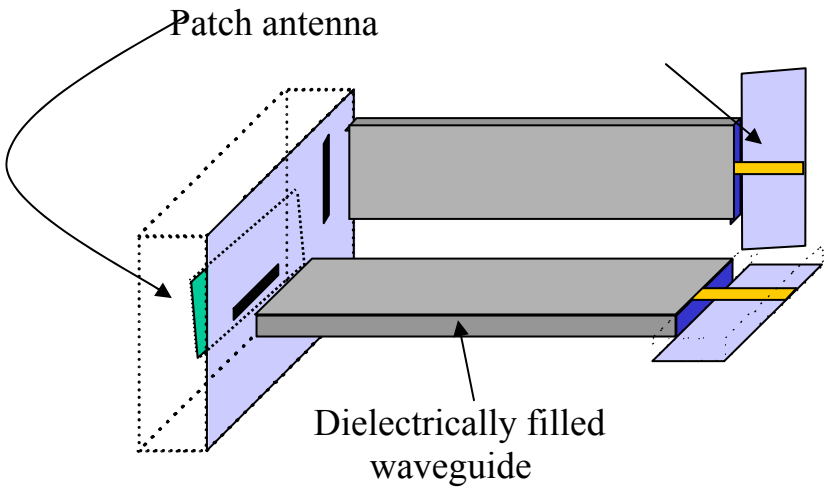

Figure 4.3: Dual polarized aperture coupled patch antenna fed by dielectric waveguides.

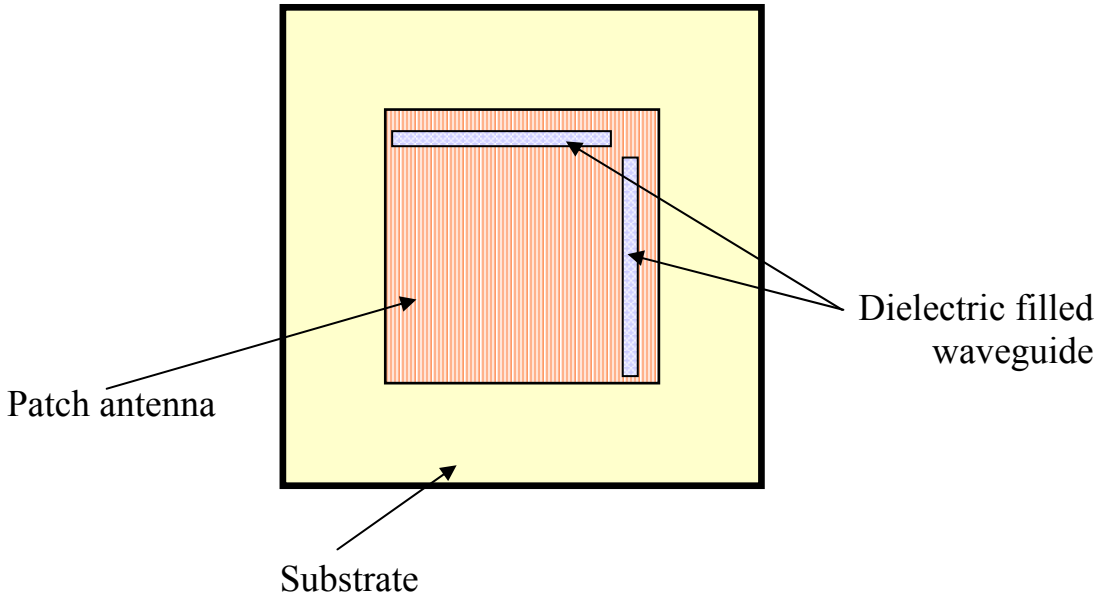

Figure 4.4: Details of the dual polarized patch antenna fed by two dielectric filled waveguide.

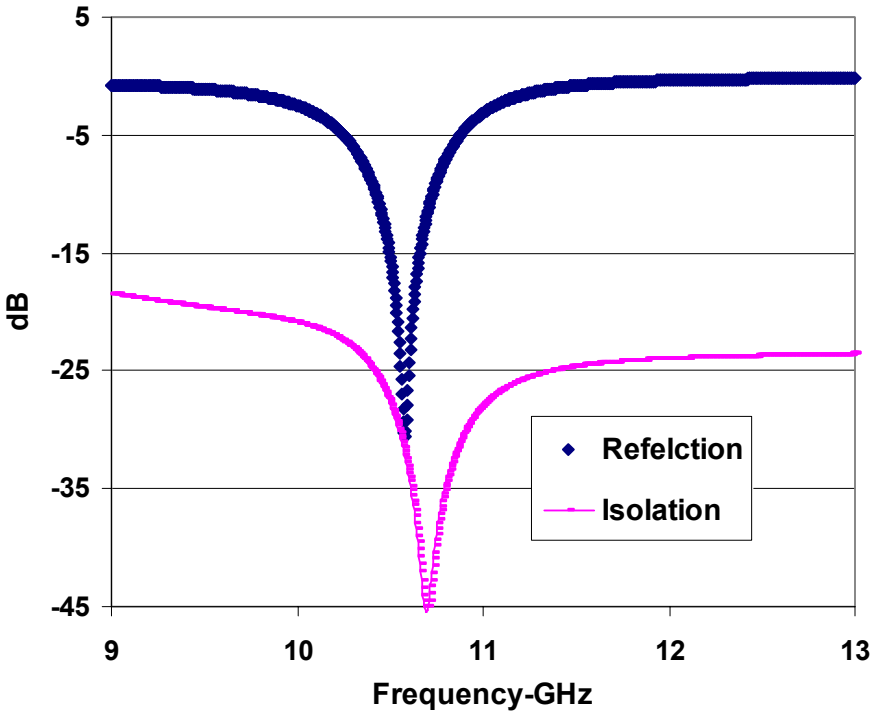

Figure 4.5: Simulated return loss and isolation of the perpendicularly fed dual polarized antenna.

The design was simulated and optimized with the results shown in Figure 4.5. The center frequency is 10.5 GHz. A 10 dB return loss over 330 MHz was achieved and the isolation between the ports is better than -20 dB. It is to be noted that this topology can be used as a transceiver since one polarization can be used for transmission while the other can be used for reception. It should be mentioned that this structure has several disadvantages. For example it is possible but difficult to machine this structure simply because of the orthogonal waveguides. Accessing microstrip lines and realizing the biasing networks is also challenging. The second approach, which is explained in the next section, appears to be a better candidate to realize a compact millimeter wave dual polarized multibeam active array.

4.4 Dual polarized perpendicularly-fed patch array spatial combiner with Rotman lenses

In what has become a classic paper, Rotman demonstrated an elegant microwave lens that can be used to divide the power among many ports. This microwave lens is capable of beam steering and scanning in different directions. Figure 4.6 shows a Rotman lens implemented in microstrip technology. The Rotman lens in this figure for example has three input ports and five output ports. Switches are employed at the input ports to control the signal flow to the lens. Only one of the three input ports will be turn on and will deliver power to the lens, the other two will be turned off. The input signal is equally divided among the five output ports with a progressive phase shift. The phase difference between the five output ports depends on the location of input port, therefore switching between the three inputs will result in three different sets of linear phase differences or phase progression across the aperture. This will scan the radiation pattern and beam steering can be achieved. It can be noted that this approach will produce discrete beam steering; the larger the number of input ports the finer the beam steer angles that can be obtained.

Active Devices can be easily incorporated into the microstrip Rotman lens as can be seen in Figure 4.6. The Rotman lens can be integrated into the perpendicularly-fed patch array spatial combiner as can be seen in Figure 4.6 and Figure 4.8. MMIC amplifiers can be bonded to the output ports. The amplified signal will travel in the microstrip transmission line and will then couple to the dielectric filled waveguide through the microstrip to

waveguide transitions. The signal out of the dielectric filled waveguide will couple to a microstrip transmission line, which will then feed the patch antenna. The signal is then radiated by this microstrip fed patch antenna. Dual polarization beam steering can be achieved by introducing another Rotman lens on the opposite side of the metal tray. The second lens is placed half way and in between the unit cells of the upper tray as can be seen in Figure 4.8.

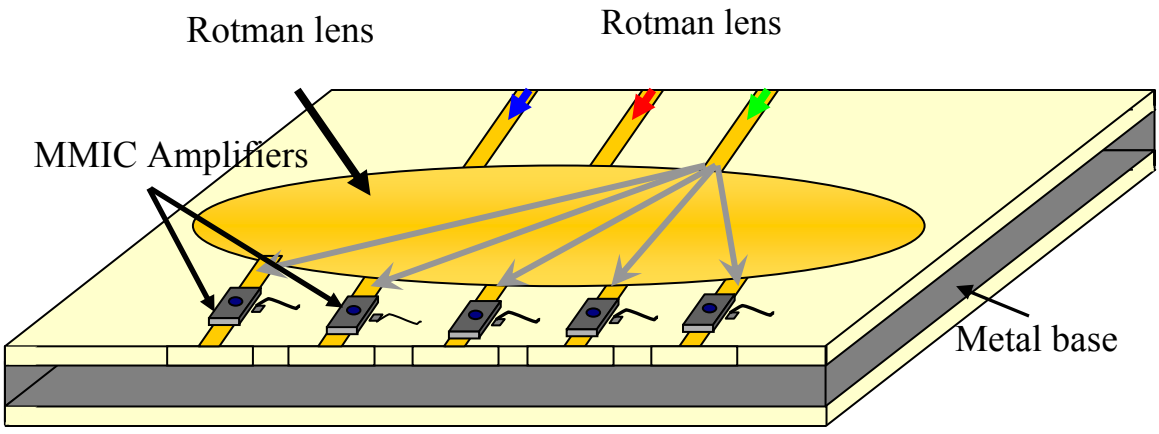

Figure 4.6: A prospective view illustrating several amplifying units on a tray that employs a microstrip Rotman lens to achieve beam steering.

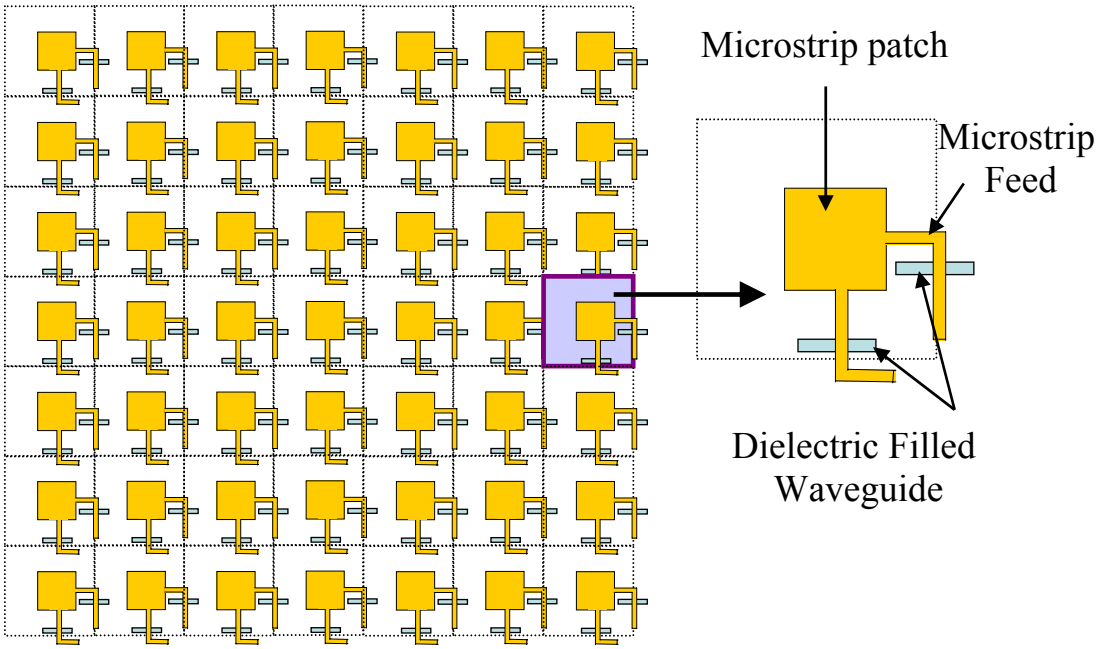

Figure 4.7: Dual patch array used as the radiating element for the dual polarized tray based perpendicularly fed 7x7 patch array employing microstrip Rotman lenses used to achieve beam steering.

The complete dual polarized perpendicularly fed patch array spatial power combiner with Rotman lens system is shown in Figure 4.8. This system has many features and functionalities. It is compact, and can produce high power at millimeter waves. In addition, it possible to beam steer the signal in the azimuth plane for two different polarizations: the horizontal and the vertical. One phase shifter is added at the input of every tray to realize beam steering at the elevation plane for both the horizontal and vertical polarizations.

This dual polarized phased array structure can be fed using the simple circuit shown in Figure 4.9 and Figure 4.10. A power divider such as Wilkinson power divider can be used to divide the power from a single input to a several outputs. These transmission line outputs will then feed the array, one transmission line for each tray. An aperture coupled feeds are used to couple the energy from the microstrip transmission line to the dielectrically filled waveguides. As can be seen from these figures there is one feeding circuitry for each polarization, therefore each polarization is controlled independently. It is to be mentioned that a Rotman lens can be used to divide the power instead of the Wilkinson power divider. This will eliminate the phase shifters placed at the input of each tray used to realize the elevation scanning. In other words a Rotman lens can be used to divide the power and feed this system, one lens for each polarization. This lens will provide the necessary constant phase shift between the trays to achieve beam steering in the elevation plane.

In this section and the pervious section, two integration methodologies were presented. Both of these systems proved to have the capability of dual polarity, beam steering, and ability to integrate active devices. After analyzing and characterizing the two design approaches, it became obvious that the system shown in Figure 4.8 is a better candidate and hence was chosen be fabricated.

The design approach or system explained in this section has many advantages over the system mentioned in section 4.3 and shown in Figure 4.2. First and foremost solid state phase shifting elements are eliminated, therefore reducing the cost of the structure. Furthermore, by eliminating the phase shifters, the biasing networks needed to control the phase shifters are removed from the system, resulting in a much simpler system. Another

advantage is the fact that it is less complicated to construct than the three dimensional structure discussed in section 4.3.

The design of this structure was divided into four sub designs, the dual polarized square patch antenna was designed first, then the dielectrically filled waveguide to aperture transition, then the dielectrically filled waveguide to microstrip transition, after that the three designs were assembled and the frequency response of this structure was obtained. Finally, the Rotman lens that is going to be integrated with this structure was designed.

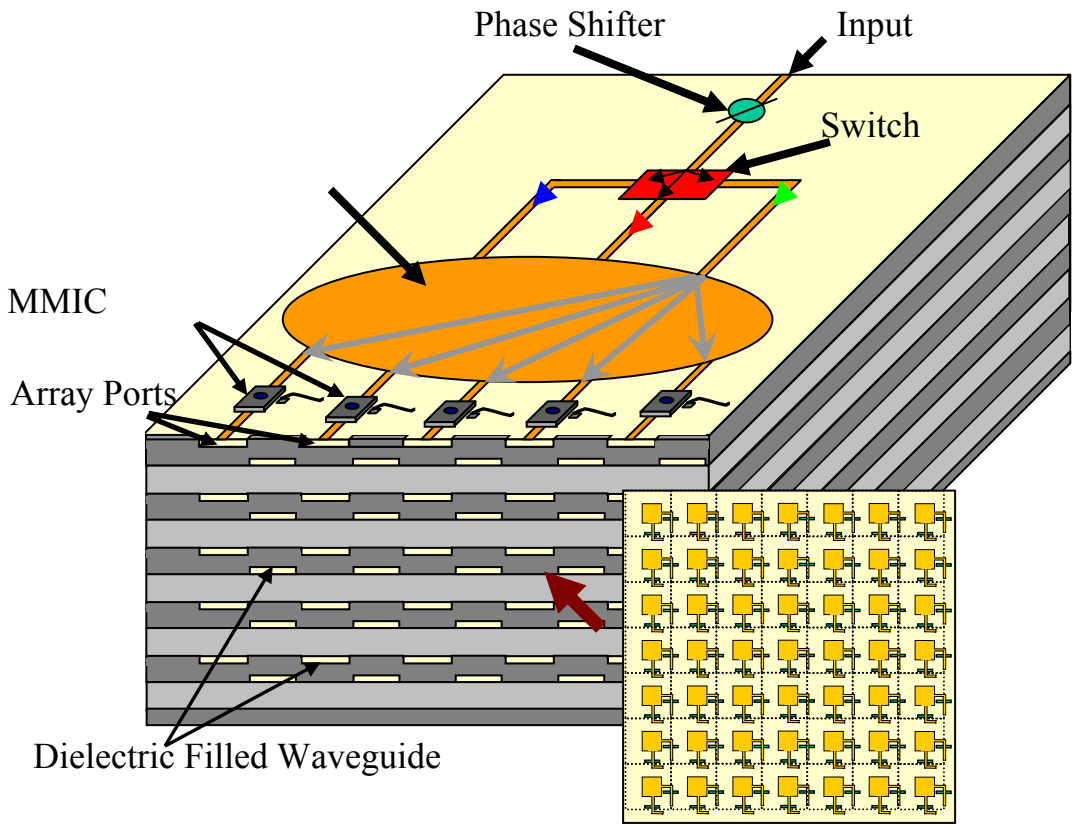

Figure 4.8: Dual polarized perpendicularly-fed patch array spatial power combiner with Rotman lenses.

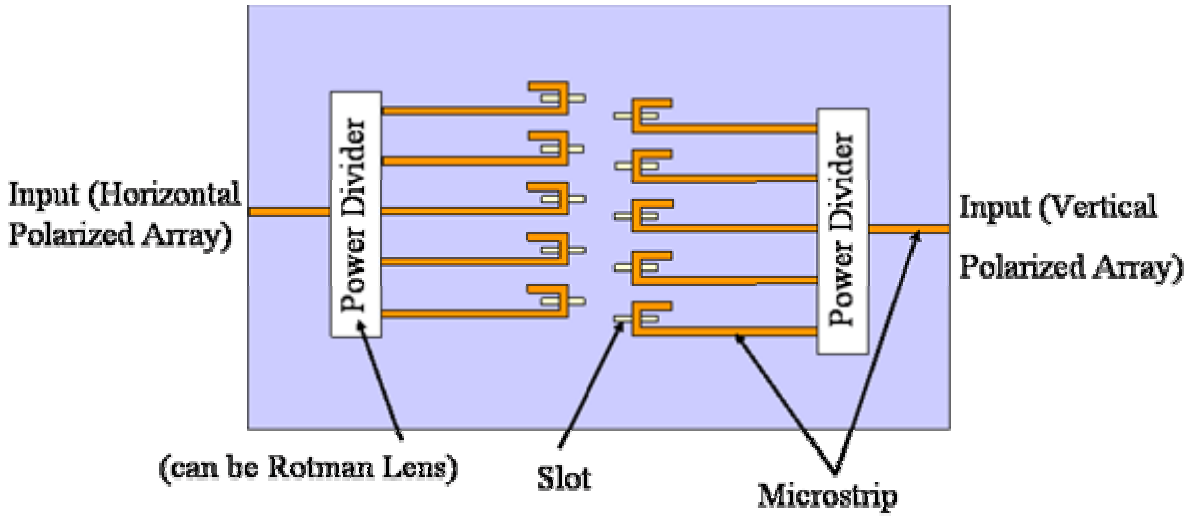

Figure 4.9: A conceptual drawing of the perpendicularly fed dual polarized phased array feeding circuitry.

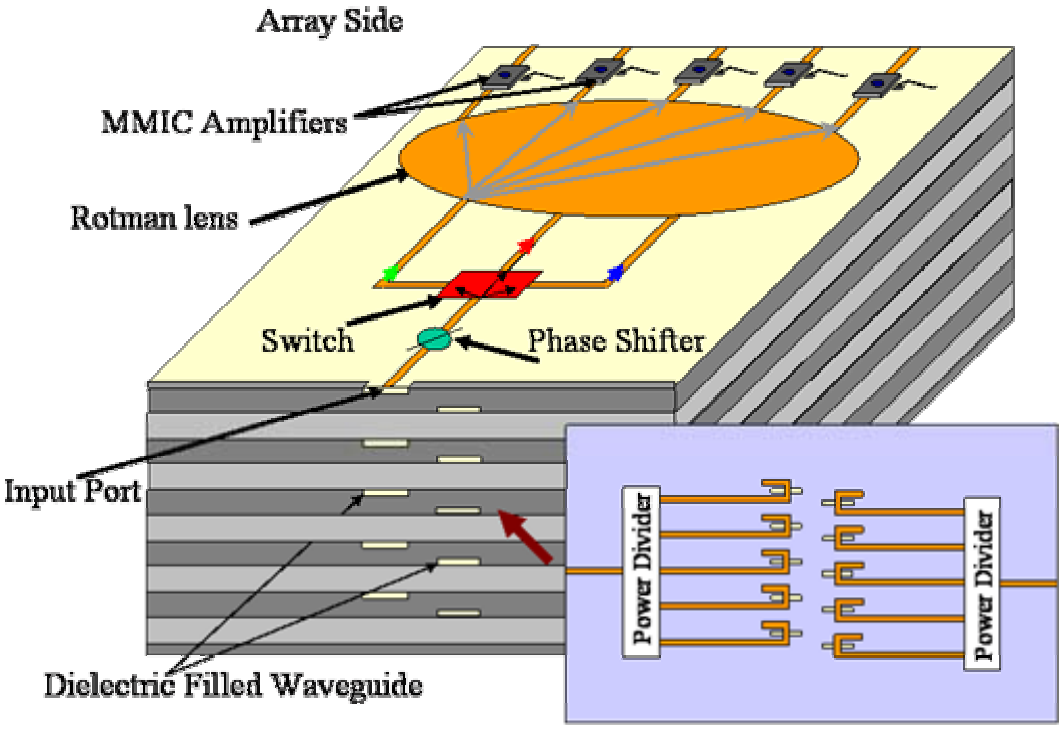

Figure 4.10: Dual polarized perpendicularly-fed patch array spatial power combiner with Rotman lenses and feeding circuitry.

4.4.1 Dual polarized patch antenna

There are a variety of dual polarized antennas that are well documented in literature. This includes patch antennas [1]-[6], horn antennas [22], tapered slot antennas [14] and many other antennas. Microstrip patch antennas are the most popular in both military and commercial applications because they are low cost, light weight, easy to integrate into arrays and circuits and have polarization diversity.

Microstrip fed patch antennas are implemented in this project to achieve dual polarity. The dimensions of this dual polarized patch were first calculated using the method outlined in [23], the design was then verified and optimized using Agilent ADS Momentum ^{TM}. The impedance of this square patch was found to be large and therefore a quarter wave matching network was used to obtain a good match. The impedance of the quarter wave matching network was calculated and found to be large, resulting in a very thin microstrip line to manufacture. Knowing that the thinnest or narrowest transmission line manufacturable or can be etched is 0.1016 mm the quarter wave matching network was set to be 0.1016 mm and an inset feed was used to obtain a good match. The length of the inset feed or the recessed microstrip line feed 'y' is critical and will affect the isolation level between the two ports, the longer the inset feed the less the isolation between the ports.

Figure 4.11 shows the layout of the square patch antenna with two orthogonal microstrip feeds used to obtain dual polarizations. The microstrip patch was designed to operate at 32.6 GHz on Rogers RT6002, with a height of 0.254 mm, dielectric constant of 2.94, and dissipation factor of 0.0012. Figure 4.11 also shows the simulated frequency response of

this patch. A 10 dB return loss over 0.65 GHz was achieved with better than -20dB isolation between the ports.

The dimensions of this dual polarized patch are as follows:

$L = 2.4892$ mm

$y = 0.254$ mm

$g = 0.127$ mm

$W_q = 0.1016$ mm

$W = 0.5588$ mm

Where L is the patch length, y is the length of the recessed microstrip line g is the gap width of the recess, W_q is the width of the quarter wave matching network and W is the width of the aperture coupled microstrip transmission line (read the next section for more detail in how this value was found). It is to be indicated that the quarter wave microstrip transmission lines were bent in order to fit the whole patch layout in a unit cell of half free space wavelength. Figure 4.12 plots the simulated E-plane radiation patterns at 32.6 GHz for port-1 and port-2. Good broadside radiation patterns with low cross polarization are observed. For port-1 the cross polarization is less than -20 dB and for port-2 it is less than – 23 dB. Also the antenna gain in the broadside direction for both ports is 6.3 dBi.

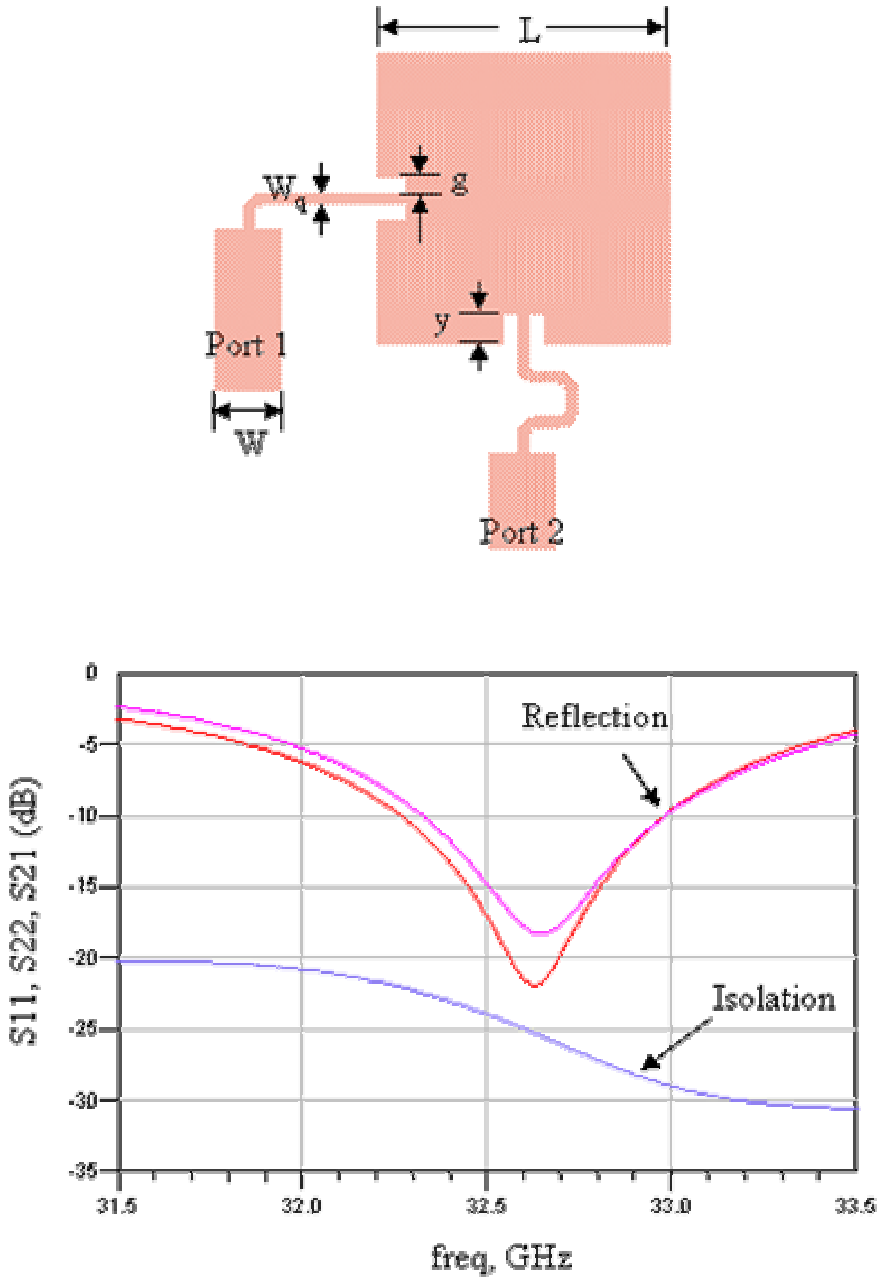

Figure 4.11: The dual polarized patch antenna layout and it frequency response.

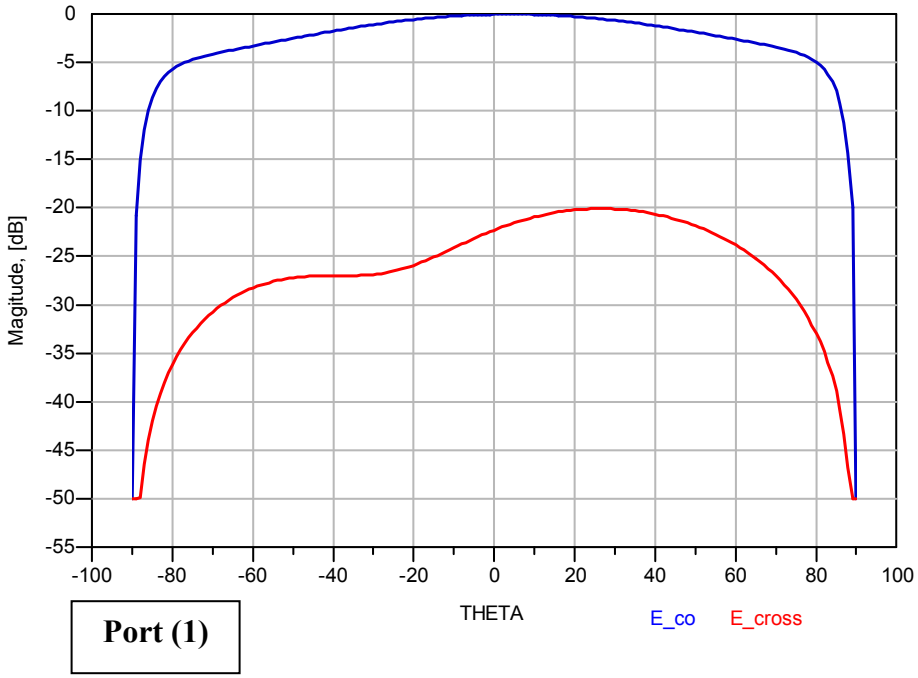

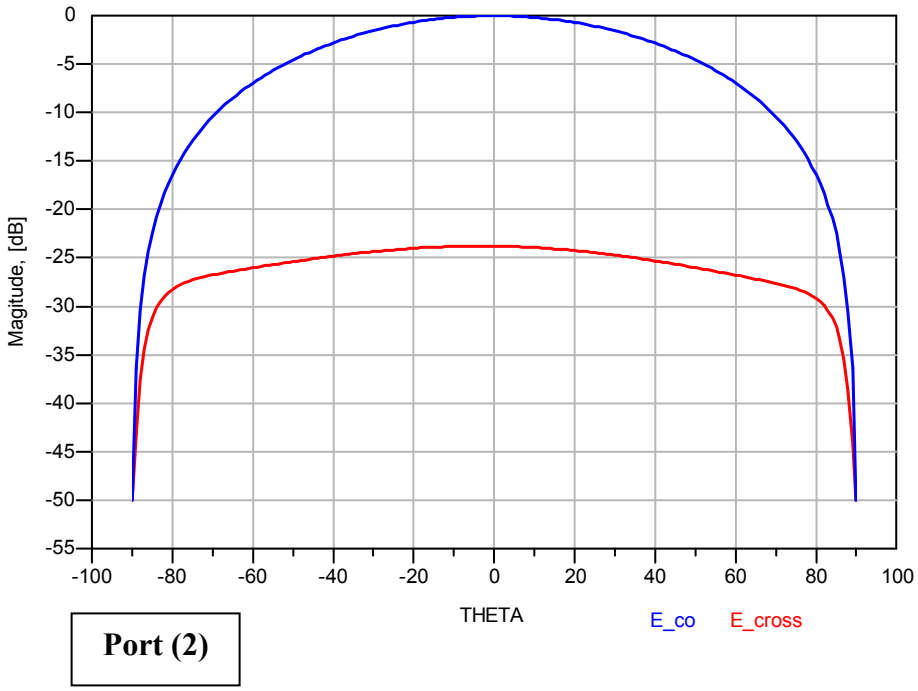

Figure 4.12: Simulated radiation patterns at 32.6 GHz for port 1 and port 2.

4.4.2 Microstrip to waveguide to aperture transition

In many applications it is necessary to connect a microstrip circuit or a microstrip antenna to a waveguide. Several waveguide to microstrip transmission lines and microstrip antennas have been developed, including ridge waveguide to microstrip [24], and aperture coupled waveguide to microstrip line or antenna [25], microstrip to waveguide transition using quasi-yagi antenna [26], waveguide to microstrip probe transition [27] and many others.

The perpendicularly-fed dual polarized patch antenna utilizes two types of microstrip to waveguide transitions; the waveguide to aperture coupled transmission line and the microstrip to dielectrically filled reduced height waveguide transition which was first developed by Ortiz and Mortazawi [28]. The microstrip to dielectrically filled waveguide transition shown in Figure 4.13 is used to couple the energy from the output ports of the Rotman lens to the dielectrically filled waveguides. In addition, the dielectrically filled waveguide to aperture microstrip transition shown in the same figure is employed to couple the energy from the waveguide to the transmission line that will eventually feed the antenna. The dielectrically filled waveguide to aperture microstrip transition has been simulated using Ansoft HFSS^{TM}. The optimal dimensions of the microstrip to dielectrically filled waveguide transition were found to be as follows:

$$a = 2.9464 \text{ mm}$$

$$b = 0.508 \text{ mm}$$

$$L = 4.6482 \text{ mm}$$

$$W_R = 0.762$$

Where a, b and L are width, height and length of the dielectrically filled waveguide which was designed on Rogers TMM4 with height of 0.508 mm, dielectric constant of 4.5 and a dissipation factor of 0.002. The width of the microstrip line (port 1 and 2) connected to this waveguide is W_R which was designed using the same substrate as the dielectrically filled waveguide. The optimal dimensions of this dielectrically filled waveguide to aperture coupled microstrip transition were found to be

$$H_p = 0.254 \text{ mm}$$

$$W = 0.5588 \text{ mm}$$

where W is the microstrip width. This microstrip will be used to feed the patch antenna and was mentioned in the pervious section. H_p is the height of Roger's RT6002 substrate with dielectric constant of 2.94.

The substrate used in the microstrip to waveguide transition (port 1) is the same substrate that will be used for the Rotman lens. The dielectrically filled waveguide is designed to support one mode, which is the TE10 mode, and the impedance of the microstrip (port 2) is the same as the impedance of the dielectrically filled waveguide.

As shown in Figure 4.14 the insertion loss of this transition is small, it is less than 0.2 dB over the entire bandwidth, which indicates a good power transmission between the two ports, and the return loss is less than -15 dB. The radiation from this aperture coupled transition was found to be negligible therefore it should not affect the radiation pattern of the antenna.

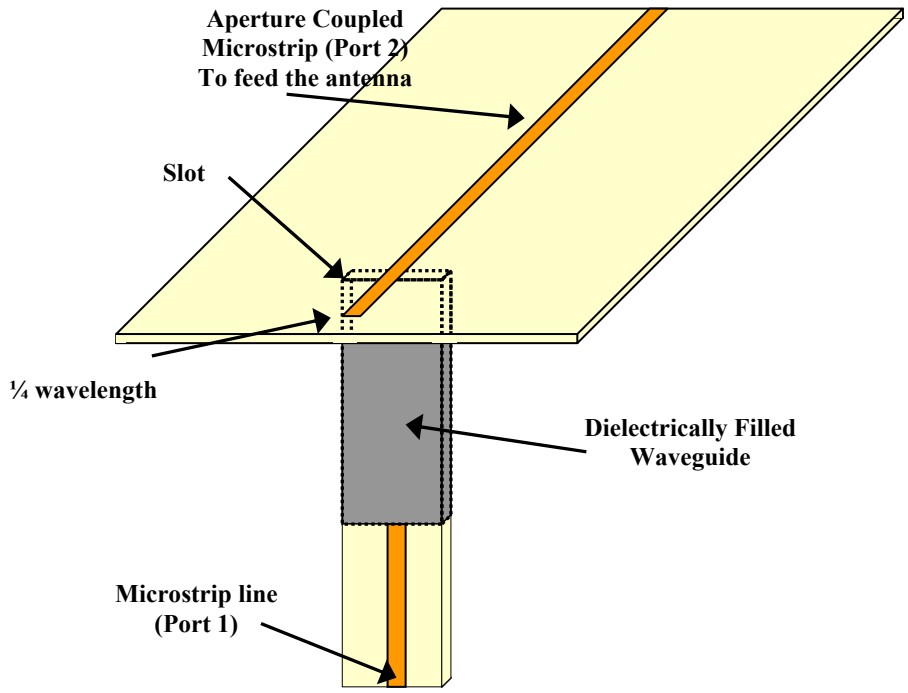

Figure 4.13: The microstrip to waveguide to aperture transition.

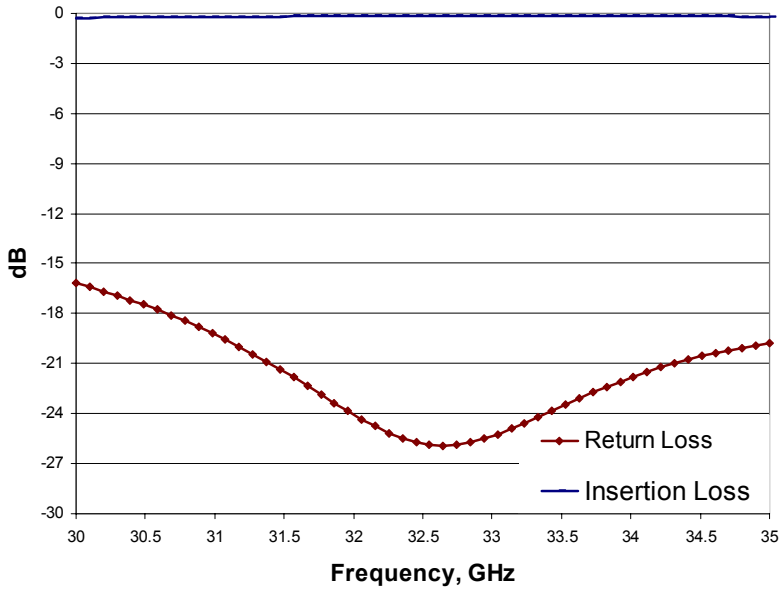

Figure 4.14: The frequency response of the microstrip to waveguide to aperture transition.

4.4.3 Unit cell design

The unit cell of the dual polarized perpendicularly fed patch antenna array is shown in Figure 4.15. This unit cell consists of a dual polarized patch antenna, aperture coupled microstrip to dielectrically filled waveguide transition, dielectrically filled waveguide to microstrip transition and input microstrip line. In this figure, a signal input in to the microstrip line at the bottom of the diagram will couple to the dielectrically filled waveguide through the microstrip to waveguide transition. The signal will then couple to the microstrip at the top of the diagram through the waveguide to aperture microstrip line transition. Finally the signal is radiated by the square patch antenna. In this diagram, one input microstrip line will feed the vertical polarization and the other input microstrip line will feed the horizontal polarization of the patch. It is to be noted that the input microstrip line shown at the bottom of Figure 4.15 will be connected to one of the output ports of the Rotman lens, therefore the number of unit cells needed or the number of the array elements will depend on the number of output ports of the Rotman Lens. As previously mentioned, one lens will control the vertical polarization and another lens will control the horizontal polarization.

The square patch antenna that was designed in section 4.4.1 was connected to the microstrip to waveguide to aperture transition that was developed in section 4.4.2. The complete design was then simulated using Ansoft HFSS^{TM}. The frequency response of the complete structure is shown in Figure 4.16. As can been seen, the return loss is better than 10 dB over 0.7 GHz of bandwidth. Also, the isolation between the two ports or the two polarizations is better than 20 dB.

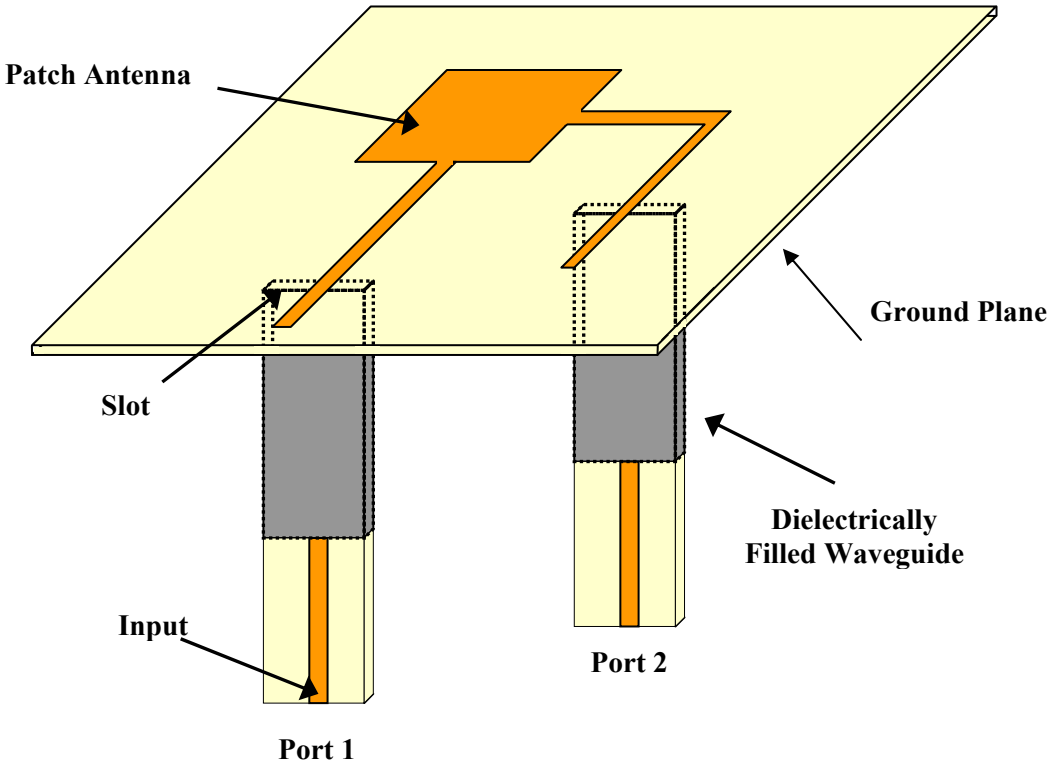

Figure 4.15: Perspective view of the dual polarized perpendicularly-fed patch unit cell.

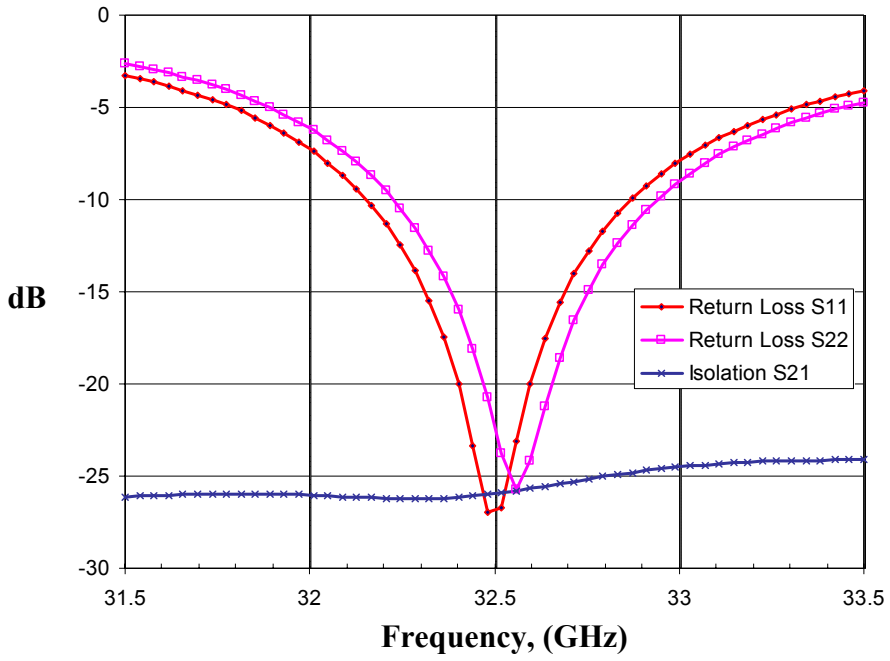

Figure 4.16: The frequency response of the dual polarized perpendicularly-fed patch.

4.5 Microstrip Rotman Lens

Conventional phased arrays use phase shifters to obtain the desired linearly progressive phase shift across the aperture to achieve beam steering. Separate phase shifters are needed for each radiating element and each phase shifter requires a control line. For systems with many array elements, phase shifters will significantly add to the cost and complexity of the system.

A practical alternative is to use a parallel-plate lens such as the Ruze [29] or the Rotman lens [30] to form multiple beams from antenna arrays. These lenses will eliminate and replace the phase shifters and the power dividers used in the conventional phased array. Furthermore, these lenses are true time delay components; hence they can operate over a large bandwidth.

The Rotman lens has less phase aberrations or phase error for the intermediate input ports compared to the Ruze lens, mainly because the Rotman lens has three focal points, where as the Ruze lens has only two focal points. The definition of a focal point, or a perfect focus, is a point on the input contour which provides an exact linear phase variation across the linear array; therefore an undistorted beam will be produced in a certain direction. A Rotman lens could be made using either waveguide or microstrip [31] technology. The main advantages of a microstrip Rotman lens are the ease of fabrication (by a simple etching process) and the size reduction due to the dielectric substrate. To control the beam steering, the Rotman lens is designed with several input ports, with each corresponding to its designated scan angle.

The design procedure of the Rotman lens includes the determination of several necessary parameters such as the desired scan angle range, the effective dielectric constant, number of array elements, and the maximum tolerable phase error.

Through calculations derived by Rotman and Turner [30], the shape (input port and array port contours) of the Rotman lens was generated, as well as the lengths of transmission lines required to insure the necessary scan angles with minimal radiated side lobes. The angular coverage was chosen to be ± 30º, therefore the focal point will be at 30º, 0º, and -30º. In other words, this Rotman lens is designed to have perfect phasing at a scan angle of 30º, 0º, and -30º. All of these calculations are normalized relative to the focal length '**f'**, which is the distance from the focal point located at the input contour of the Rotman lens at an angle of 30º to the center of the output contour of the lens. There are several functions which determine the input and output shapes of the Rotman lens. A significant design parameter is the length '**g**', which is dependent upon the desired scan range. The optimal lens input to output distance '***g'*** can be found by equation 4.1. The calculated shape is shown in Figure 4.17.

$$\mathbf{g} = 1 + \frac{\alpha^2}{2} = 1 + \frac{(30\text{deg})^2}{2} = 1 + \frac{0.5236^2}{2} = 1.3708 \qquad \textbf{(4.1)}$$

Finally, meander lines are necessary on the output side to obtain a planar array. The parallel-plate height should be less than half a dielectric wavelength. This is to ensure that only the TEM mode can propagate. The power spreading in the parallel-plate region is linear with distance, rather than square of distance in three dimensional spreading.

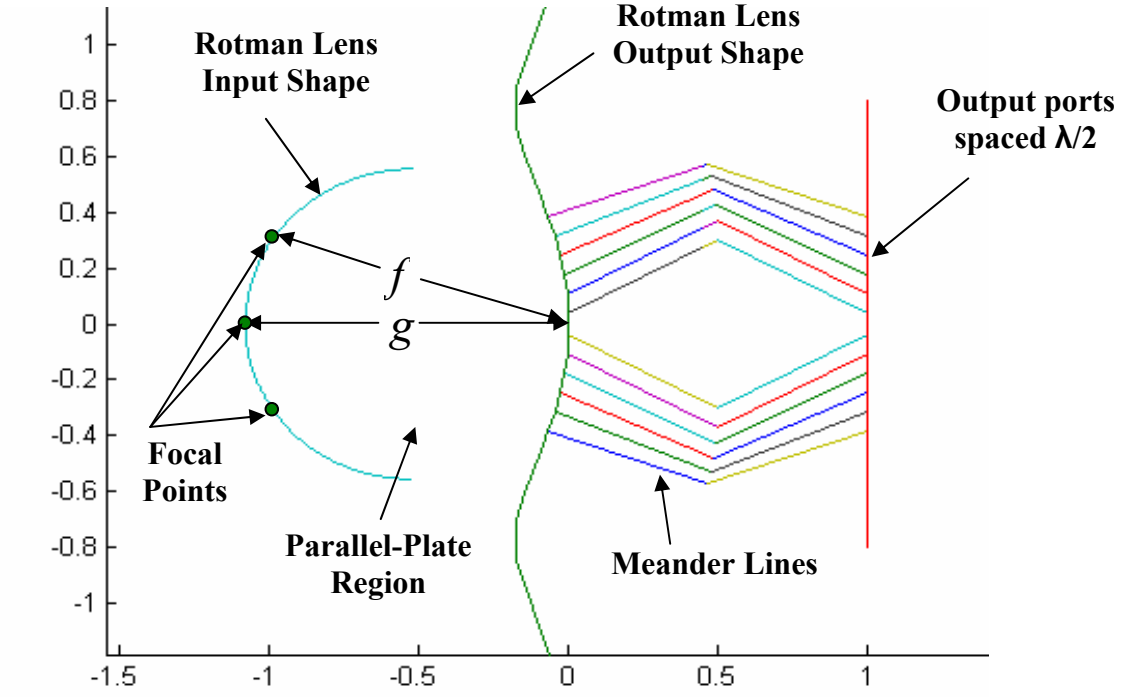

Figure 4.17: Calculated shape of the Rotman lens, optimized for a 30 degree scan angle.

In order to successfully implement a phase difference at the output ports, the path lengths from the input to the output ports must correspond to the desired scan angle. This Rotman lens is designed to have no phase or path errors in the path length at -30º, 0º, and 30º. Other angles or intermediate input ports within the scanning range will have some path length errors. The path length errors for several angles have been computed for '***g***' = 1.076 and are plotted versus the aperture length '**η**' in Figure 4.18. As expected at 30º (a focal point) there are no path errors. The output ports will exist from η = -0.5 to η = 0.5. Therefore, in the worst case, the normalized path length error will not exceed ± 0.00035, which occurs at a scan angle of 20 degrees. It is to be noticed that the path error increases as the point moves away from the center.

For a large array on the order of 100 λ, the phase error due to this method becomes significantly high. Improved approaches [32]-[33] were developed to minimize this phase error. This was done by replacing the circular input contour with a carefully calculated non-circular input contour. Again, this improvement is only evident for an array with a very large aperture.

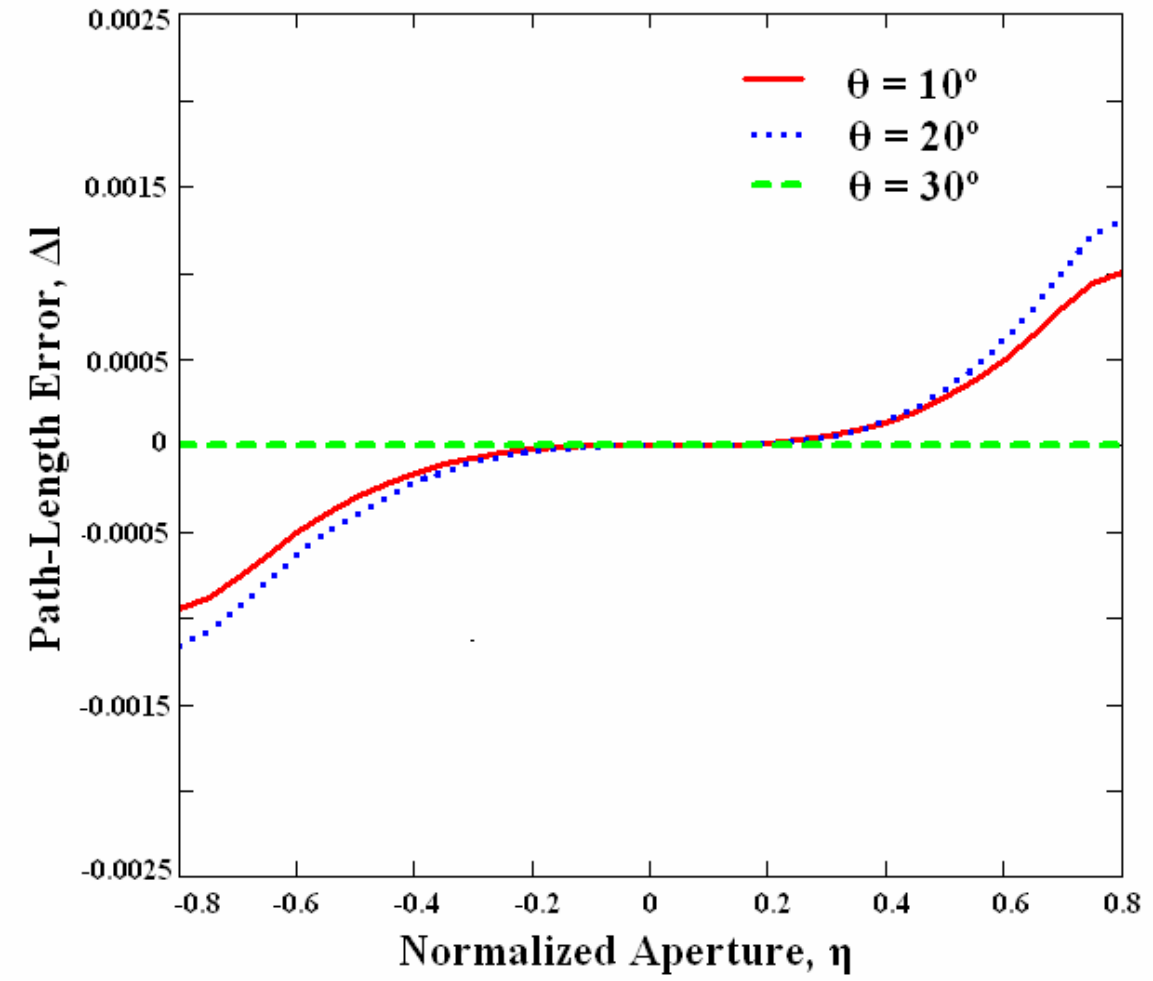

4.18: Normalized Path length error 'Δl' versus the normalized aperture length 'η' for '***g'*** = 1.076, at 10º, 20º and 30º.

To determine the scaling factor '**f**' several parameters need to be determined first; this includes the maximum path error tolerable, the number of array elements and spacing between antenna elements. The maximum path error is set to be ± 0.00035. This corresponds to half aperture length η = 0.5. To avoid grating lobes, antenna theory rules suggest keeping the element spacing 'd' below the inequality of equation 4.2, hence the spacing between antenna elements is set to be equal to λ/2, where λ is the free space wavelength of the operating frequency.

$$d \leq \frac{\lambda}{(\sin(\theta)+1)} \qquad \textbf{(4.2)}$$

θ is the scan angle.

The number of antenna elements '**N**' was chosen to be 9 elements and the length of the antenna array is given by

$$L = (N-1) * d \qquad \textbf{(4.3)}$$

and the scaling factor can be found by

$$\mathbf{f} = \frac{L}{\eta} \qquad \textbf{(4.4)}$$

This procedure will give the minimum scaling factor and therefore the smallest Rotman lens size possible given the required angular coverage, maximum path error, number of antenna elements, and element spacing. For a microstrip lens built in a certain dielectric material, the scaling factor should be divided by the square root of effective dielectric constant [34].

4.5.1 Microstrip Rotman Lens at X-Band

The purpose of this X-band design is to fully characterize the design of Rotman lens and measure its performance. Successful results will insure that the design procedure followed is correct and therefore similar performance will be expected for the Ka band Rotman lens that will be designed and employed in the dual polarized perpendicularly-fed array.

A Microstrip Rotman lens has been designed using a program developed based on pervious reports and references [29], [35]-[37]. This Lens has 9 array elements and 7 input ports, and has been simulated using ADS Momentum^{TM}. Figure 4.19 shows the simulated Rotman lens; all of the ports are numbered. The antenna array ports are numbered from 14 to 22, where the input ports are numbered from 1 to 9. The remaining ports will not be used and will always be terminated as the phase error of these ports is large. A microstrip tapered transition is used between the aperture width of the input/output contour and the thin 50Ω microstrip line. It was suggested by Smith [37] that the flare angle of this microstrip tapered transition to be less than 12º. In addition, the input ports and the output ports should point to the center of the opposite lens contour. Both of these design considerations were followed in the design of this lens.

Simulation was performed on this lens, and all of the lens transmission lines were connected to matching ports with 50Ω impedance. Figure 4.20 and 4.21 illustrate the phase across the array ports when the lens is fed from port 1 and port 4 which will produce radiation patterns with peaks at 0º and 30º respectively. The results were as expected, there were no phase variations in the first case, and thus no beam steering will

be expected. The scattering parameters of this lens were used to calculate the radiation pattern (refer to Appendix A for the program) of the 9 element antenna array (ports 14 to 22). The element spacing is set to be λ/2 at 10 GHz. Figure 4.22 shows the calculated radiation patterns of an omni-directional antenna array fed by this simulated Rotman lens. These four radiation patterns are a result of the lens being fed from the input ports 1, 2, 3 and 9 which correspond to beam at 0º, 10º, 30º and -30º respectively. As can been seen, the results are satisfactory and as expected.

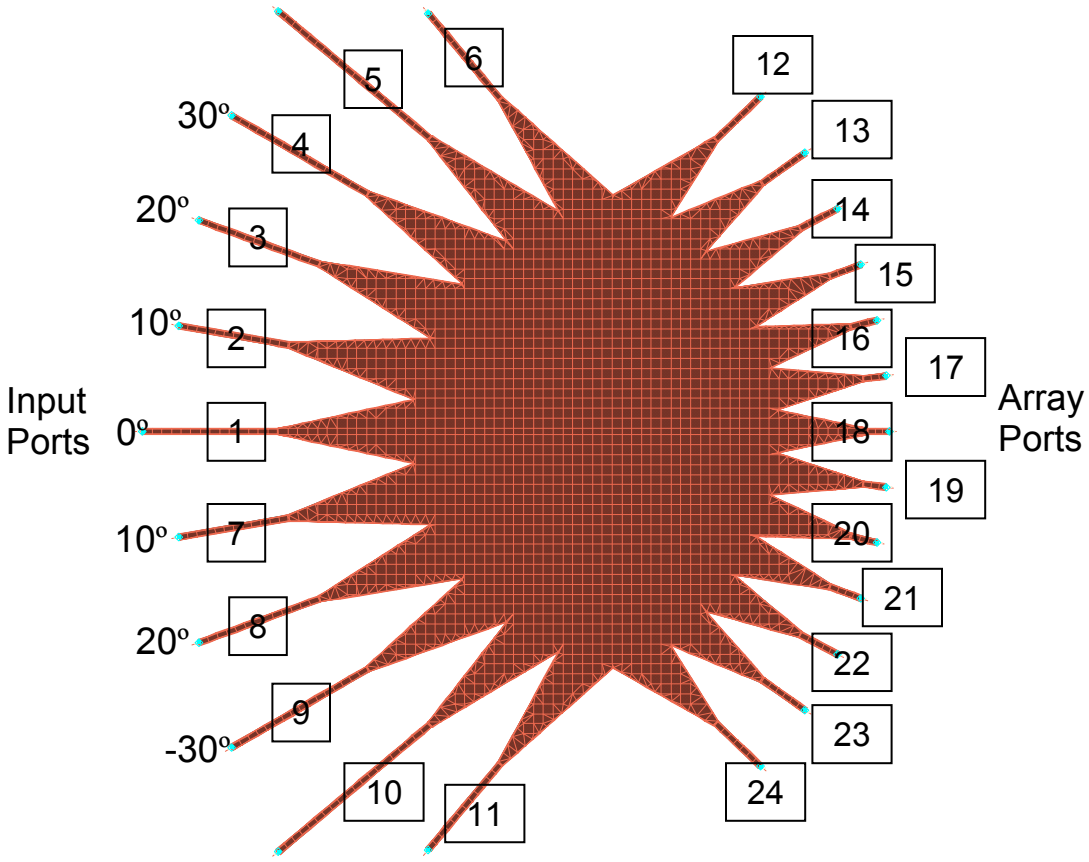

Figure 4.19: The simulated Rotman lens.

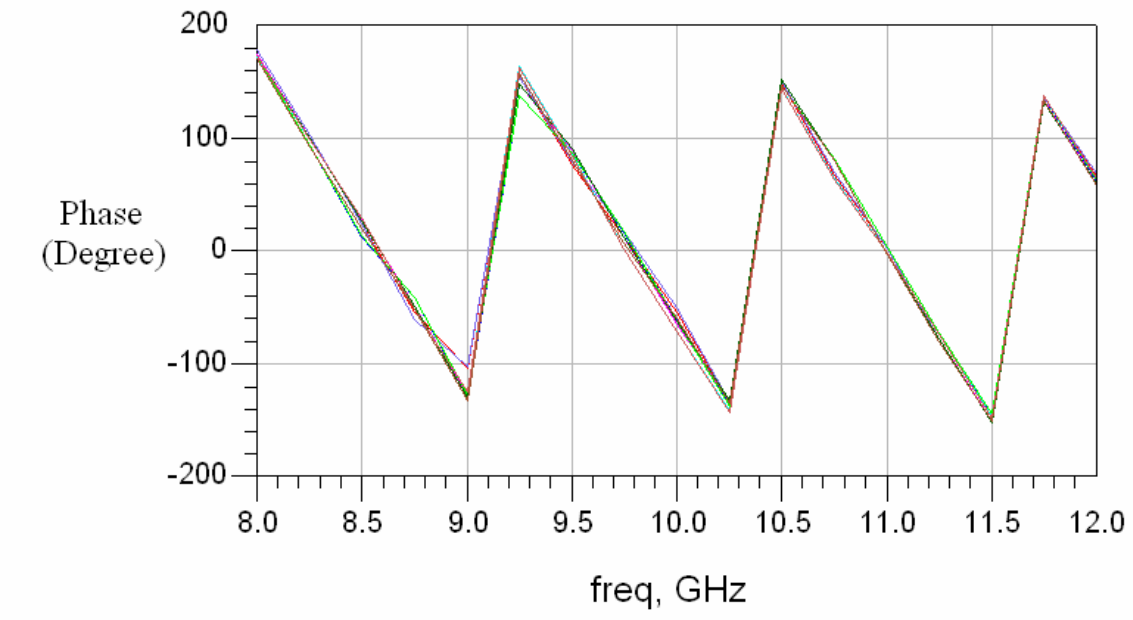

Figure 4.20: The phase across the array ports when the lens is fed from the port that will produce radiation pattern with peaks at 0º

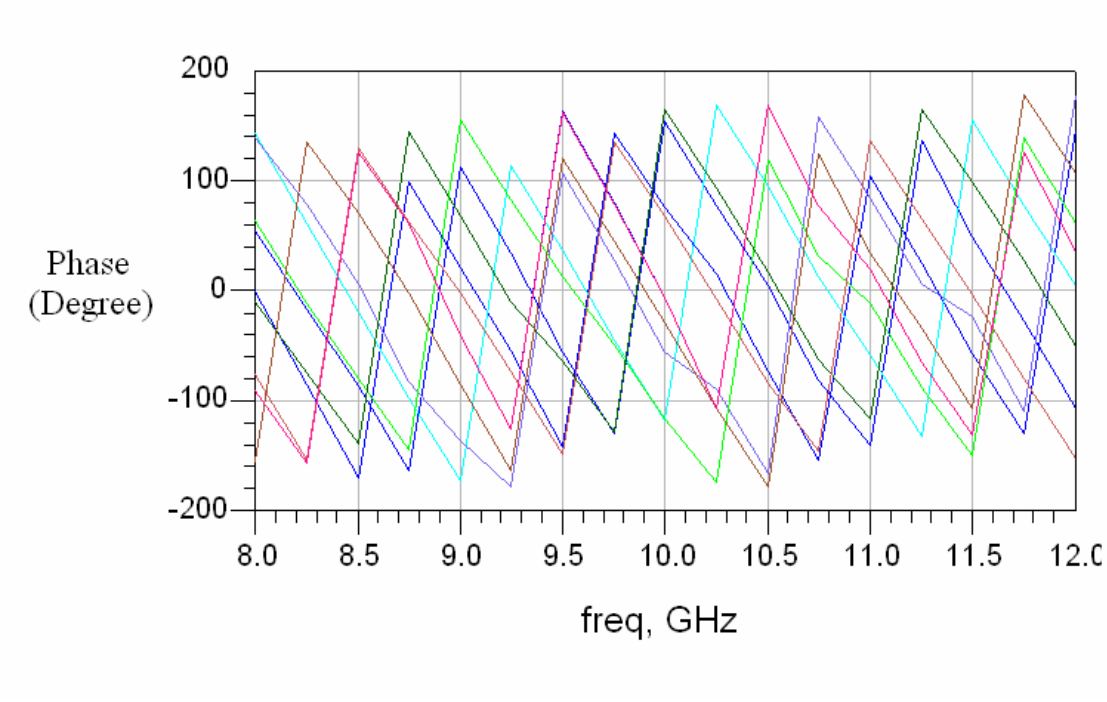

Figure 4.21: The phase across the array ports when the lens is fed from the port that will produce radiation pattern with peaks at 30º.

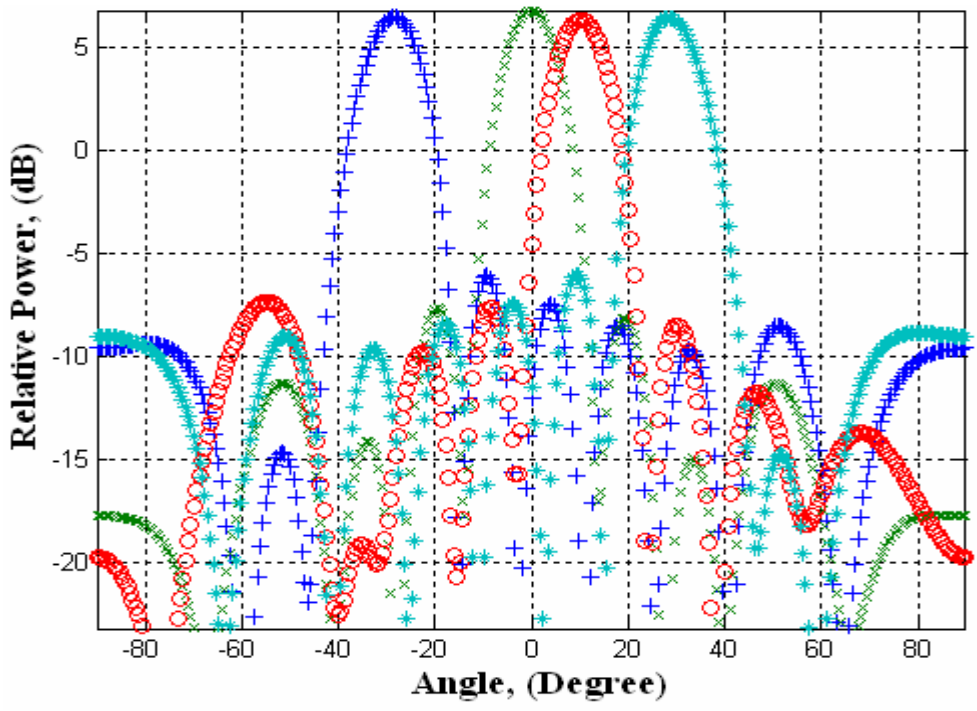

Figure 4.22: Calculated array factor of an antenna array fed by the simulated Rotman lens at 10 GHz.

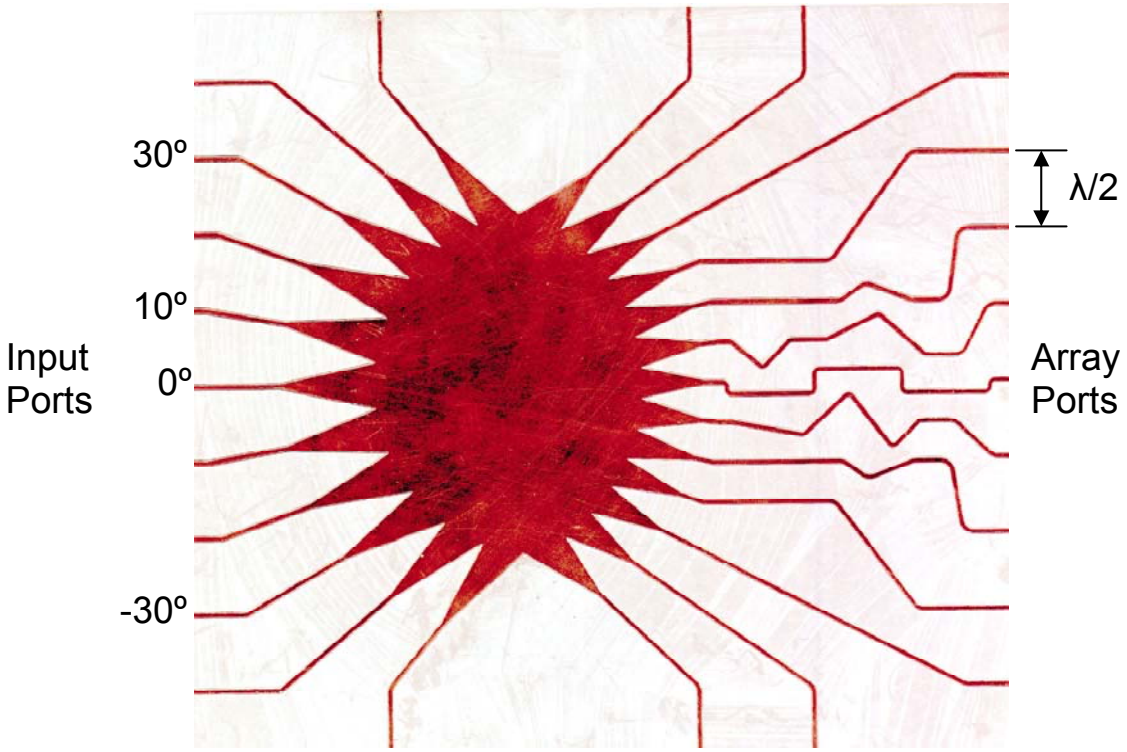

Figure 4.23: A scanned photo of the fabricated Rotman lens.

This lens is then fabricated on 0.635 mm thick Rogers Duroid RT6006 substrate with dielectric constant $\varepsilon_r = 6.15$. A scanned photo of the Rotman lens is shown in Figure 4.23. Meander lines were necessary on the output side to obtain a planer array. This extra transmission line should have the same length for all of the antenna ports (ports 14 to 22), this is to maintain the phase differential of the Rotman lens. SMA launchers were used to connect the Rotman Lens to the network analyzer.

An Agilent network analyzer E8364B is used to measure the scattering parameters for this Rotman lens. One port of the network analyzer was connected to the input of the lens while the second port of the network analyzer was connected to the output ports one by one, the remaining ports of the lens were terminated with matching 50Ω terminations. Figure 4.24 shows the reflection coefficient of the input ports 1 and 4. It is less than -10 dB over the bandwidth. The reflection coefficient of the other input and output ports are very similar, indicating very good match between the microstrip transmission line and the lens. Also the coupling between the input ports and the coupling between array ports is better than -15 dB; this is shown in Figure 4.25. The measured phase of the output ports or antenna elements when the lens is fed from port 1 (0º) is shown in Figure 4.26. As can be seen the phase across the antenna array is very similar.

The calculated radiation patterns if this lens feeds an omni-directional antenna array are plotted for four inputs ports 1, 2, 4 and 9 (for scan angles of 0º, 10º, 30º and -30º respectively) and shown in Figure 4.27. The results follow the design and simulation predictions. It is to be noted that the side lobes for both the simulated and the measured lens are less than -13 dB. Figure 4.28 shows a plot of the measured insertion loss of X-band microstrip Rotman lens when it is fed from port 1, it is calculated to be 5.0 dB at 10

GHz. Most of the loss is due to the fact that a significant portion of the incident wave will be absorbed/lost at the sides of the lens, (port 12, 13, 23 and 24) which is called spill over power. Figure 4.29 shows a photograph of the fabricated X-band Rotman lens.

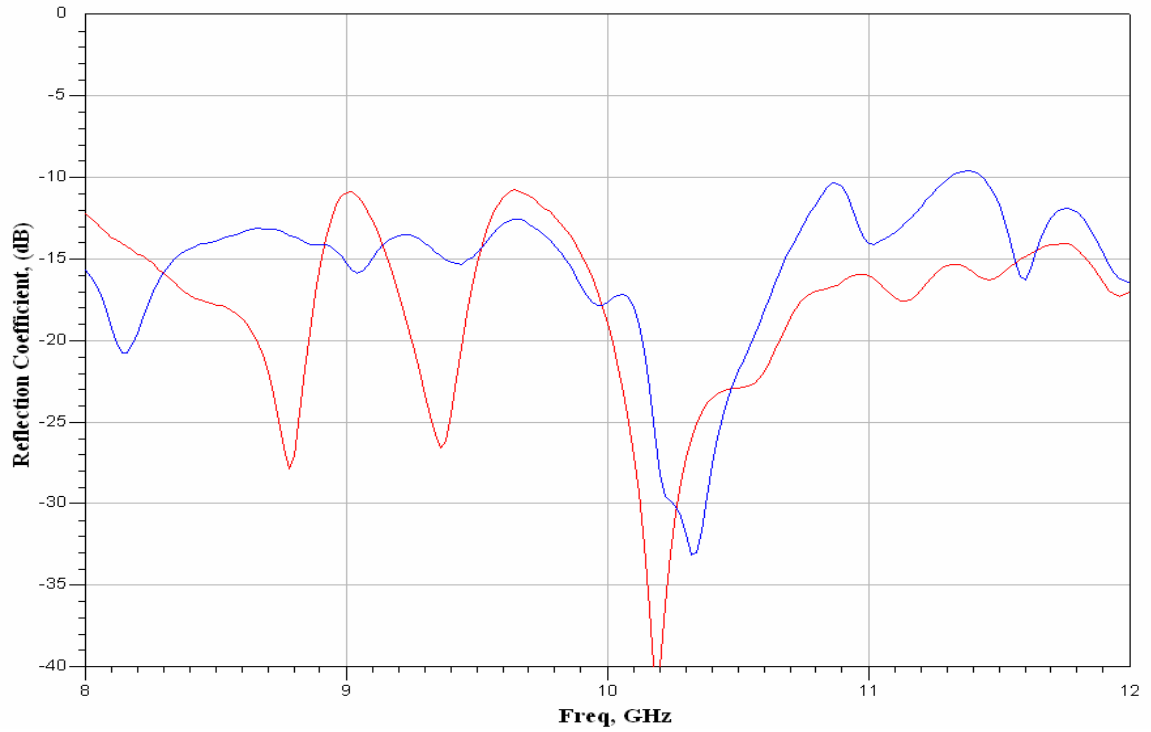

Figure 4.24: The reflection coefficient of the input ports 1 and 4.

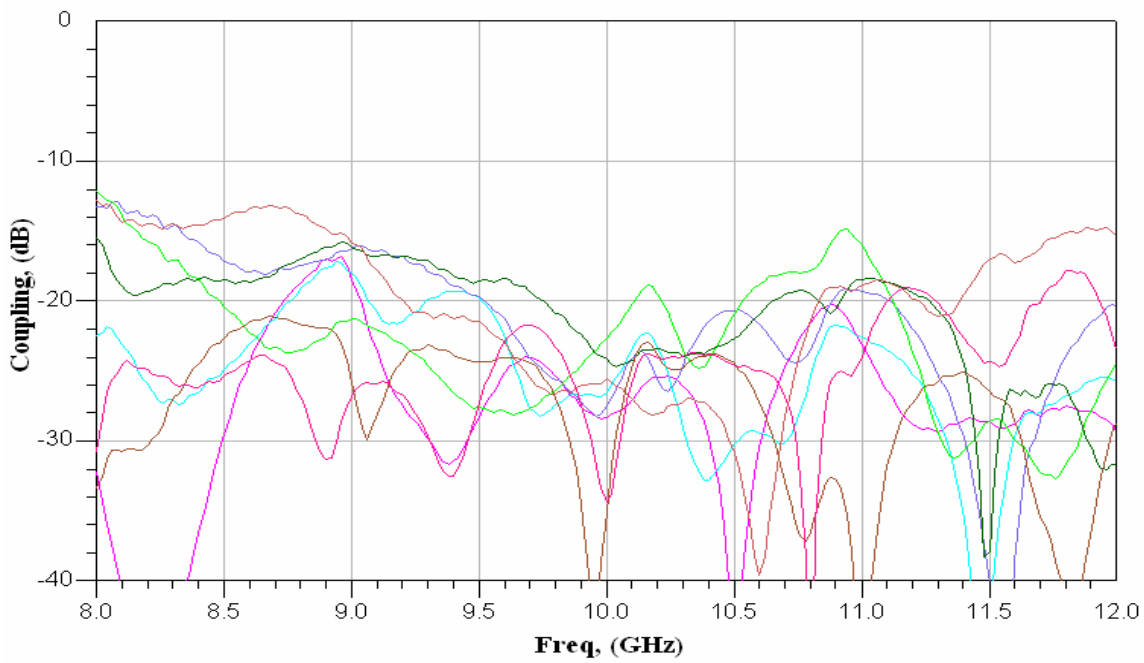

Figure 4.25: The coupling between the input ports and the coupling between array ports.

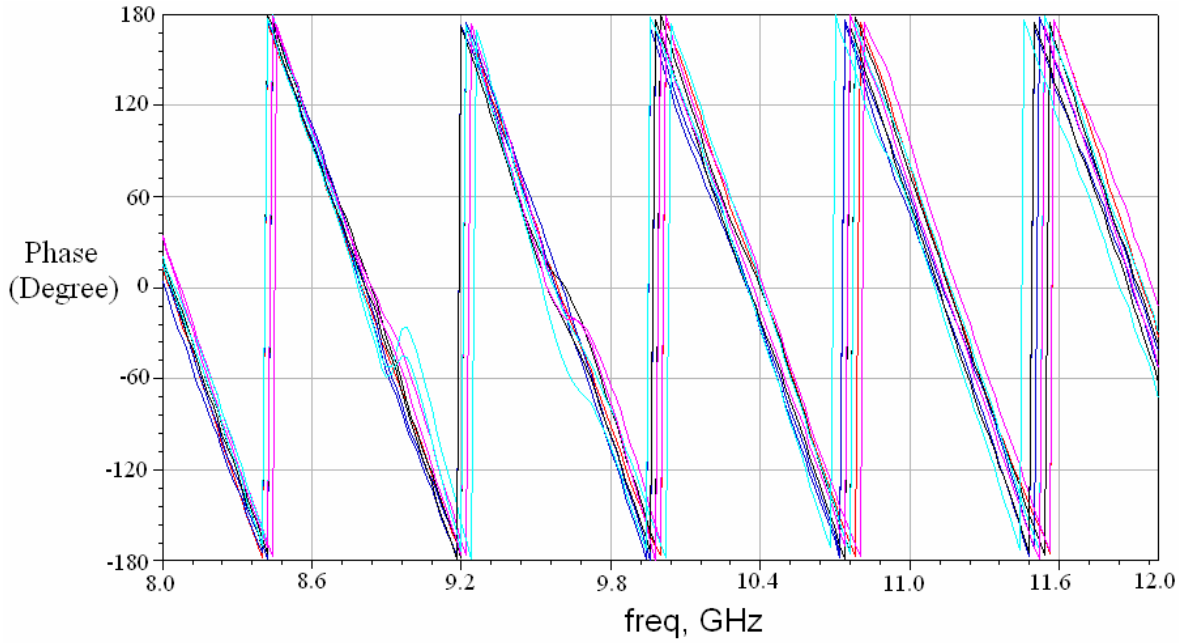

Figure 4.26: The phase across the array ports when the lens is fed from the port (1) the port that will produce radiation pattern with peaks at 0º.

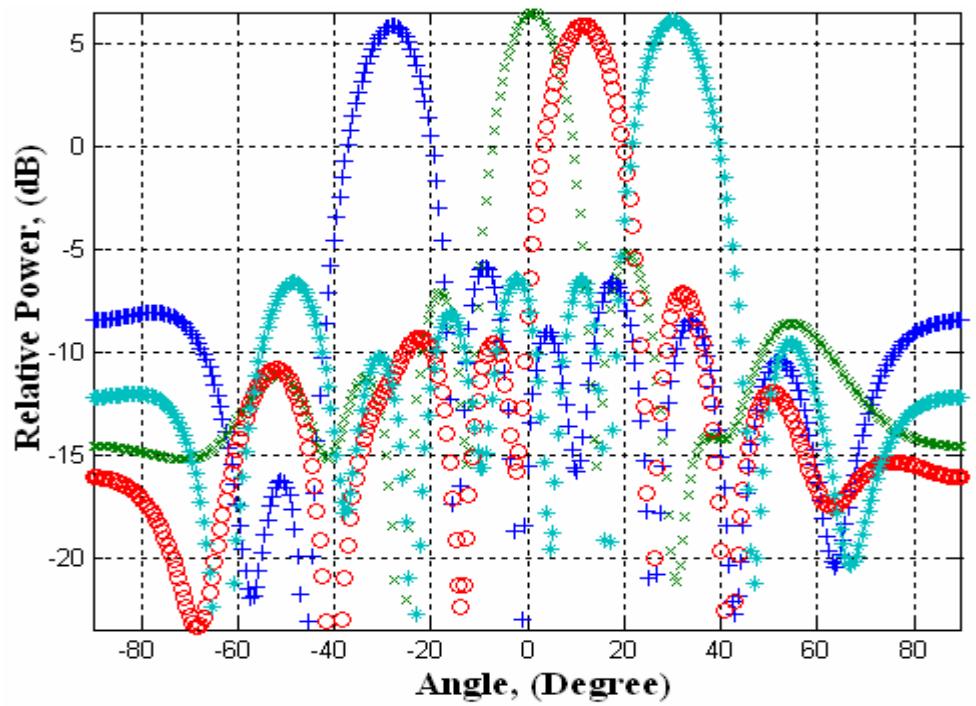

Figure 4.27: Calculated array factor of an antenna array fed by the fabricated Rotman lens at 10 GHz.

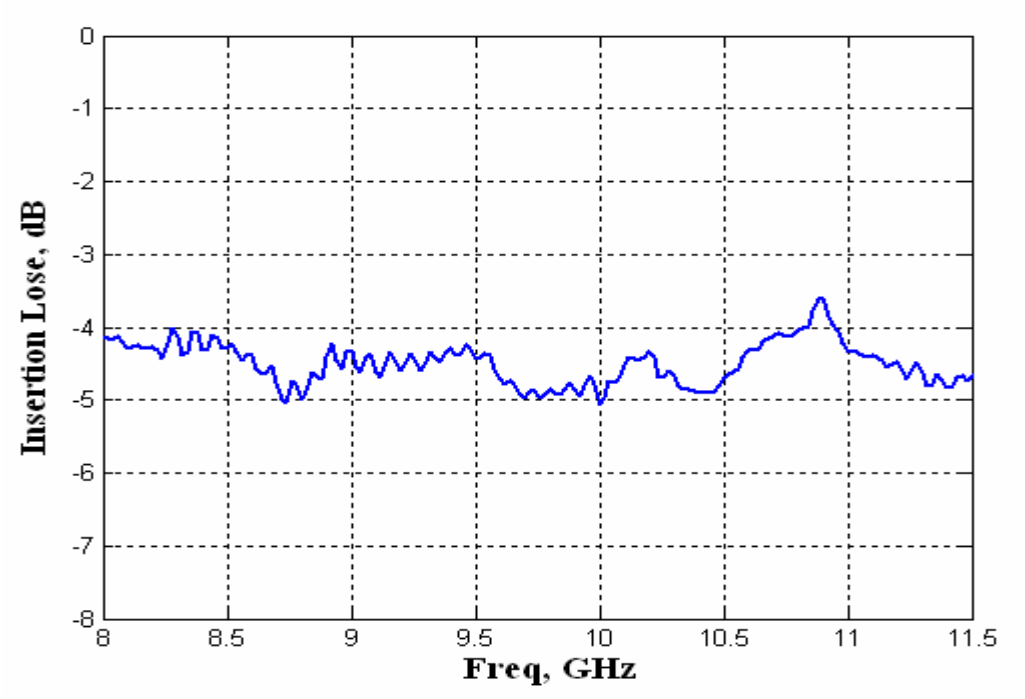

Figure 4.28: The measured insertion loss of the X-band microstrip Rotman lens when it is fed from port 1.

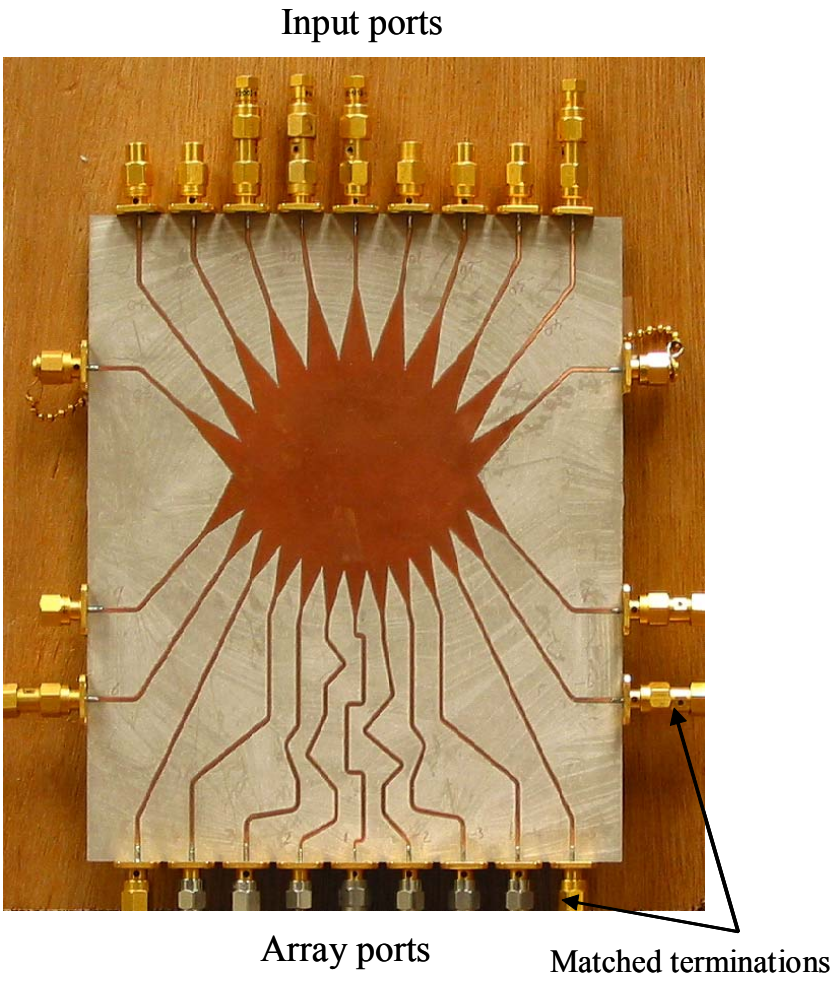

Figure 4.29: A photograph of the fabricated X-band Rotman lens.

4.5.2 Ka-band Microstrip Rotman lens

A Ka-band Microstrip Rotman lens has been designed using the same program that was used to design the X-band Rotman lens. This lens has 7 inputs designed to produce beams at 0º, ±10º, ±20º, and ±30º where the three focal points (inputs) are at port 1, 4 and 9, corresponding to scan angles at 0º, 30º and -30º, respectively. This Ka-band lens has 9 array elements (numbered form 14-22) spaced $\lambda/2$ at 32.6GHz.

This design has been simulated using ADS Momentum™ with a mesh density of 7 cells per wavelength. This Ka-band Rotman lens will be used in the perpendicularly-fed dual polarized patch array, which uses a microstrip to dielectrically filled waveguide transition; therefore the dielectric constant of the substrate for this lens should be the same as the dielectric constant of the dielectrically filled waveguide. Also, the substrate thickness of the lens should be the same as the height of the dielectrically filled waveguide. Additionally, the microstrip width of the antenna array ports of the lens should be the same as the microstrip width used in the microstrip to dielectrically filled waveguide transition, which is 0.762 mm. Based on the dielectrically filled waveguide parameters discussed in section 4.4.2, the lens was designed on 0.508 mm think Roger's TMM4 substrate, with dielectric constant $\varepsilon_r = 4.5$.

One of the important design considerations when using dielectric substrate at millimeter-wave is surface waves (substrate modes) and the possibility of exciting higher order modes excitation. It is known that dielectric substrates make very good dielectric waveguides [38]-[39] with a fundamental mode that has no cutoff frequency. As the substrate becomes electrically thick (which can happen when the frequency is increased or by actually using a thicker substrate) more substrate modes can be excited. Therefore

some power can be lost into these modes. As the substrate coupling levels become large, a deleterious effect on the design performance can be expected and significant fractions of the input power will be lost. It has been shown for example that most of the power of the isolated printed antenna elements goes into dielectric, in the ratio $\varepsilon_r^{3/2}$:1, as opposed to radiated power [40]-[41].

Given the dielectric constant, dielectric thickness , and the operation frequency for a certain substrate, it is possible to determine the number of modes are excited in the substrate and their polarization. It is to be realized that the higher the dielectric constant, dielectric thickness, or the frequency, the more modes that can be excited in a given substrate. Information such as the propagation constant β of any mode at any frequency can be found graphically. For this grounded substrate with dielectric constant $\varepsilon_r = 4.5$, dielectric thickness d = 0.508 cm and operating of 32.5 GHz and using the dispersion relations, the existing modes are determined.

Figure 4.30 shows that there is only one guided mode, which is the TM_0. Modes that intersect with the circle of radius V are existing modes in the dielectric waveguide. The effective dielectric constant is also plotted as a function of frequency in Figure 4.31. Again one mode exists for this grounded substrate. An interesting observation is that as the frequency increases, the effective dielectric constant modes increases, approaching a the relative dielectric constant of the substrate. It is now safe to proceed with the design knowing that there are no higher order substrate modes.

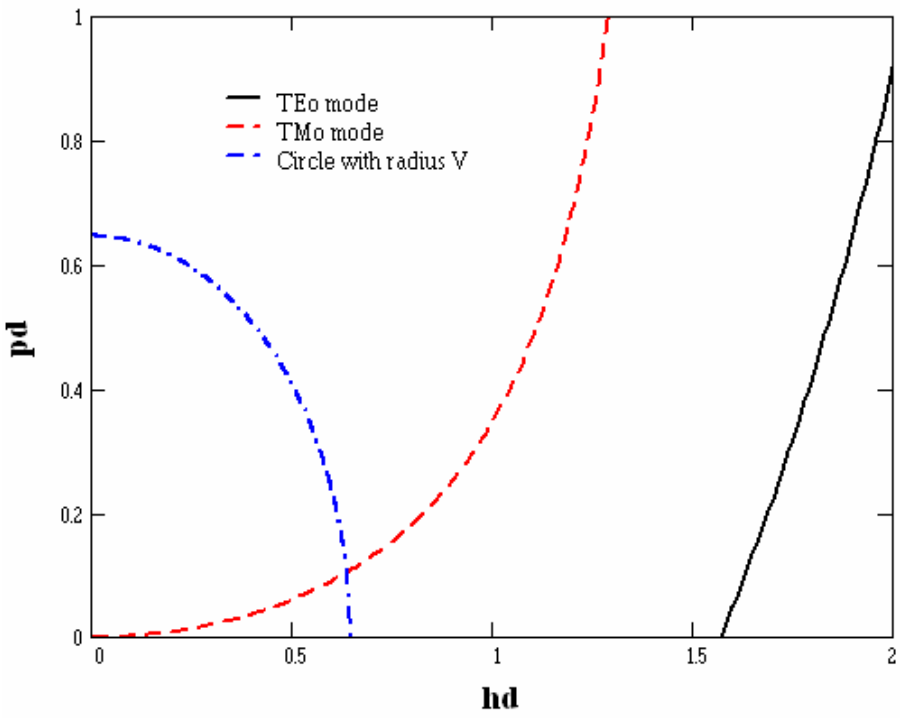

Figure 4.30 Graphical representation of the dispersion relations for the modes that exist in a grounded substrate with ε_r=4.5 and d=0.508mm thick at 32.5 GHz.

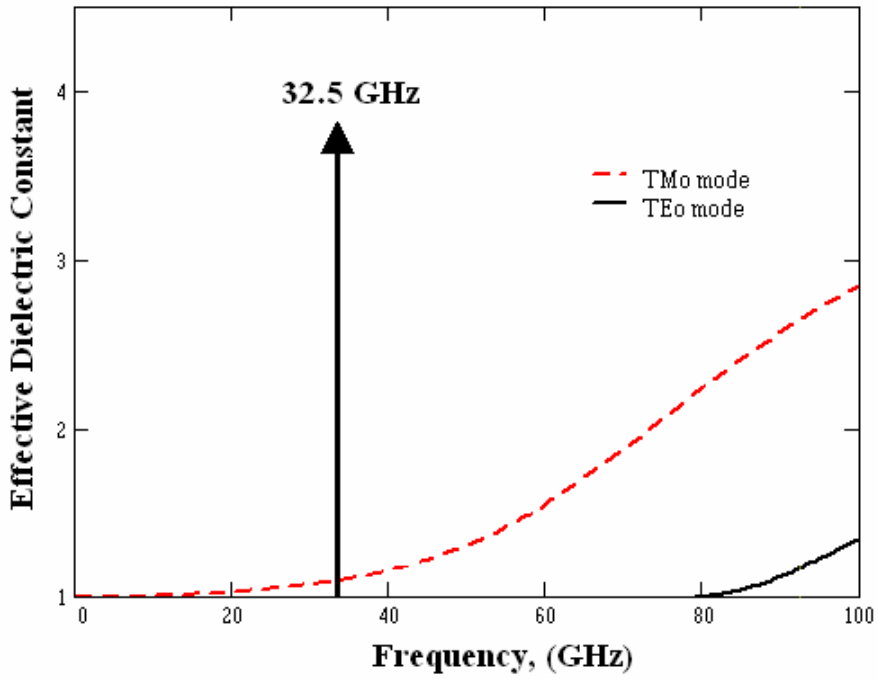

Figure 4.31: Plot of the effective dielectric constant as a function of frequency for a grounded substrate with ε_r =4.5 and dielectric thickness = 0.508 mm.

Figure 4.32 shows the simulated Rotman lens. Figure 4.33 illustrates the phase across the array ports when the lens is fed from port 1 which will produce radiation patterns with peaks at 0º. As can be seen, there are no phase variations at the output ports and therefore no beam steering will be expected. During the simulation of this lens it was noticed that the larger mesh density, the more identical the phase response will be between the output ports, concluding that 7 cells per wavelength, which is the maximum the available computer memory can handle and simulate, is not fine enough to render an accurate simulation results. The reflection coefficients of all the lens ports were les than 10 dB and the coupling coefficients between the ports were less than 15 dB over a broad bandwidth.

The radiation pattern is then calculated using the scattering parameters obtained for the simulation, for an antenna array with element spacing of half of free space wavelength at 32.6 GHz.

Figure 4.34 shows the calculated radiation patterns of an antenna array fed by this simulated Rotman lens. As can been seen the results are satisfactory, and the beam pointing directions are as expected with seven beams covering an area of ±30º with 10º steps. The side lobes were less than 13dB for all of the radiation patterns.

The final Rotman lens design that is going to be used on the perpendicularly-fed dual polarized array is shown in Figure 4.35. Transmission lines were added to connect the output ports (ports 14 to 22 of Figure 4.32) to a linear antenna array. These transmission lines should have the same length, to ensure that the phase differential of the Rotman lens is intact. The separation between adjacent transmission lines was kept equal to, or larger than, five times the thickness of the substrate, to minimize coupling between them.

Consequently, it was necessary to meander these transmission lines. These transmission lines may be bended in different manors in order to save space and/or to improve the lens efficiency. Other techniques can also be developed, which are still being investigated.

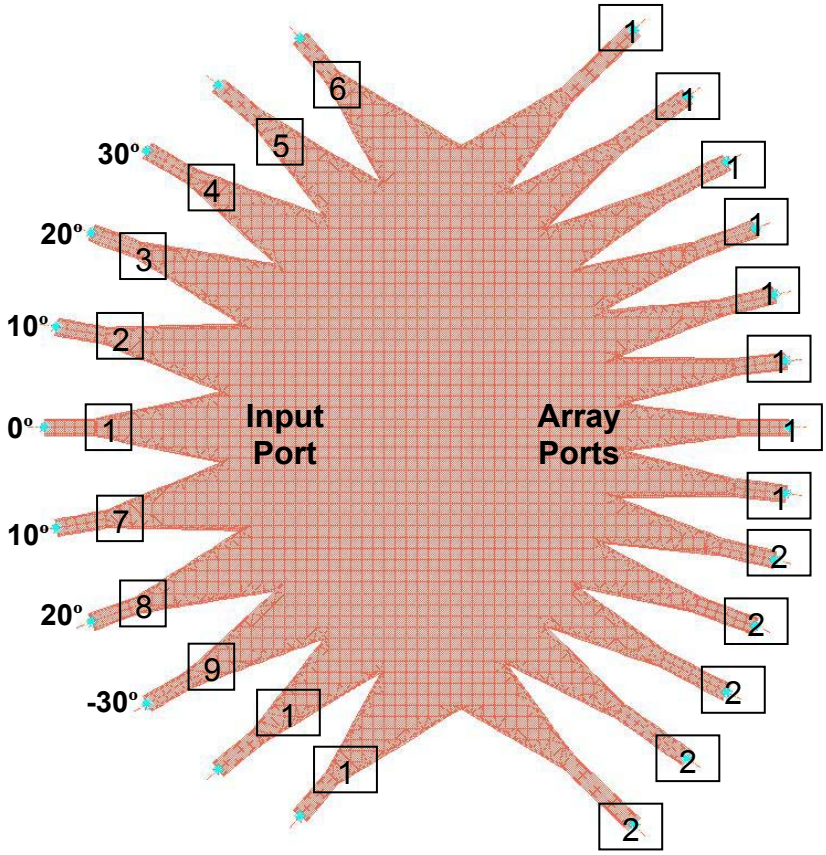

Figure 4.32: The simulated Ka-band Rotman lens.

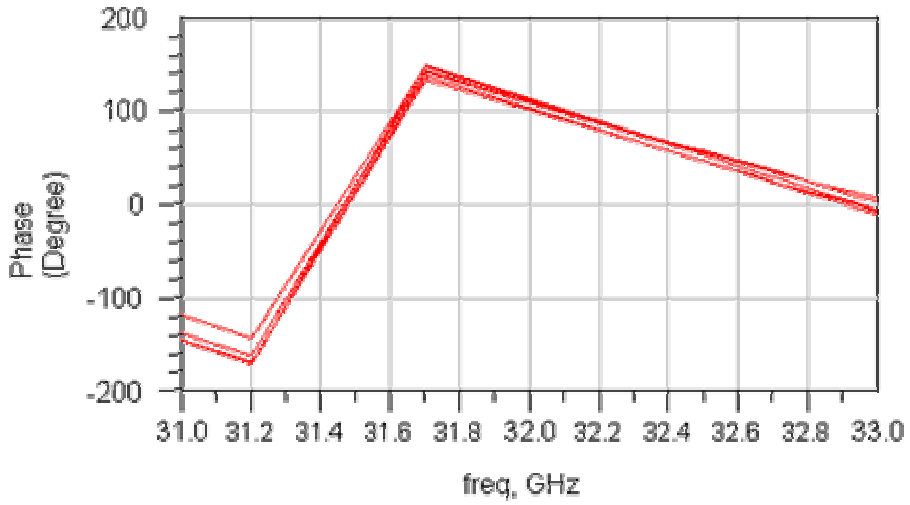

Figure 4.33: The phase across the array ports when the lens is fed from port 1 which will produce radiation pattern with peaks at 0º. (Simulation)

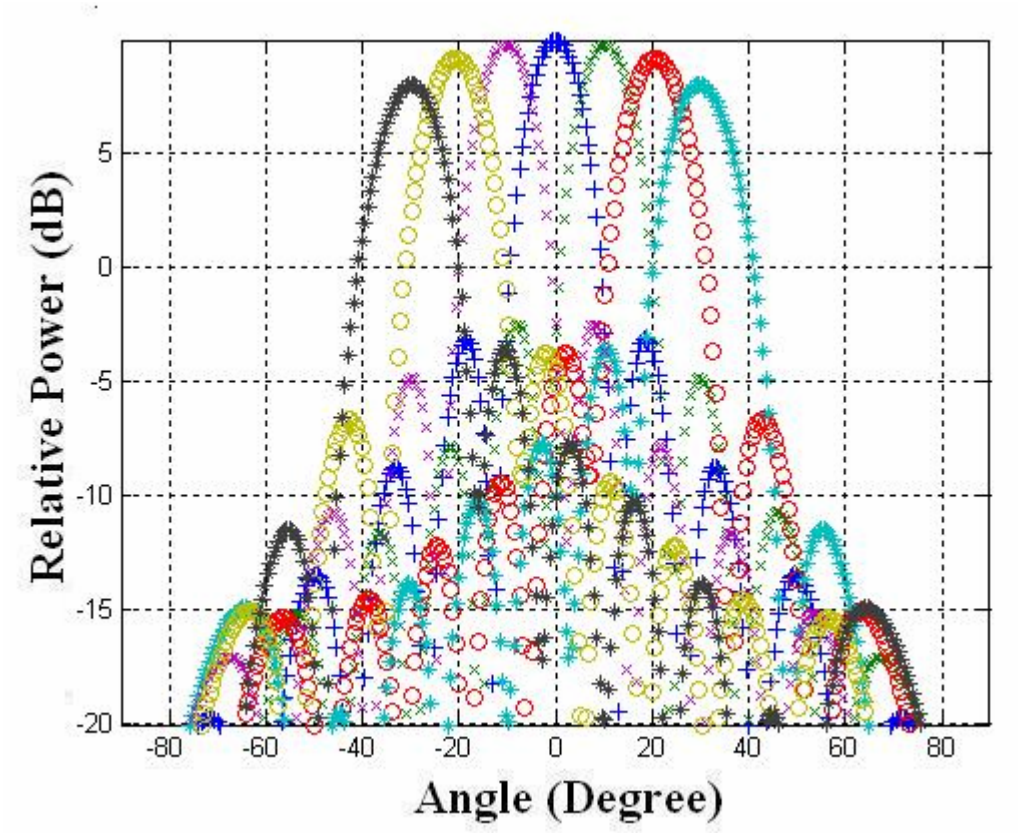

Figure 4.34: Calculated radiation patterns of an antenna array fed by the simulated Rotman lens at 32.6 GHz.

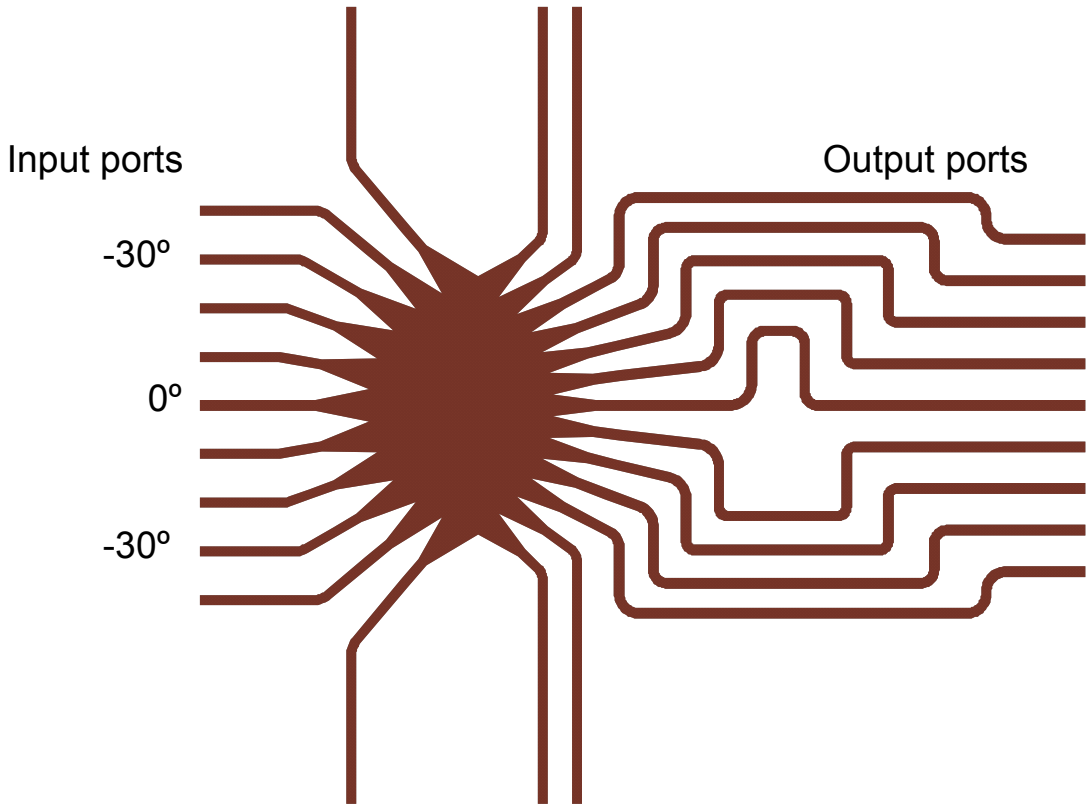

Figure 4.35: The Mask of the Ka-band Rotman lens.

4.5.3 Microstrip Patch Antenna Array fed by Rotman Lens

Rectangular microstrip patch antennas were designed using ADS Momentum™ to operate at 32.6 GHz. The dimensions of the antenna are as follows:

L = 1.8631mm

W = 2.8067 mm

Where L is the resonant length of the antenna and W is the width of the antenna. Nine antennas were then connected to the 9 outputs of the lens. Figure 4.36 shows the Rotman lens fed patch antenna array. A quarter wave matching network was needed to match the

microstrip impedance to antenna input impedance. The purpose of this design is to test the performance of this Ka-band Rotman lens.

This design was fabricated and tested; Figure 4.37 shows a photograph of the fabricated microstrip antenna array fed by a Rotman lens. The lens was measured in the far field in an anechoic chamber. Figure 4.38 shows the measurement setup that was used, where R is a distance in the far field of the antennas. A receiving standard gain horn antenna was used as a receiver in the measurements. The transmitting patch array is rotated and the radiation pattern is measured. The signal is then switched between the seven input ports to steer the beam.

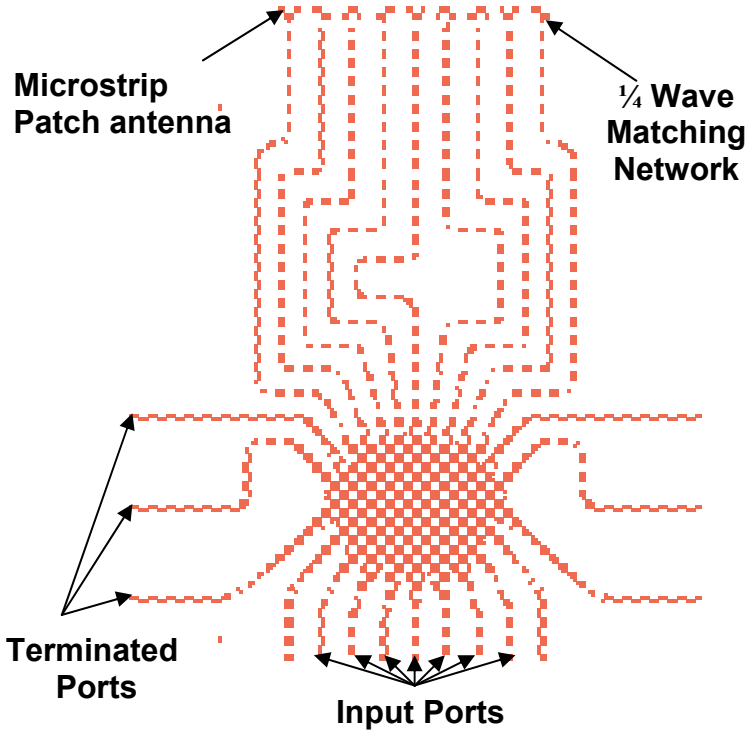

Figure 4.36: Array of microstrip patch antennas fed by Rotman Lens.

Figure 4.39 shows the measured radiation patterns for this design. All of the measurements were taken at 32.55 GHz. As can be seen, the desired scan angles are met. The side lobe level was less than 8.5 dB in the worst case. This result was comparable to a similar design [8]. To absorb the 'spilt over' power to the sides of the lens absorbing material pieces (Emerson and Cuming ^{TM} BSR-1/ss 6M) that can be seen in the photograph (Figure 4.39) are used.. Shown in Figure 4.40 is the reflection coefficient of a 50Ω transmission line measured with and without absorbing material. It is clear that the improved the reflection coefficient to more than 10 dB over a broad bandwidth. The use of the absorbing material proved to be an effective way to absorb the spilt over power at the edge of the lens, and will help to reduce the side lobe levels [9]. To investigate the reason for the high side lobe levels, the Ka-band Rotman lens was simulated again, but this time with the input ports left open without terminations. The input signal was fed into port 9, which corresponds to the -30º scan angle. The radiation pattern is then calculated using the simulation results. Figure 4.41 shows a comparison between the measured antenna array fed by the Rotman lens (green) and the calculated radiation pattern of the Rotman lens with the inputs port left without termination. A fairly close similarity between the two radiation patterns can be observed and in both cases the side lobe level increased when compared with the radiation patterns of Figure 4.34 when all the ports were terminated. This verifies the importance of input ports terminations. One way to realize this is to use a non-reflective switch at the input ports. This is commercially available, such as the MACOM^{TM} non-reflective switch MA4AGSW1A. This switch will allow the signal to be absorbed rather than reflect back to the lens.

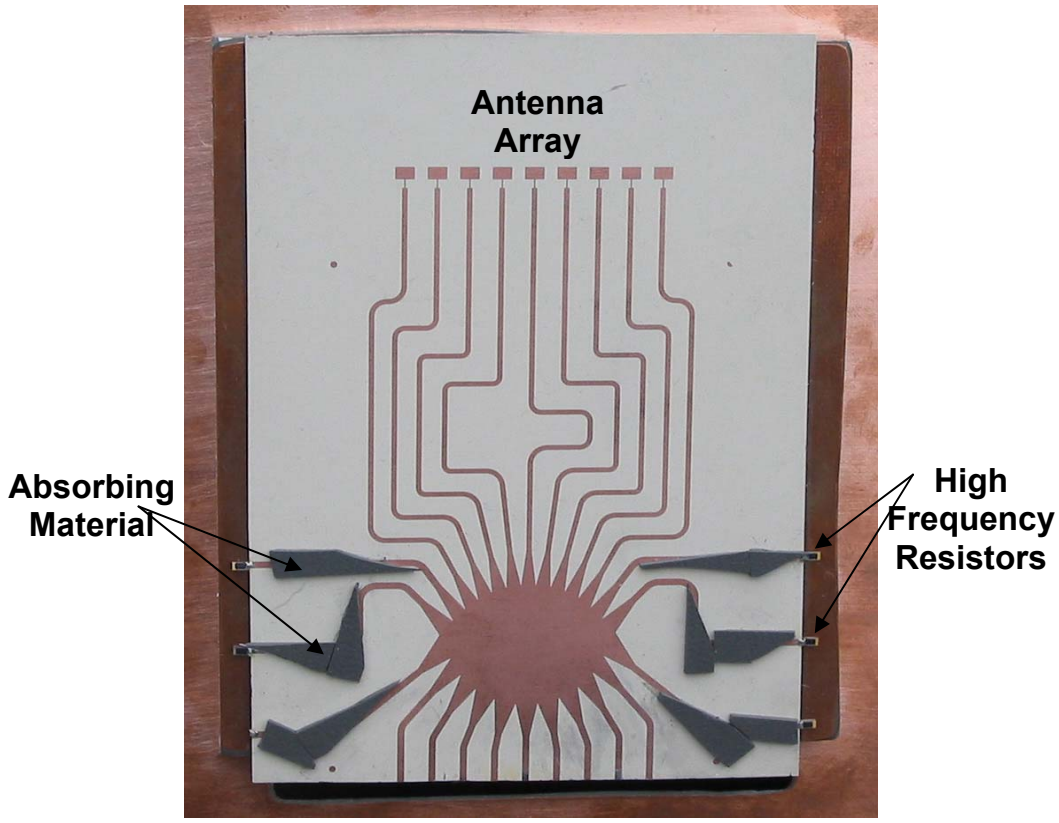

Figure 4.37: A photograph of the fabricated antenna array fed by Rotman lens.

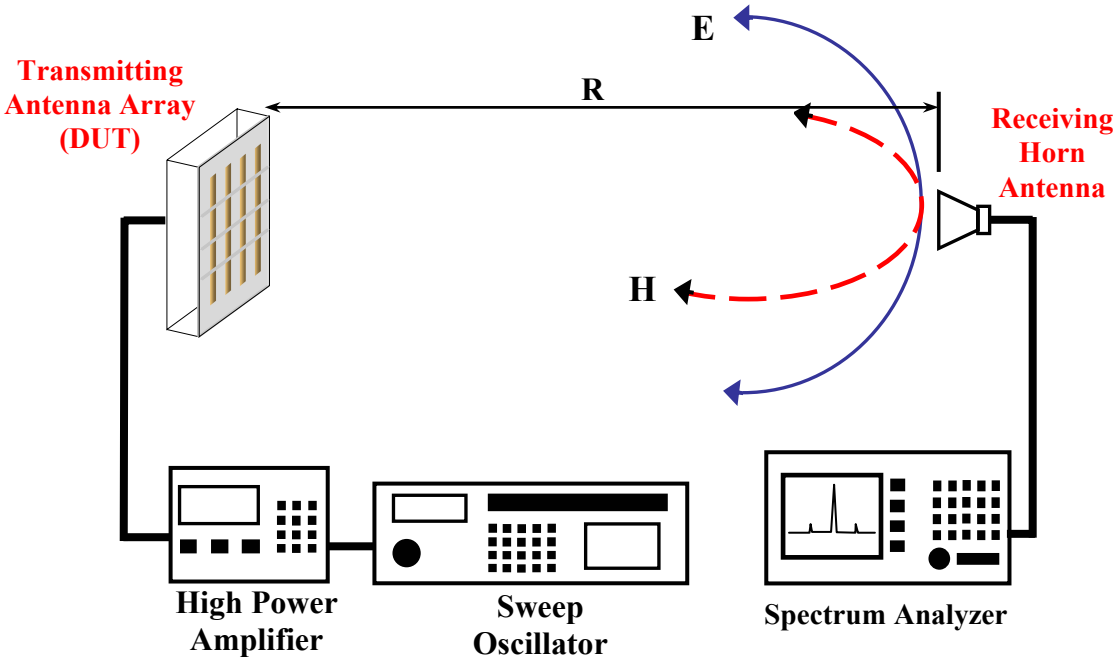

Figure 4.38: Experimental setup for the measurement of the antenna array in the far field.

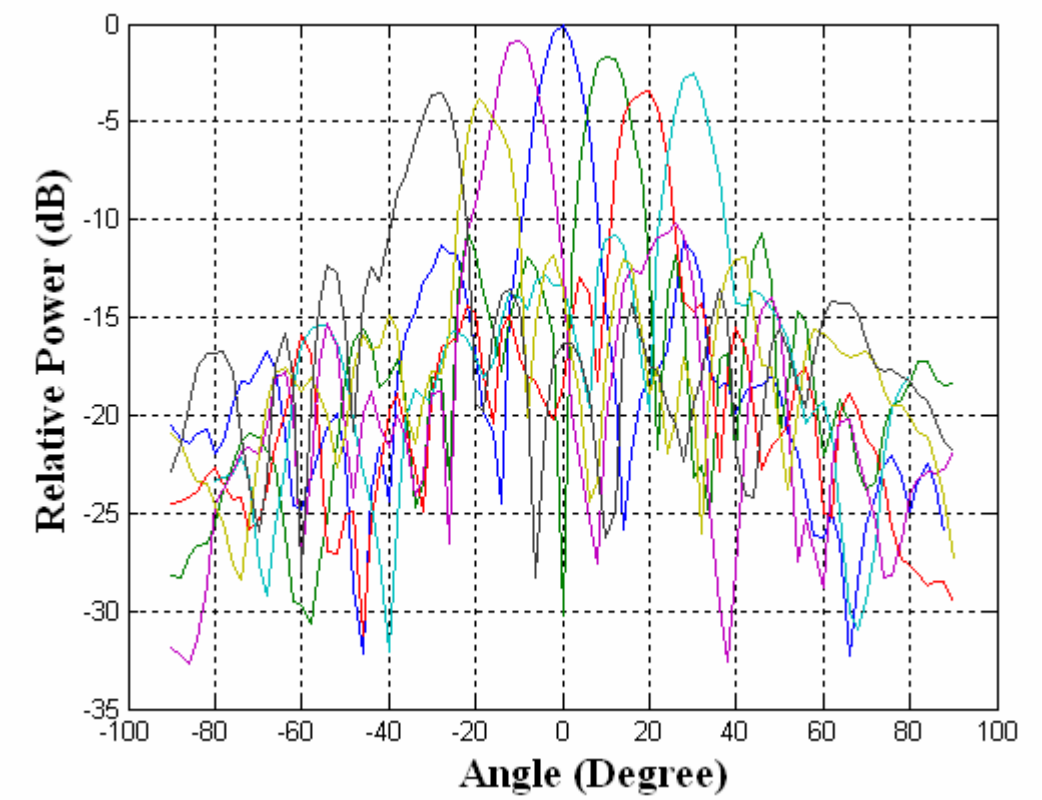

Figure 4.39: Measured radiation patterns of the microstrip patch antenna array fed by Rotman lens at 32.55 GHz.

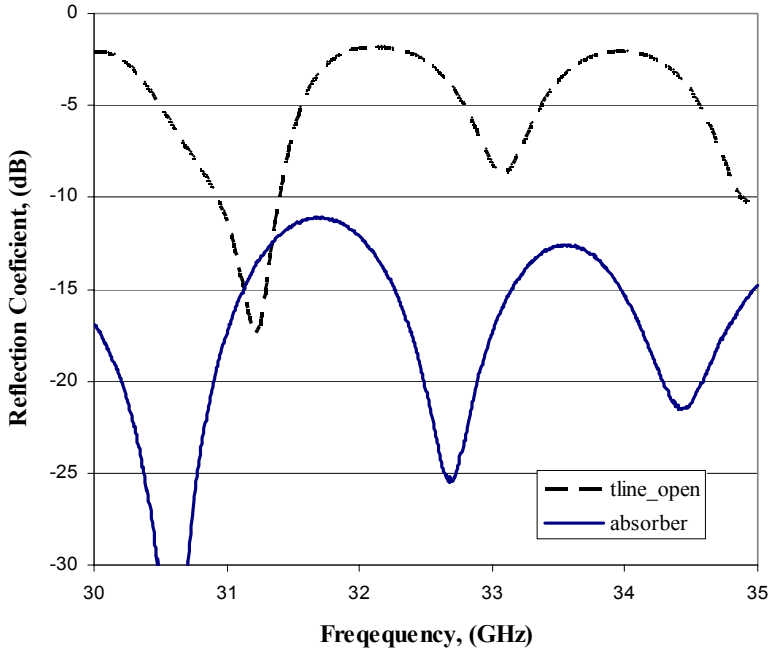

Figure 4.40: The reflection coefficient of open ended transmission line with absorbing material (solid), and without absorbing material (dashed).

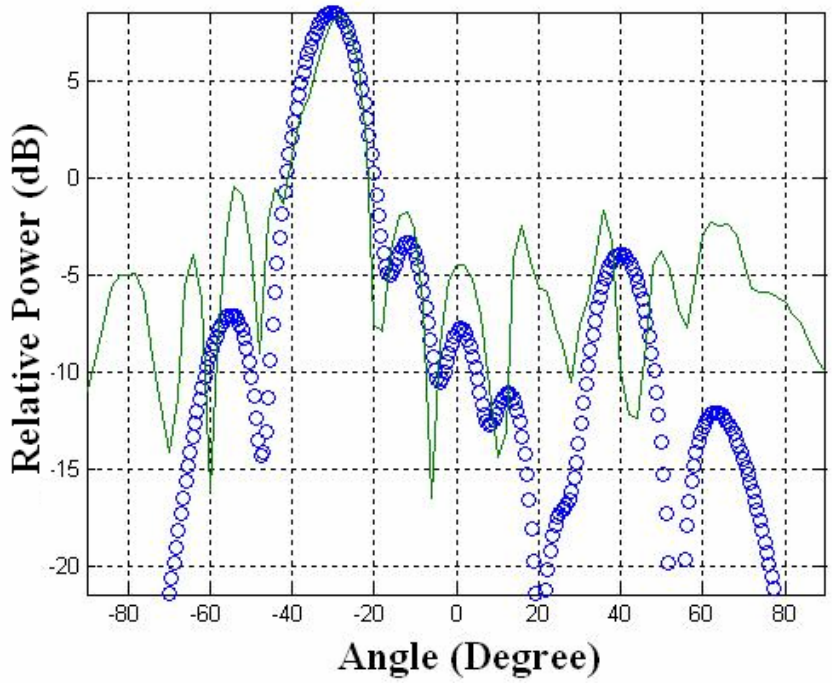

Figure 4.41: A comparison between the measured antenna array fed by the Rotman lens (solid-green) and the calculated radiation pattern of the Rotman lens with the input ports left open and without termination (dotted-blue).

4.6 1X9 Dual polarized perpendicularly-fed patch array spatial combiner with Rotman lenses

The Design of the Ka-band Dual polarized perpendicularly-fed patch array has been completed. A 1x9 dual polarized patch array fed by Rotman lenses is shown in Figure 4.42.

This structure is an assembly of three parts: the Rotman lens, microstrip line to dielectrically filled waveguide to aperture coupled microstrip transition and the dual polarized patch antenna. As shown in this Auto CAD drawing of the whole design, 2.4mm connectors (signal launchers) were placed at each input port of the Rotman lens to feed the system. Beam steering can be realized by switching between the input ports. It is to be mentioned that the scan angle, or coverage area of this lens is ± 30º and the 7 input ports of the lens allow for a scanning range from -30 to 30 degrees in 10 degree steps. It is to be noted that the Rotman lens can be easily redesigned with a different number of input or output ports. An electronic switch can be used to switch between the beams instead of the 2.4 connectors used in this prototype design. A good candidate at this frequency is a 1 to 8 switch available by MACOM™ (MA4AGSW8-2).

The top view of the structure is shown in Figure 4.42, since the bottom view is identical to the top view. One Rotman lens will beam steer the horizontal polarization while the other lens will beam steer the vertical polarization. One can therefore demonstrate beam steering capability in the azimuth plane of the structure for both the vertical and horizontal polarizations using one tray. Interestingly enough, two independent signals can be sent at different frequencies and radiate at two different polarizations. This structure can also be

used to transmit and receive simultaneously as one polarization can be used to transmit and the other to receive. Figure 4.43 shows the mask of the 1x9 dual polarized patch antenna array.

A photograph a fabricated Rotman lens and perpendicularly fed patch array is shown in Fig. 4.44. This photograph depicts a single tray of the phased array. Only the top view of the structure is shown, the bottom view of this structure is identical to the top view. The aluminum structure was machined using a CNC (Computer Numerical Control) machine.

The Rotman lens and waveguide transition were fabricated on Rogers TMM4 substrate with a dielectric constant of 4.5. The patch array was fabricated on Rogers RT6002 with a dielectric constant of 2.94. Each input port was fed through a 2.4 connector. As shown in the photograph, there are 7 input beam ports, and 9 output beam ports to form a 1x9 linear array with half wavelength spacing between elements. It is to be mentioned that the absorbing materials (Emerson and Cuming^{TM} BSR-1/ss 6M) are used to absorb the 'spilt over' power to the sides of the lens.

Using an anechoic chamber and a standard gain horn as was shown in Figure 4.38, the radiation patterns were measured for the 1x9 dual polarized patch array fed by Rotman lenses. The measured pattern for the vertically polarized beam steering is depicted in Figure 4.45 and that for the horizontally polarized beam steering is shown in Figure 4.46. The desired scan angles from –30 to +30 degrees in 10 degree increments were achieved at 32.9GHz for each of the seven input beam ports and for each polarization. The sidelobes were found to be under 8.0dB for all the beams. The measured cross polarization radiation was found to be better than –16dB for both the vertical and horizontal ports.

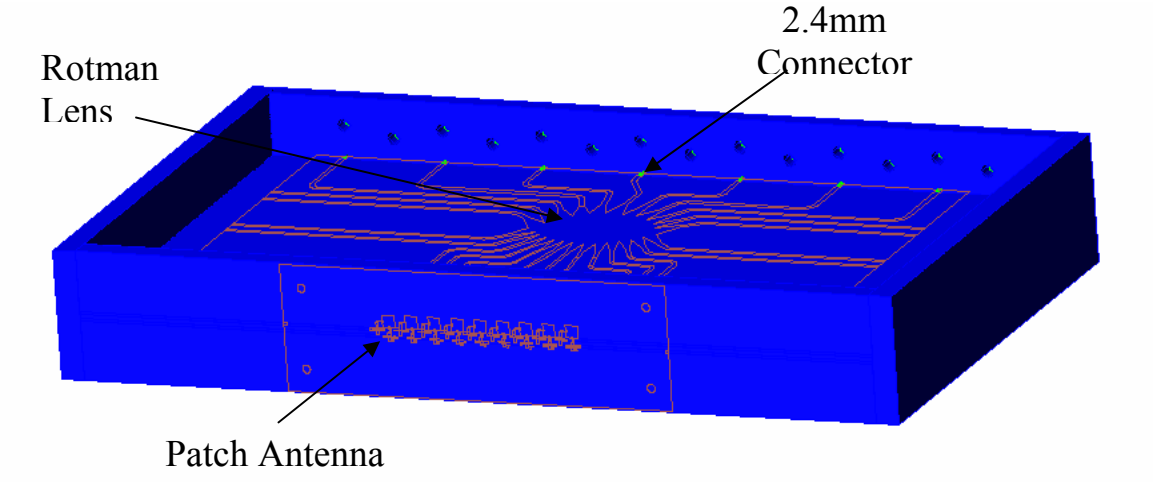

Figure 4.42: Auto CAD drawing of a 1x9 perpendicularly-fed patch array fed by Rotman lens.

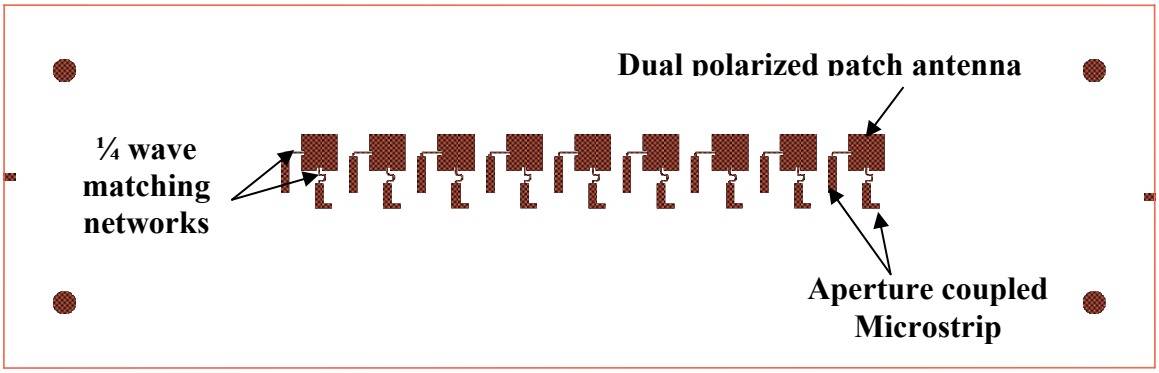

Figure 4.43: The mask of the 1x9 dual polarized antenna array.

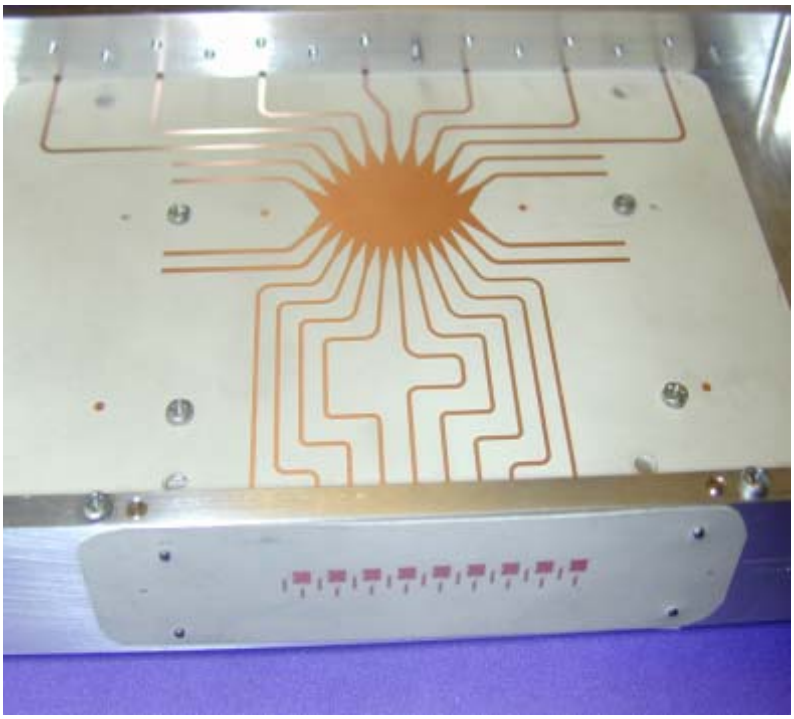

Figure 4.44: Photograph of a 1x9 dual polarized patch array fed by Rotman lenses.

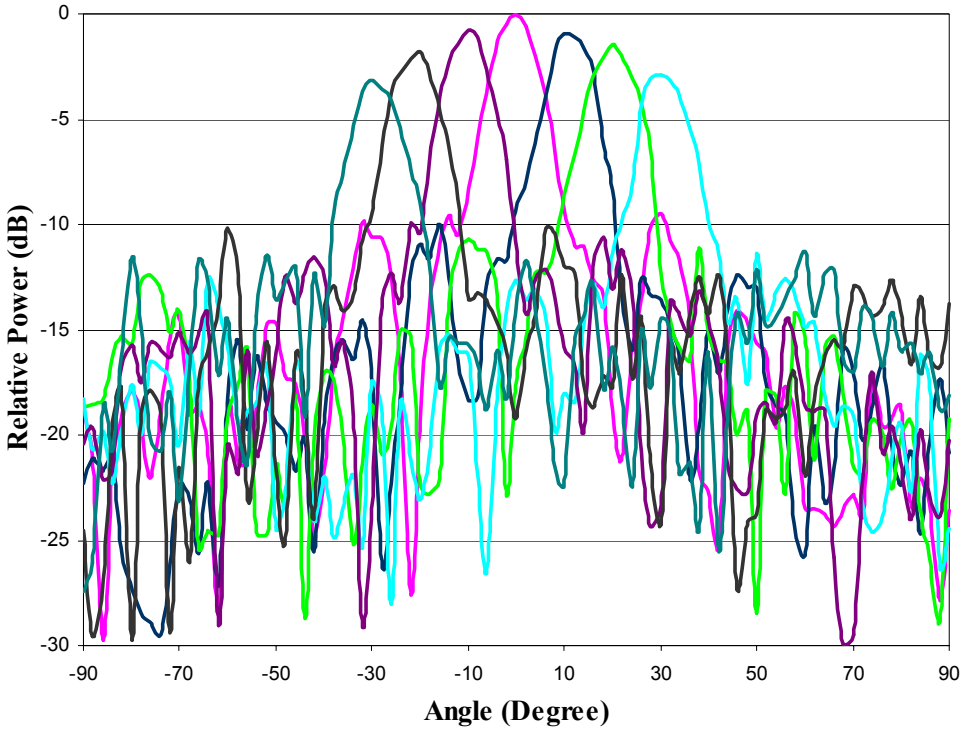

Figure 4.45: Measured radiation patterns for the vertical polarization at 32.9GHz.

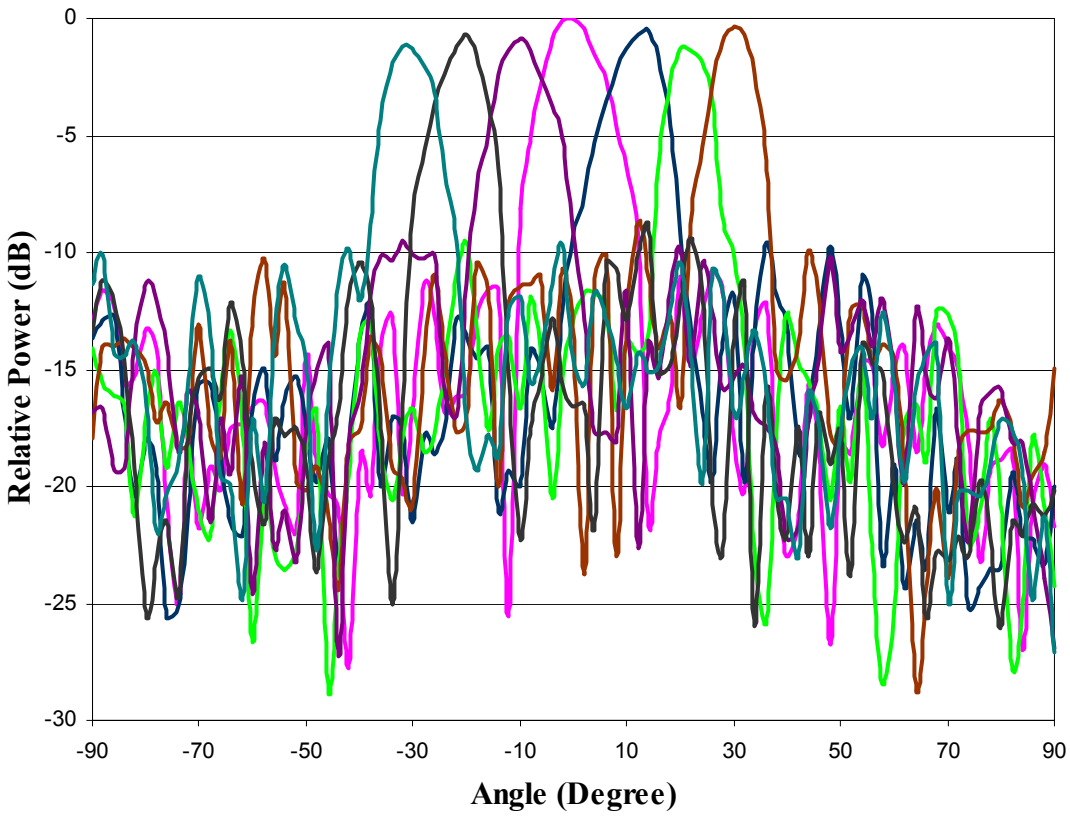

Figure 4.46: Measured radiation patterns for the horizontal polarization at 32.9GHz.

4.7 References

[1] R. M. Cox, J. R. Sebring," MLS- A Practical Application of Microwave Technology" IEEE Trans. On Microwave Theory and Tech., Vol. MTT-24, No. 12, pp. 964-971, Dec. 1976

[2] S. F Peik, and J. Heinstadt," Multiple Beam Microstrip Array Fed by Rotman Lens", IEE Antennas and Propagation April 1995. pp. 348-351.

[3] J. Butler. and R. Lowe. ," Beamforming Matrix Simplifies Design of Electronically Scanned Antenna ,"*Radion Electronic Desig., 9, pp 170-173, 1963.*

[4] K. Chang, M. Li, T. Y. Yun, C. T. Rodenback, " Noval Low-Cost Beam Steering Techniques", IEEE Trans. On Antenna and Propagation., Vol. 50, no. 5, May 2002.

[5] P. Liao and R.A. York,"A New Phase-Shifterless Beam Scanning Technique Using array of Coupled Oscillators" IEEE Trans. On Microwave Theory and Tech., Vol. MTT-41, No. 10, pp. 1810-1815, Oct. 1993.

[6] A. Tombak, and A. Mortazawi," Design of Novel Low-Cost Phased Arrays Based on the extended Resonance Technique" IEEE antenna and Propagation Symp, Vol. 4 June 2003 pp. 672-675.

[7] C. Metz, J. Grubert, J. Heyen, A. F. Jacob, S. Janot, E. Lissel, G. Oberschmidt, L. C. Stange, "Fully Integrated Automotive Radar Sensor With Versatile Resolotion" IEEE Trans. On Microwave Theory and Tech., Vol. 49, No. 12, pp. 2560-2566, Dec. 2001.

[8] M. Hansieshi, M. Konno" Dual-Polarized Antenna Fed by Dog-Bone SlotsRecent" *IEE interntional conf. on, Ant and Prog., pp. 45-48, April 2001.*

[9] H. Wong, K. B Ng and K. M Luk," A Dual-Polarized L-probe Patch Antenna" Microwave Conference APMC2001 Asia-Pacific, vol.2, pp. 930-933, 2001.

[10] J. R Sandford and A. Tengs, "A Two Substrate Dual Polarized Aperture Couple Antennas and Propagation Society International Symposium, AP-S. Digest , vol.3, pp1544 -1547, 1996.

[11] B. G Porter, L. L Rauth, R. Mura, and S.S Gearhart "Dual Polarized slot-coupled patch antennas on Duroid with Teflon lenses for76.5GHz automotive radar systems," IEEE trans. Antenna and Propagat, vol 47 pp 1836-1842, 1999.

[12] D. M Pozar and S. D Stephen,"A Shared-Aperture Dual Polarized Microstrip" *IEEE Trans, Ant Prog, pp. 150-157,Feb 2001.*.

[13] *Gao, S.C.; Li, L.W.; Leong, M.S.; Yeo, T.S.*, "A novel dual-polarized, wide-band microstrip patch antenna with aperture coupling," IEEE Antenna and Propagat International Sym.., vol. 4 pp.78-81, 2001, Volume: 4 , 2001.

[14] *Holter, H.; Tan-Huat Chio; Schaubert, D.H.* **,"**Experimental results of 144-element dual-polarized endfire tapered-slot phased arrays**,"** *IEEE Trans, Ant Prog, pp 1707-1718,November 2000.*

[15] J. McSpandden, L. F Kai Chang "Ka-band Beam Steering Reflectarray Study," *IEEE Trans, Ant Prog., pp 1662-1665, October 1999.*

[16] X. Qin, W. Zhang, C. Domier, N. Luhmann, W. Berk, S. Duncan and D. Tu,"Monolithic Millimeter-Wave Beam Control Array," Digest of *IEEE Microwave Theory Tech Symp, pp 1669-1673, 1995.*

[17] J. C Chiao, Y. Fu, D. Choudhury, and L. Y Lin, "Microwave Beam-Steering Grid," *IEEE MTT-S Int. Microwave Symp. Dig, June 1999.*

[18] E. O Rausch, A. F Peterson, and W. Wiebach, "Electronically Scanned Millimeter Wave Antenna using a Rotman lens," *IEE Radar., Publication# 449, October 1997.*

[19] N. G. Alexopoulos, P. L. E Uslenghi, and G. A. Tadler, " Antenna Beam Scanning by Active Impedance Loading," IEEE Trans. Antennas Propagation., Vol. AP-22, pp. 722-723, Sept. 1974

[20] C. Chekroun, D. Herrick, Y. Michel, R. Pauchard and P. Vidal," RANDAT: New method of Electronic Scanning, " Microwave Journal, pp. 45-53, Feb. 1981.

[21] W. Lam, C. F. Jou, N. C. Luhmann, Jr. and D. B Rutledge, " Diode Grids for Electronically Beam Scanning and Frequency Multiplication," Int. J. Infrared and Millimeter Waves, Vol. 7, pp. 27-41. 1986.

[22] *W. F Crosswell, R.E. Roddewig, C.G. Pewsey, R.L. Moye, W.L. Jones*, "A waveguide fed composite horn antenna**,"** IEEE Antenna and Propagat International Sym.., vol. 4 pp.338-341, Volume: 1 , 1988.

[23] C.A. Balanis, Antenna Theory: Analysis and design, Wiley, New York,1984.

[24] J. Machac and A. Klaasen," On the transition from ridged waveguide to microstrip**"** Proc. 19th European Microwave Conf., 1989, pp. 1265-1269.

[25] A. C. Buck and D. M. Pozar, “Aperture coupled microstrip antennas with a perpendicular feed**,”** IEEE Electron, letts., pp. 125-126, 1986.

[26] N. Kaneda, Y. Qian. I. Itoh, "A broad band microstrip to waveguide transition using quasi yagi antenna," *IEEE MTT-S Int. Microwave Symp. Dig*., pp. 1431-1434, 1999.

[27] Y. Leong, and S. Weinreb, “Full band waveguide to microstrip probe transition s," *IEEE MTT-S Int. Microwave Symp. Dig, pp. 1435-1138, 1999.*

[28] S. Ortiz and A. Mortazawi, "A perpendicularly-fed patch array for quasi-optical power combining," *IEEE MTT-S Int. Microwave Symp. Dig*., vol. 2, pp. 667-670, 1999.

[29] J. Ruze, “ Wide Angle Metal Plate Optics”, Proc. IRA, 38, pp. 53-59, 1950.

[30] W. Rotman and R. F Turner, “Wide Angle Lens for Line Source Applications,”*IEEE Trans, Ant Prog., AP-11, pp. 623-632, 1963.*

[31] A. K. S. Fong. And M. S. Smith, “A Microstrip Multiple Beam Forming Lens,”*Radion Electron. Eng., 1984, 54, pp. 318-320.*

[32] T. Katagi., S. Mano and S. Sato, “An Improved Design of Rotman Lens Antennas,” *IEEE Trans. On Antennas and Propagation, Vol. AP-32, No. 5, pp. 524-527, May 1984.*

[33] Y. M. Tao and G. Y. Delisle,” Design of Compact Integrated Rotman Lens for Multiple Beam Array,” Digest of ISAE’ 97, Xi’an, China, pp. 22-26, August 1997.

[34] R. C. Hansen, “Design Trades for Rotman Lenses,” *IEEE Trans. On Antennas and Propagation, Vol. 39, No. 4, pp. 464-472,April 1991.*

[35] J. Kim, F. Barnes, "Scaling and focusing of the Rotman lens," *IEEE Antennas and Propag. Int. Symp., pp. 773-776 Vol. 2, July 2001.*

[36] Y. M. Tao and G. Y. Delisle," Multiple Beam Antenna Arrays for Indoor Communications" Digest of ANTEM'96, Montreal, August 1996.

[37] L. Musa and M. S. Smith, " Microstrip Port Design and Sidewall Absorption for Printed Rotman Lenses", IEE Proceedings,Vol.136, P. H, No.1, pp. 53-58, Feb 1989.

[38] R.E Collin, Field Theory of Guided Waves. New York: McGraw-Hill, 1960.

[39] C. H. Walter, Traveling Wave Antennas. New York: McGraw-Hill, 1965, pp.290-299.

[40] I. E. Rana and N. G. Alexopoulos, "Current distribution and input impedance of printed dipoles," IEEE Trans. Antennas Propagat., vol. AP-29, pp.99-105, Jan. 1981.

[41] N. G. Alexopoulos and D. R. Jackson, "Fundamental substrate (cover) effects on printed circuit antennas," IEEE Trans. Antennas Propagat., vol. AP-32, pp.807-816, Aug. 1984.

Chapter 5

Conclusions and Future Work

5.1 Conculsions

Spatial power combining techniques offer a promising approach to realize compact, reliable , lightweight, higher-power and economical systems at millimeter wavelengths. This work focuses on the tray based perpendicularly fed array systems, and several design issues such as bandwidth improvement, power combining efficiency, dual polarity and beam steering were addressed in this thesis.

In this work, an enhanced bandwidth tray-based spatial power-combining array structure based on a perpendicularly-fed antenna is proposed. This structure has the advantage of minimal interactions between the radiated fields and the active devices. Additionally, increased stability is provided, while providing a robust and reliable performance. Dielectrically filled miniature horn arrays were employed for both the receiving and transmitting radiating elements of this 5x5 amplifier array. A peak gain of 15.8 dB at 9.9 GHz and a 3-dB bandwidth of 13% were measured. Gain, bandwidth and power measurements are consistent with simulation predictions.

Experimental and numerical investigations on a 49-element Ka-band amplifier array have been conducted. This study is aimed at determining the origin of various losses in the amplifier array. Passive simulation data confirms that the load seen by the active devices

is well matched and that most of the power is coupled to the LSE_{10} mode. This means that coherent power combining should take place if there is no phase and amplitude variation due to the active devices and phase correcting dielectric lenses.

A complete structure of the tray based spatial power combiner requires electronic beam controllers for beam steering. Two design methodologies for dual polarized antennas, phase shifting components, feeding networks and active devices were investigated. Both of these approaches are based on a modified perpendicularly-fed patch array spatial power amplifier. A design strategy was developed to realize this dual polarized perpendicularly-fed patch array by employing Rotman lenses to scan the beam. The design of this structure was divided into four stages the dual polarized square patch antenna was designed first, then the dielectrically filled waveguide to aperture transition, then the dielectrically filled waveguide to microstrip transition. Finally, the Rotman lens that is going to be integrated with this structure was designed.

A Ka-band array of microstrip patch antennas fed by a Rotman Lens was designed, fabricated and tested. The scan angle, or coverage area, of this lens and consequently the system is ± 30º. Seven input ports of the lens allow for a scanning range from -30 to 30 degrees in 10 degree steps. This lens is used in the tray based perpendicularly fed dual polarized multibeam array. This dual polarized system is therefore expected to have a scan range of ± 30º for both the horizontal and vertical polarizations.

A multibeam spatial power combining phased array system has been designed and fabricated at Ka band. Beam forming and steering is obtained through the use of Rotman lenses. The system demonstrated the capability of both vertical and horizontal polarizations with ±30 degree beam steering. The cross polarization was measured to be

less than –16dB for both the vertical and the horizontal polarizations. Through simulations, greater than 20dB isolation between the vertical and horizontal polarizations is achieved, with a 10dB return loss of 700MHz.

5.2 Future Work

Microstrip based systems offer several advantages in contrast to other conventional transmission line systems: they are straightforward to design and simulate, they allow for ease of fabrication and rapid prototyping, and they can be easily integrated into a complete system consisting of components such as amplifiers, filters, or couplers. However, in the millimeter-wave frequency band, the losses associated with microstrip designs start to become significant. As an alternative, a waveguide based multibeam system can be implemented. Very little losses are associated with waveguide based systems since the electromagnetic wave is completely confined within the waveguide. In addition, waveguide based systems offer superior bandwidth. Based on the above discussion, the future work of this project includes the implementation of a waveguide based multibeam system for the millimeter-wave frequency band. The waveguide based multibeam system will undergo a similar design procedure as the microstrip based system. This procedure includes the design of the Rotman lens as the phase shifting component, the scheme to achieve dual polarization, and finally, the design of dual polarized antennas intended for a planar array. Figure 5.1 shows the proposed waveguide based dual polarized perpendicularly fed miniature horn array. as can been seen, two separate miniature horn antennas can be used for each unit cell where one would be used for the horizontal polarization and the other would be for the vertical polarization. The miniature horn antennas, which can be achieved through dielectric loading, must be small enough to allow for half wavelength spacing between elements. To avoid grating lobes, both vertical and horizontal elements must fit within a unit cell size of $\lambda/2$ by $\lambda/2$. The output ports from the Rotman lens would operate in the TE_{10} mode, which must allow for vertical

polarization. To achieve a horizontal polarization, a 90 degree waveguide polarization converter (found in literature) canl be implemented. The output ports of the Rotman lens would be fed into the step twist junctions, and the output of the step twist junctions would then be fed into an array of horn antennas. Two separate horn antennas per unit cell offer several advantages; the main advantage is its large bandwidth. Also, the cross polarization radiation is minimal since the vertical and horizontal waveguides remain separate and there is very little coupling.

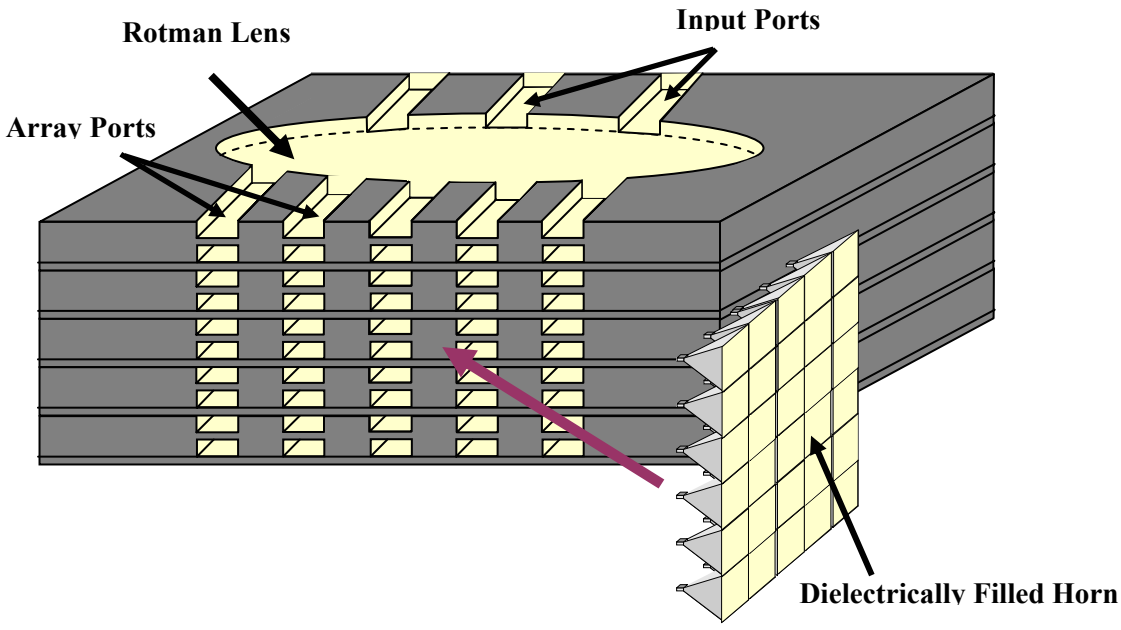

Figure 5.1 Waveguide based dual polarized perpendicularly fed miniature horn array.

Appendix A

MATLAB Program used to calculate the radiation patterns of an antenna array if it is fed by a given set of scattering parameters:

```
% Measured S-parameters are loaded, the S-parameters are in real and imaginary format.
clear all; clc;

Data(4,1).s=load('sb0ap4.txt'); Data(4,2).s=load('sb0ap3.txt');
Data(4,3).s=load('sb0ap2.txt'); Data(4,4).s=load('sb0ap1.txt');
Data(4,5).s=load('sb0a0.txt');   Data(4,6).s=load('sb0an1.txt');
Data(4,7).s=load('sb0an2.txt'); Data(4,8).s=load('sb0an3.txt');
Data(4,9).s=load('sb0an4.txt');

% This offset can be used to investigate the phase at each port, but should not be used in
the final plot.

offset(1)=0; offset(2)=0; offset(3)=0; offset(4)=0; offset(5)=0; offset(6)=0; offset(7)=0;
offset(8)=0; offset(9)=0;

for i=1:9

   S21(4,i).freq=Data(4,i).s(:,1);
   S21(4,i).s21=Data(4,i).s(:,2)+j*Data(4,i).s(:,3);
   S21(4,i).s21=abs(S21(4,i).s21).*exp(j*angle(S21(4,i).s21)+j*offset(i)*pi/180);

end;

lmax=length(S21(4,i).freq);
findex=round(linspace(1,lmax,17));

for k=findex

   theta=[-pi/2:0.01:pi/2];
   frequency=S21(4,i).freq(k);
   freq_operation=32.6e9; % Frequency of operation.
   Spacing =0.5;
% The spacing between the antenna elements, it is 0.5 of a wavelength at operating
frequency only.

 AF_summation4=0;
```

```
    for i=1:9

% Calculating the Array Factor.

AF_summation4=AF_summation4 +
abs(S21(4,i).s21(k)).*exp(j*i*2*pi*(frequency/freq_operation)*Spacing*sin(theta)+j*ang
le(S21(4,i).s21(k)));

    end;

% Calculating the Radiatin Patterns
    EF=cos(theta);

    RP4=AF_summation4.*EF;

    AF_forplot4=20*log10(abs(RP4));

    figure(1);
    plot(180/pi*theta,AF_forplot4);
    maxpoint=max([max(AF_forplot4)]);
    axis([min(theta)*180/pi max(theta)*180/pi maxpoint-30 maxpoint]);
    xxx=sprintf('%s','Frequency = ',num2str(S21(4,i).freq(k)/1e9),' GHz');
    title(xxx);
    grid;

    pause;
end;
```